공학박사학위논문

Synthesis and Characterization of Polymer Nanocomposites with Improved Physical Properties Using Graphene Derivatives as Fillers for Various Applications

그래핀 유도체를 기반으로 하는 물성이 우수한 고분자 나노복합재료의 합성 및 분석, 그리고 다양한 분야로의 응용

2016년 8월

서울대학교 대학원

화학생물공학부

임 민 영

그래핀 유도체를 기반으로 하는 물성이 우수한 고분자 나노복합재료의 합성 및 분석, 그리고 다양한 분야로의 응용

Synthesis and Characterization of Polymer Nanocomposites with Improved Physical Properties Using Graphene Derivatives as Fillers for Various Applications

지도교수 이 종 찬 박사

이 논문을 공학박사학위 논문으로 제출함.

2016 년 8 월

서울대학교 대학원

화학생물공학부

임 민 영

임민영의 박사학위논문을 인준함.

2016 년 8 월

위 원 장 (인)

부위원장 (인)

위 원 (인)

위 원 (인)

위 원 (인)

Synthesis and Characterization of Polymer Nanocomposites with Improved Physical Properties Using Graphene Derivatives as Fillers for Various Applications

by

Min-Young Lim

Adviser: Professor Jong-Chan Lee, Ph. D.

Submitted in Partial Fulfillment
of the Requirements for the Degree of
DOCTOR OF PHILOSOPHY

August, 2016

School of Chemical and Biological Engineering
College of Engineering
Graduate School
Seoul National University

Abstract

Polymer nanocomposites containing graphene have drawn much attention for scientific interests and industrial purposes over the past few years because they can have much improved performance. However, the poor compatibility of graphene with polymers limits the practical application for the polymer nanocomposites. Therefore, the modification of graphene is strongly needed to increase the miscibility with the polymer. In addition to the improved compatibility with the polymer, surface modification of GO with a unique functional moiety can be also very advantageous for the polymer nanocomposites with desired functionality, because the functional moiety on GO can impart the special functionality to the polymer nanocomposites. Therefore, various approaches to prepare graphene-derivatives modified with various kinds of chemical moieties including polymers for the improved compatibility with the polymers were introduced in this study. The physical properties of polymers were much improved by using such graphene derivatives as the fillers of polymer nanocomposites.

Firstly, polyketone (PK) nanocomposites were prepared by a solution casting method using 1,1,1,3,3,3-hexafluoro-2-propanol as a solvent and polyamide 6 grafted graphene oxides (PA 6-GOs) as filler materials. PA 6-GOs were obtained

by in-situ polymerization of ε-caprolactam using GOs having different amounts of oxygen functional groups. The PK nanocomposites containing only an extremely small amount of the PA 6-GOs (~ 0.01 wt%) showed much improved mechanical properties compared to PK. This could be ascribed to the homogeneous dispersion of the graphene-based filler materials in the polymer and specific interactions such as dipole-dipole interactions and/or the hydrogen bonds between the fillers and polymer matrix. For example, when 0.01 wt% of PA 6-GO having less oxygen functional groups was used as a filler for the composite, the tensile strength, Young's modulus, and elongation at break of the composite increased by 35, 26, and 76 %, respectively. When 0.01 wt% of PA 6-GO having larger content of oxygen functional groups and PA 6 was used, Young's modulus decreased, while the tensile strength increased by 37 %, and the elongation at break increased tremendously by 100 times, indicating that very tough polymeric materials could be prepared using a very small amount of the graphene-based fillers.

Secondly, PK nanocomposites were prepared by a polymer powder coating method using carbon nanomaterials, such as carbon nanotube (CNT), graphene oxide (GO), and antioxidant grafted GOs as filler materials. The antioxidant grafted GOs were obtained by grafting hindered amine and hindered phenol, respectively, onto the surface of the GOs. The PK nanocomposites containing the carbon nanomaterials showed much improved thermal stabilities and mechanical

properties compared to PK. In particular, we found that the antioxidant grafted GOs are more effective in increasing the thermal properties of PK than CNT and GO without any antioxidant moieties. The enhanced thermal stability and mechanical property by the antioxidant grafted GOs can be explained by the combined antioxidant ability of the antioxidant functional groups and the rigid conjugated carbon units in the GOs having the ultrathin sheet shapes.

Finally, poly(vinyl alcohol) (PVA) nanocomposites were prepared by a solution casting method using a reduced graphene oxide coated with tannic acid (rGO-TA) as a filler. The rGO-TA was simply prepared by mixing tannic acid (TA) with graphene oxide (GO). The simple mixing process was found to be effective to reduce GO and to produce covalently-grafted TA layers on the reduced GO. The mechanical properties of PVA were much improved by the addition of rGO-TA because the TA layers increased the compatibility of the reduced GO with PVA matrix. For example, Young's modulus and elongation at break values of PVA were increased by 34.0 and 56.9%, respectively, by adding 1.0 wt% of rGO-TA. In addition, the PVA nanocomposites showed excellent humidity sensing properties over the wide relative humidity range and the long-term stability due to the conductive property of the reduced GO and the enhanced mechanical strength by the effective incorporation of rGO-TA into the PVA matrix.

Keyword: Graphene, polymer nanocomposite, polyketone, poly(vinyl alcohol), mechanical property, thermal stability, toughness.

Student Number: 2012-30956

TABLE OF CONTENT

Chapter 2

Improved strength and toughness of polyketone nanocomposites using extremely small amount of polyamide 6 grafted graphene oxides

Chapter 3

Effect of antioxidant grafted graphene oxides on the mechanical and thermal properties of polyketone nanocomposites

Chapter 4

Poly(vinyl alcohol) nanocomposites containing reduced graphene oxide coated with tannic acid for humidity sensor

List of Figures

List of Tables

Chapter 1

Introduction

1.1. Carbon nanomaterials

Carbon nanomaterials, such as carbon nanotubes (CNTs), graphene, and graphene oxide (GO), have a unique place in nanoscience and have drawn much attention for scientific interests and industrial applications due to their outstanding mechanical, chemical, thermal, and electrical properties (Fig. 1) [1-7] . Accordingly, they have a great potential to use in a wide range of possible applications such as sensors, energy storage and conversion, drug delivery, field emission devices, nanoelectronics, and composite materials [6, 7].

Since the discovery of CNTs [5, 8], which have cylindrical structures made of carbon with unique mechanical and electronic properties, physicists and material scientists were fascinated with this new form of carbon that changed the paradigm of the three basic forms of carbon, such as diamond, graphite and amorphous carbon, and a lot of research has been conducted to use beneficial characteristics of CNTs for the practical applications in the last two decades [7]. In particular, although the physical properties of CNTs are still being discovered and debated with interest, they have a very broad range of electronic, thermal, and structural properties that change depending on the different types of nanotubes such as the diameter, length, and chirality during their growth [9].

Recently, graphene, the newly discovered two-dimensional atomic carbon sheet, is among the most interesting carbon nanomaterials in terms of properties and possible applications due to its exceptional mechanical, thermal, electrical, and optical properties [1-3, 6, 10]. It has a strong mechanical strength (~ 1.0 TPa of Young's modulus), thermal conductivity (~5000 W m^{-1} K^{-1}), high intrinsic mobility (200,000 cm^2 v^{-1} s^{-1}), optical transparence (~ 97.7%), and large specific surface area (theoretically 2630 m^2 g^{-1} for single-layer graphene) [1, 6, 10], and these ascendant physicochemical properties can make graphene extraordinarily perspective as next generation materials for nanoscience.

GO, a single-layer of graphite oxide, is the specific branch of graphene research [2]. It is usually produced by the chemical oxidation of graphite, with subsequent dispersion and exfoliation in water or suitable organic solvents (Fig. 2) [4]. In particular, after oxidation, various kinds of oxygen functional groups, such as carboxylic acid, hydroxide, epoxide, and ketone groups, were introduced onto the graphene layer and the oxidized graphite can be easily exfoliated into individually dispersed single layer of graphite oxide, GO, by sonication due to the strong repulsion between negative-charged GO layers and the enlarging interlayer distance [1]. In addition, GO is known to be non-conductive materials with a conductivity of ~10^{-4} S m^{-1} because of the destruction of the conjugated graphitic region from the oxidation, while it can be reduced to restore conjugated structure

producing reduced graphene oxide (rGO) with a conductivity of ~10^2 S m^{-1} [3, 11]. Therefore, it can be considered as a precursor for graphene synthesis by either chemical or thermal reduction processes.

1.2. Graphene-based polymer nanocomposites

Polymer nanocomposites containing nanofillers have been widely studied for scientific interests and industrial purposes over the past few decades because they can have high performances at low filler contents and numerous applications [12-18]. Especially, the remarkable improvements in mechanical and thermal properties of the polymer nanocomposites are known to be closely related to the interface structure and good interfacial interaction between fillers and polymer matrix [19], because the nanocomposites have a large interfacial area to filler volume and a significant load transfer across the interface can result in the mechanical and functional performances of the polymer nanocomposites [20]. Recently, carbon nanomaterials, such as carbon nanotubes (CNTs), graphene, and graphene oxide (GO), have been used to improve the performance of polymer nanocomposites as filler materials because they can show an extraordinary reinforcing efficiency as the fillers for the polymer nanocomposites [13, 15, 21-24]. In particular, graphene-based polymer nanocomposites have been widely studied over the past few years because they can have much improved performance by adding only a very small amount of graphene-based materials as the fillers. Graphene, as a single layered two-dimensional atomic carbon sheet, is the most often used filler material due to its extraordinarily reinforcing efficiency

in electronic, thermal, and mechanical properties [13, 15]. In addition, GO has been suggested as a very promising candidate for the filler materials because GO can be easily prepared in a large scale by the chemical exfoliation of natural graphite and GO can be also easily modified to increase the miscibility with the polymers using various approaches because of various kinds of oxygen functional groups, such as carboxylic acid, hydroxide, epoxide, and ketone groups, in GO [1, 3].

Recently, graphene-based nanomaterials, such as graphene and GO, have been also explored as a new class of antioxidants due to their physical barrier property with two-dimensional structure, ultrahigh surface area, and inherent radical scavenging ability [25]. In detail, when the graphene-based nanomaterials are used as fillers for polymer nanocomposites, their ultrahigh surface area provides good site availability and large capacity for free radical scavenging in the polymer matrix, resulting in the remarkable improvement in thermal stability of the polymer nanocomposites. Therefore, the graphene-based nanomaterials have attracted great attention as the filler materials in the fields of the high-performance polymer nanocomposites for scientific interests and industrial purposes.

1.3. Motivation

Graphene-based polymer nanocomposites have drawn much attention for scientific interests and industrial purposes over the past few years because they can have much improved performance. Since the remarkable improvements in mechanical and thermal properties of the polymer nanocomposites are closely related to the interface structure and good interfacial interaction between the fillers and the polymer matrix as aforementioned, designing and tuning of interface between the reinforced fillers and the polymer should be considered to achieve high performances of the polymer nanocomposites at low filler contents. In particular, although graphene is the most often used filler materials, the application of graphene as the filler for the polymer nanocomposites has been limited due to the poor compatibility with polymers forming non-uniform domains in the polymer matrix, then the effective increase of the mechanical properties of the polymer could not be achieved. Therefore, the development of the preparation method for graphene-based materials having excellent dispersibility in the polymer matrix and good interfacial adhesion with the polymer is a significant issue in the field of the graphene-based polymer nanocomposites to achieve the optimum performance of the polymer nanocomposites.

In this study, we attempted to develop various approaches to prepare graphene-derivatives modified with various kinds of chemical moieties including polymers for the improved compatibility with the polymers. As a result, the physical properties of the polymers were much improved by using such graphene derivatives as the fillers of the polymer nanocomposites. For example, when only 0.01 wt% of GO derivatives containing polyamide 6 chains were mixed with aliphatic polyketone (PK), the tensile strength increased by 40 %, and the elongation at break increased tremendously by 100 times.

1.4. References

[1] Zhu YW, Murali S, Cai WW, Li XS, Suk JW, Potts JR, et al. Graphene and graphene oxide: Synthesis, properties, and applications. Adv Mater. 2010;22(35):3906-24.

[2] Chen D, Feng H, Li J. Graphene oxide: preparation, functionalization, and electrochemical applications. Chem Rev. 2012;112(11):6027-53.

[3] Dreyer DR, Park S, Bielawski CW, Ruoff RS. The chemistry of graphene oxide. Chem Soc Rev. 2010;39(1):228-40.

[4] Chua CK, Pumera M. Chemical reduction of graphene oxide: a synthetic chemistry viewpoint. Chem Soc Rev. 2014;43(1):291-312.

[5] Iijima S. Helical microtubules of graphitic carbon. Nature. 1991;354(6348):56-8.

[6] Novoselov KS, Fal'ko VI, Colombo L, Gellert PR, Schwab MG, Kim K. A roadmap for graphene. Nature. 2012;490(7419):192-200.

[7] De Volder MF, Tawfick SH, Baughman RH, Hart AJ. Carbon nanotubes: present and future commercial applications. Science. 2013;339(6119):535-9.

[8] Park SJ, Cho MS, Lim ST, Choi HJ, Jhon MS. Synthesis and dispersion characteristics of multi-walled carbon nanotube composites with poly(methyl methacrylate) prepared by in-situ bulk polymerization. Macromol Rapid Comm.

2003;24(18):1070-3.

[9] Schrettl S, Frauenrath H. Elements for a rational polymer approach towards carbon nanostructures. Angew Chem Int Edit. 2012;51(27):6569-71.

[10] Xu Z, Gao C. In situ polymerization approach to graphene-reinforced nylon-6 composites. Macromolecules. 2010;43(16):6716-23.

[11] Gao W, Alemany LB, Ci LJ, Ajayan PM. New insights into the structure and reduction of graphite oxide. Nature Chem. 2009;1(5):403-8.

[12] Stankovich S, Dikin DA, Dommett GH, Kohlhaas KM, Zimney EJ, Stach EA, et al. Graphene-based composite materials. Nature. 2006;442(7100):282-6.

[13] Kim H, Abdala AA, Macosko CW. Graphene/polymer nanocomposites. Macromolecules. 2010;43(16):6515-30.

[14] Kuilla T, Bhadra S, Yao D, Kim NH, Bose S, Lee JH. Recent advances in graphene based polymer composites. Prog Polym Sci. 2010;35(11):1350-75.

[15] Potts JR, Dreyer DR, Bielawski CW, Ruoff RS. Graphene-based polymer nanocomposites. Polymer. 2011;52(1):5-25.

[16] Salavagione HJ, Martinez G, Ellis G. Recent advances in the covalent modification of graphene with polymers. Macromol Rapid Comm. 2011;32(22):1771-89.

[17] Verdejo R, Bernal MM, Romasanta LJ, Lopez-Manchado MA. Graphene filled polymer nanocomposites. J Mater Chem. 2011;21(10):3301.

[18] Sun Y, Shi G. Graphene/polymer composites for energy applications. J Polym Sci Part B: Polym Phys. 2013;51(4):231-53.

[19] Paul DR, Robeson LM. Polymer nanotechnology: Nanocomposites. Polymer. 2008;49(15):3187-204.

[20] Ma J, Meng QS, Michelmore A, Kawashima N, Izzuddin Z, Bengtsson C, et al. Covalently bonded interfaces for polymer/graphene composites. J Mater Chem A. 2013;1(13):4255-64.

[21] Watts PCP, Fearon PK, Hsu WK, Billingham NC, Kroto HW, Walton DRM. Carbon nanotubes as polymer antioxidants. J Mater Chem. 2003;13(3):491-5.

[22] Moniruzzaman M, Winey KI. Polymer nanocomposites containing carbon nanotubes. Macromolecules. 2006;39(16):5194-205.

[23] Spitalsky Z, Tasis D, Papagelis K, Galiotis C. Carbon nanotube–polymer composites: Chemistry, processing, mechanical and electrical properties. Prog Polym Sci. 2010;35(3):357-401.

[24] Verdejo R, Bernal MM, Romasanta LJ, Lopez-Manchado MA. Graphene filled polymer nanocomposites. J Mater Chem. 2011;21(10):3301-10.

[25] Qiu Y, Wang ZY, Owens ACE, Kulaots I, Chen YT, Kane AB, et al. Antioxidant chemistry of graphene-based materials and its role in oxidation protection technology. Nanoscale. 2014;6(20):11744-55.

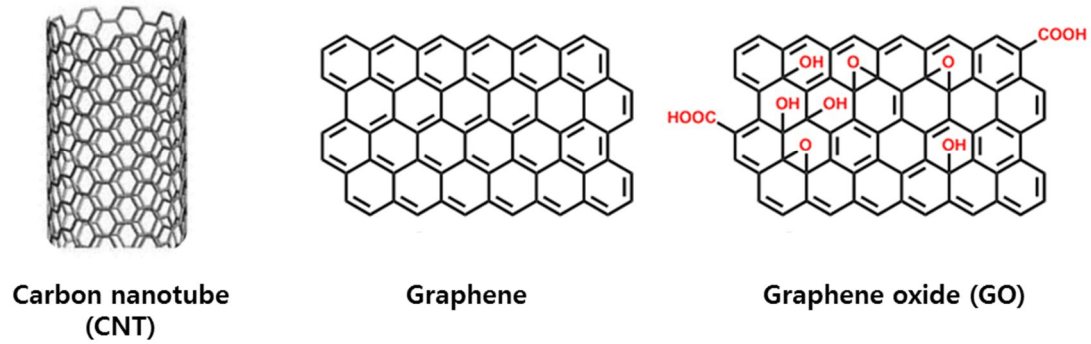

Fig. 1.1 Chemical structure of carbon nanotube (CNT), graphene, and graphene oxide (GO)

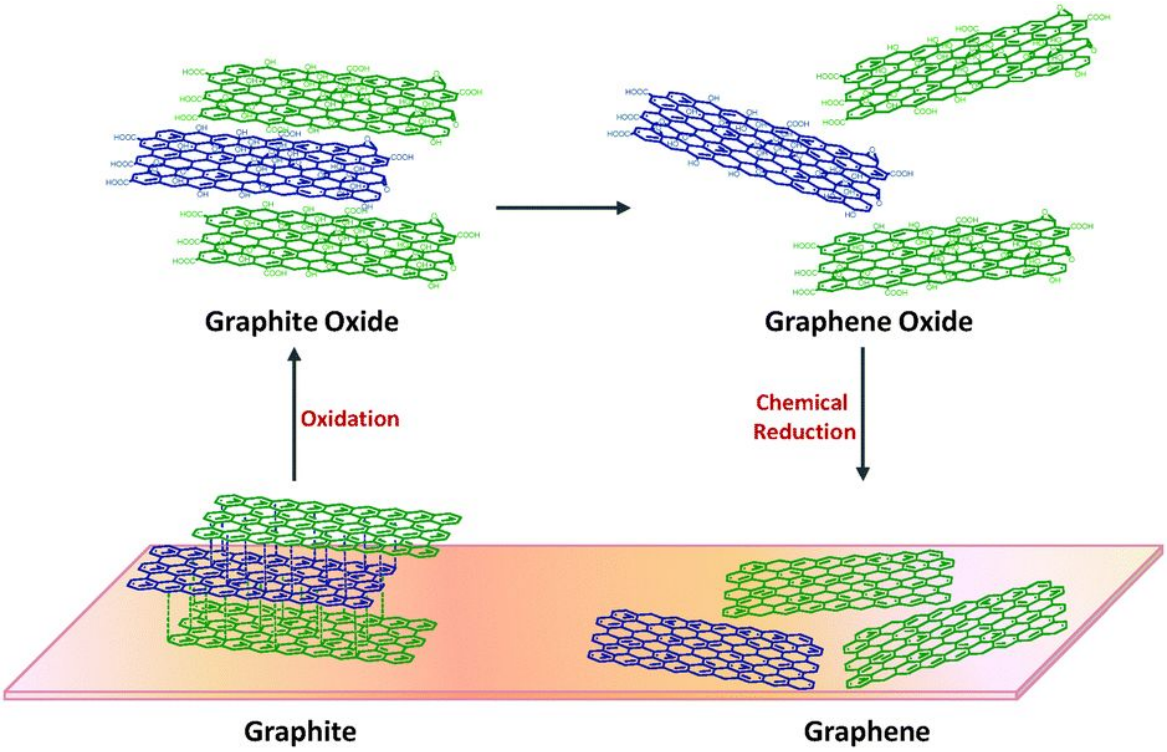

Fig. 1.2 Schematic illustration of preparation of GO [4]

Chapter 2

Improved strength and toughness of polyketone nanocomposites using extremely small amount of polyamide 6 grafted graphene oxides

2.1. Introduction

Polymer nanocomposites containing nano-sized filler materials have been widely studied for scientific and industrial purposes over the past few decades because they can have much improved performance [1-5]. The remarkably improved mechanical and thermal properties of the polymer nanocomposites have been known to be closely related to the interface structures and good interfacial interactions between nano-sized fillers and a polymer matrix [6-8]. Since the interfacial areas between the fillers and the polymer matrix are very large, a significant load transfer across the interface is possible, if there are large interactive forces between the fillers and the polymers [5]. Normally, the interaction between the polymer matrix and the fillers in the polymer nanocomposites could be increased by modification of the surfaces of the fillers.

Carbon nanomaterials have been widely applied to improve the performance of polymer nanocomposites, because the modified carbon nanomaterials can control the interactive forces between the fillers and the polymer matrix [9-13] . Recently, graphene, a single layered two-dimensional atomic carbon sheet, has been widely applied as a filler due to its extraordinary reinforcing efficiency of the electronic, thermal, and mechanical properties [11,12]. Particularly, much improved

composite performance was observed by adding only a very small amount of graphene-based materials (about 0.1 – 1.0 wt%) to the polymers, because graphene has extremely large surface area and specific interactions between the graphene and the polymer can be expected [14-17]. Therefore, graphene-based polymer nanocomposites have been considered as very promising materials for engineering plastic applications [2,11,12,18]. For the polymer nanocomposites to have advanced properties, homogeneous dispersion of fillers in the polymer matrix and compatibility between fillers and polymers are strongly needed. When graphene is modified properly, the compatibility with the polymer matrix could be improved, producing polymer nanocomposites materials having uniformly-dispersed graphenes [18,19]. In addition, it was possible to control the interface parameters, such as grafting density, grafting chain length, and functional groups on the graphene surface.

Aliphatic polyketones (PK) are alternating olefin/carbon monoxide (CO) copolymers prepared using ethylene and/or propylene with CO as a co-monomer [20,21]. PK could be considered as high-performance thermoplastic polymers because they have good chemical resistance, mechanical properties, and low gas permeability [22]. Accordingly, there has been of great interest in a wide range of possible applications of the PK polymers, while they have not been introduced to the market. We strongly believe that further works on the synthesis, rheology, and

processing of PK are necessary to use them in practical applications [23-30]. In particular, the introduction of graphene-based materials as fillers in a PK matrix could produce composite materials with integrated properties for possible applications.

In this work, we tried to prepare PK nanocomposites using graphene-based nanofillers. Graphene oxide (GO) having various oxygen functional groups, such as carboxylic acid, hydroxyl, epoxide, and ketone groups were used because they can interact with the ketone groups in PK. However, we could not make any PK nanocomposite materials with improved mechanical and physical properties using graphene or GO, because they are not miscible with PK; only phase-separated domains were observed from the PK nanocomposite films that contained the graphene or GO. To impart miscibility to GO with PK, polyamide 6 (PA 6) was attached to GO, because PA 6 is known to be miscible with PK [31-33]. It was not possible to attach PK on GO, because PK is prepared by coordination polymerization using a catalyst composed of metallic complexes [20,21]. Surprisingly, we found that the addition of only a very small amount of GO with PA 6, such as 0.01 wt%, to PK improved the mechanical properties of PK significantly.

2.2. Experimental

Materials

Polyketone (PK) was kindly supplied by Hyosung (Korea) and used as received. The glass transition and melting temperatures are 10 ºC and 220 ºC, respectively. Melt index is 60 g/10 min. The PK used in this study is an alternating copolymer prepared by ethylene, propylene and carbon monoxide as monomers; the molar contents of 1-oxo-trimethylene and 1-oxo-2-methyltrimethylene are 94 mol% and 6 mol%, respectively (Fig. 1a). Graphite powders were received from BASF (Germany). Phosphorus(V) oxide (P_2O_5), sodium nitrate ($NaNO_3$), potassium permanganate ($KMnO_4$), hydrogen peroxide (H_2O_2), ε-caprolactam (CL), 6-aminocaproic acid, and 1,1,1,3,3,3-hexafluoro-2-propanol (HFIP), all from aldrich, were used as received. All other reagents and solvents were used as received from standard vendors.

Preparation of GO

GO was synthesized from graphite powders through the modified Hummers method [34]. 1.0 g of graphite powders and 0.5 g of P_2O_5 were added to 6.0 mL of

98% H_2SO_4. The mixture was kept at 85 ºC for 5 h. Deionized water (200 mL) was added to the mixture and left overnight. Then the mixture was filtered through anode aluminum oxide (AAO) membrane filter with 0.2 μm pore size and washed with deionized water continuously. The solid was dried in vacuum at 35 ºC overnight. 1.0 g of the dried product (pre-oxidized graphite) and 0.5 g of $NaNO_3$ were added to 23 mL of 98% H_2SO_4 in an ice bath and kept at this temperature for 40 min without stirring. Then 3.0 g of $KMnO_4$ was slowly added with stirring to keep the temperature below 10 ºC. The mixture was heated to 35 ºC and stirred for 2 h and then 140 mL of deionized water and 10 mL of 30 % H_2O_2 were added. Then the mixture was centrifuged (10000 rpm for 30 min) and the supernatant decanted. The solid was washed with water and centrifugation with 250 mL of 10 % HCl at least 3 times until the pH was 7. After vacuum filtration the solid was dried overnight at 35 ºC. The resulting solid was called GO 1 (less oxidized GO). GO 2 (more oxidized GO) was obtained using the same procedure except the amount of $KMnO_4$ (6.0 g) and the reaction time (18 h).

Preparation of PA 6 grafted GO

PA 6 grafted GO (PA 6-GO) was obtained using GO 1 as follows: 4.5 g of ε-caprolactam (CL) and 50 mg of GO 1 were added into 10 mL of anhydrous DMF

and the mixture was sonicated for 1 h. Then 0.5 g of 6-aminocaproic acid was added into the solution and the solution was purged under N_2 for 1 h. The solution was heated at 180 ºC for 1 h and heated at 250 ºC for 5 h with stirring. After the mixture was cooled to room temperature, the black product was washed with warm water and then dried in vacuum at 35 ºC overnight. Then the product was purified by centrifugation with formic acid and washing by 1,1,1,3,3,3-hexafluoro-2-propanol (HFIP) to obtain purified PA 6 grafted GO (PA 6-GO1) without separated PA 6 not grafted on the GO. PA 6-GO2-1 was obtained using the same procedure except that different GO (GO 2) was used as a starting material. PA 6-GO2-2 was obtained using GO 2 by changing the reaction time from 5 h to 10 h. Fig. 1b shows the structures of different PA 6-GOs.

Preparation of PK nanocomposites

0.1 mg of PA 6-GO1 was added to 1.0 g of HFIP and then sonicated for 30 min to make a homogeneous dispersion of the filler in the solvent. 1.0 g of PK powders was dissolved in 10 g of HFIP. The dispersed HFIP solution of PA 6-GO1 was added to the PK solution and sonicated for 30 min. The mixture solution was poured on a glass plate and dried at room temperature overnight, then the dried film was peeled off from the substrate and heated at 50 ºC for 3 days under

vacuum to make sure to remove any possible remaining solvent in the composite film [35, 36]. The obtained PK nanocomposite with 0.01 wt% of PA 6-GO1 was noted as PA 6-GO1 0.01/PK. Neat PK and other nanocomposites samples were also prepared by the same procedure. The name of other PK nanocomposites and their feed ratios are listed in Table 1.

Characterization

X-ray photoelectron spectroscopy (XPS) was recorded on a KRATOS AXIS-His using MgKα (1254.0 eV) as the radiation source. Spectra were collected over a range of 0-1200 eV, followed by high resolution scan of the C 1s and N 1s regions. Thermal gravimetric analysis (TGA) was performed in a Q-5000 IR from TA Instruments, using a heating rate of 10 ^{o}C/min under a nitrogen atmosphere. The thermal transition temperatures of the polymers were examined by differential scanning calorimetry (DSC) using TA Instruments DSC-Q1000 under a nitrogen atmosphere. Samples with a typical mass of 3.0-7.0 mg were encapsulated in sealed aluminum pans. The samples were first heated to 240 ^{o}C and then quenched to -50 ^{o}C. This was followed by a second heating scan from -50 ^{o}C to 240 ^{o}C at a heating rate of 10 ^{o}C/min. The viscosity was measured by Ubbelohde viscometer to get the inherent viscosity (η_{inh}) of free PA 6 [37]. The viscosity

measurements were took in formic acid solution of PA 6 with a concentration of 3.0 g/L, in an Ubbelohde viscometer at 25 ^{o}C. For the simplification, a single point measurement was carried out. It can be assumed that the inherent viscosity (η_{inh}) equals the intrinsic viscosity in a single point measurement [38]. The viscosity average molecular weight (M_{η}) was calculated from Mark-Houwink equation using η_{inh} [39]. Fractured surface morphologies of the composite films were inspected by scanning electron microscopy (SEM) using a field emission scanning electron microscope (FESEM, JEOL JSM-6701F). Fourier-transform infrared (FT-IR) spectra of films were recorded on a Cary 660 FT-IR spectrometer (Agilent Technology) at ambient temperature. Data were collected over 30 scans at 4 cm^{-1} resolution. The mechanical properties were measured using a universal testing machine (LS1SC, LLOYD Instruments). The dumbbell specimens were prepared using the ASTM standard D638 (Type V specimens dog-bone shaped samples). Type V specimens were prepared using die cutting to the dimensions: W = 3.18 ± 0.03 mm, L = 9.53 ± 0.08 mm, G = 7.62 ± 0.02 mm, and R = 12.7 ± 0.08 mm. The tensile properties of the membrane samples were measured in air at 23 ^{o}C under a 45% relative humidity (RH) with a gauge length and cross head speed of 15 mm and 10 mm/min, respectively. The storage modulus (G') values of the composites are measured using a dynamic mechanical analyzer (DMA) (model DMA/SDTA861e, Mettler Toledo). The film samples are heated from 0 ^{o}C to 60

^{o}C at the heating rate of 5 ^{o}C/min. The G' values are measured at a constant frequency of 1 Hz with a static force of 1 N.

2.3. Results and Discussion

Preparation of PA 6-GOs

GOs with different degrees of oxidation, named as GO 1 and GO 2, were synthesized by a modified Hummers method using 3 weight and 6 weight equivalent amounts of $KMnO_4$, respectively (Fig. 1b). The XPS spectra in Fig. 2 of GO 1 and GO 2 show four peaks: C-C (284.5 eV), C-O (286.5 eV), C=O (287.5 eV), and O-C=O (288.5 eV), as previously reported [15,40,41]. GO 1 was found to have 38.9 % and 61.1 % of oxidized carbon and graphitic carbon, respectively, while GO 2 has 48.6 % and 51.4 % [41]. Therefore, the XPS results clearly indicate that GO 2 is more oxidized and contains a larger amount of oxygen functional groups than GO 1.

PA 6 chains were attached to GO by the in-situ polymerization of ε-caprolactam using 6-aminocaproic acid as an initiator. The ring-opening polymerization of ε-caprolactam on GO is possible, because the amine group in 6-aminocaproic acid can be reacted with the oxygen functional groups such as carboxylic acid and epoxy groups on GO, and then the ring opening initiation of oxygen functional groups with ε-caprolactam is possible [39,42-44]. However, the homopolymers of ε-caprolactam (free PA 6) could also be formed because unreacted 6-aminocaproic

acid or other possible impurities such as water can be reacted with ε-caprolactam to initiate the ring-opening polymerization. Since the solubilities of GO containing PA 6 and the homopolymer (PA 6) are very different, the homopolymer could be separated by centrifuge process and washing by HFIP which can dissolve the PA 6 homopolymer while not the PA 6-GOs. These separated homopolymer is called "separated PA 6" in this paper. Others also prepared PA 6 grafted GO and separated PA 6 homopolymer, using similar processes [39,42]. The existence of grafted PA 6 chains on GO sheets could be confirmed by the XPS spectrum of PA 6-GO1 (Fig. 2c); N1s peak at 400.9 eV clearly indicates the existence of nitrogen element in PA 6-GO1.

The molecular weight of the PA 6 on GO could be estimated by measuring the molecular weight of the separated PA 6 extracted from the reaction mixture of GO and ε-caprolactam. Since the ring-opening polymerizations on GO and outside of GO start at the same time, it is very probable that the molecular weights of PA 6 on GO and the separated PA 6 are close [45]. Although their molecular weights might be different, the molecular weight of the separated PA 6 from the reaction mixture for PA 6-GO having grafted PA 6 with a larger molecular weight should be larger than that of the separated PA 6 from another mixture of PA 6-GO having grafted PA 6 with smaller molecular weight. If we could detach the grafted PA 6 on GO and measure the molecular weight of the detached PA 6, then direct

comparison of the effect of the grafting chain length is possible. However the grafted PA 6 on GO is connected to GO by amide and/or ester groups and the polymer backbone of PA 6 is composed of the amide groups, so it is not possible to detach them effectively. Therefore, the molecular weight of the grafted PA 6 was estimated by measuring the molecular weight of the separated PA 6.

Since the Mark-Houwink constants are available for PA 6, M_η of the separated PA 6 was obtained by measuring η_{inh} as listed in Table 2. The molecular weights of the separated PA 6 from 6-GO1 and PA 6-GO2-1 are quite close, because they were prepared from the same reaction conditions (250 ^oC for 5 h), while the molecular weight of the separated PA 6 from PA 6-GO2-2 prepared from longer reaction time (250 ^oC for 10 h) is slightly larger than those of other PA 6-GOs. Furthermore, the melting temperature behavior of the separated PA 6 (Table 2) agrees with the molecular weight behavior. From the DSC and viscosity results, and by assuming that the molecular weight behavior of grafted PA 6 follows that of separated PA 6, it could be expected that the grafting chain length of PA 6-GO1 and PA 6-GO2-1 are close, and that of PA 6-GO2-2 is slightly larger than the others.

The grafting density and residual functional groups of the PA 6-GOs could be estimated by TGA curves shown in Fig. 3. It is well- known that the weight decreases at temperature below 300 ºC due to oxygen functional groups such as

carboxylic acid, hydroxyl, epoxide, and ketone in GO, and those between 300-500 ºC are due to the PA 6 [39,42,46]. According to the TGA results, the content of oxygen functional groups increases in the order of PA 6-GO1, PA 6-GO2-2, and PA 6-GO2-1; their weight loss below 300 ºC for these samples are 1, 5, and 20 wt%, respectively. PA 6-GO1 prepared from GO 1 shows the smallest oxygen functional group content, because GO 1 was synthesized in milder oxidation reaction conditions than GO 2. Although PA 6-GO2-1 and PA 6-GO2-2 were prepared from the same GO (GO 2), PA 6-GO2-2 contains less oxygen functional groups because the oxygen functional groups are further reduced due to the longer reaction time at 250 ºC; the polymerization times for PA 6-GO2-1 and PA 6-GO2-2 are 5 h and 10 h, respectively. It is known that the reaction temperature of 250 ºC is enough to reduce some of the oxygen functional groups in GO, and obviously, longer reaction time could reduce more oxygen functional groups in GO [47,48].

The PA 6 contents estimated by the TGA curves increase from PA 6-GO1 to PA 6-GO2-1 and PA 6-GO2-2; they are 37, 48, and 58 wt% for PA 6-GO1, PA 6-GO2-1, and PA 6-GO2-2, respectively. Since the more oxidized GO 2 has more reactive sites than the less oxidized GO 1, PA 6-GO2-1 and PA 6-GO2-2 prepared from more oxidized GO 2 have larger PA 6 content than PA 6-GO 1 prepared from less oxidized GO 1 having less oxygen functional groups. PA 6-GO2-2 has larger

PA 6 content than PA 6-GO2-1, because although they were prepared using the same GO 2, PA 6-GO2-2 was prepared from longer polymerization time, so it could have increased grafting density. From the TGA results and assumption that the grafting chain lengths of PA 6-GO1 and PA 6-GO2-1 are quite close and that of PA 6-GO2-2 is slightly larger than the others, it can be assumed that the grafting density of PA 6 increases from PA 6-GO 1 to PA 6-GO2-1 and PA 6-GO2-2.

The chemical structures of PA 6-GOs in Fig. 1b show the content of the oxygen functional groups and the grafted PA 6. To increase understanding of the effect of their content on the properties of the PK nanocomposites, these structures are somewhat exaggerated. The interface parameters of PA 6-GOs such as the grafting chain length, grafting density, and residual oxygen functional groups on the GO surface could be controlled by varying the degrees of oxidation of GO and polymerization time. The control of interface parameters can provide a chance to control the contact area between the fillers and the polymer and achieve good interfacial adhesion [14].

Polyketone nanocomposites with PA 6-GO

Mechanical properties

PK nanocomposite films were prepared for the measurement of mechanical properties using a solution casting method. HFIP was used for the preparation of the polymer solutions with PA 6-GOs, because HFIP is a good solvent for PK and it can disperse PA 6-GOs very well. As mentioned in the introduction, GO cannot be used as a filler to improve the mechanical properties of the PK, because GO is not miscible with PK and forms aggregated GO clusters in HFIP (Fig. 4a). When we tried to use other solvents such as *N,N*-dimethylacetamide (DMAc), *N,N*-dimethylformamide (DMF), and *N*-methyl-2-pyrolidinone (NMP) to disperse GO, the PK was not soluble. However, when PA 6-GOs were mixed with PK in HFIP, PA 6-GOs were well-dispersed in HFIP (Fig. 4b), and the PK nanocomposites containing PA 6-GOs (PA 6-GO/PK composites) were found to have much improved mechanical properties, as shown in Fig. 5 and listed in Table 1. Although formic acid and *m*-cresol were found to dissolve both PK and PA 6-GOs, we did not use them because of the toxic and corrosive property of the formic acid and the high boiling point (~200 ^{o}C) of *m*-cresol, then the removal of the solvent after the casting process is not easy.

The tensile strength values of PK nanocomposites were much increased from 68.6 MPa (tensile strength of PK) to 86.0, 94.1, and 92.9 MPa by adding 0.01 wt% of PA 6-GO1, PA 6-GO2-1, and PA 6-GO2-2, respectively. When the content of PA 6-GO1, PA 6-GO2-1, and PA 6-GO2-2 was increased further from 0.01 to 0.10

wt%, the reinforcing efficiency of PA 6-GOs decreased for all the samples, although the decrease was less for the PA 6-GO2-1/PK nanocomposite (Fig. 5a). Therefore, the maximum tensile strength was obtained when the content of PA 6-GOs was only 0.01 wt%, possibly due to the good dispersion of the PA 6-GOs and the formation of specific interactions between the fillers and the PK matrix, while when the content of fillers was larger than the critical point of 0.01 wt%, the efficiency of the reinforcement decreased, possibly due to the aggregation of the PA 6-GOs in the polymer matrix [49]. Although the aggregation of the PA 6-GOs in the range of 0.02 to 0.10 wt% could not be observed by the naked eye in the mixtures of PA 6-GO1 and PK in HFIP and the PK nanocomposites films, as shown in Fig. 4c and d, when the contents of PA 6-GOs were larger than 0.10 wt%, the phase-separated domains could even be observed by the naked eye in the PK nanocomposites film (Fig. 4e).

The Young's modulus of PA 6-GO1/PK and PA 6-GO2-2/PK (the nanocomposites containing PA 6-GO1 and PA 6-GO2-2) also showed the maximum value when the filler content was 0.01 wt%, while that of PA 6-GO2-1/PK (the nanocomposites containing PA 6-GO2-1) decreased from 4090 to 2820 MPa with the increase of the content of PA 6-GO2-1 from 0 to 0.10 wt% (Fig. 5b).

The elongation at break behavior of PA 6-GO1/PK and PA 6-GO2-2/PK is similar to that of PK. In contrast, the elongation at break values of PA 6-GO2-

1/PK are much larger than that of PK and other nanocomposites (Fig. 5c). These results can be explained by the stress-strain curves for PK nanocomposites. Stress-strain curves of PK, PA 6-GO1 0.01/PK, and PA 6-GO2-2 0.01/PK show brittle fracture behavior without significant deformation, while that of PA 6-GO2-1 0.01/PK shows ductile fracture behavior with a large amount of plastic deformation (Fig. 6). In particular, the nanocomposite film containing 0.01 wt% of PA 6-GO2-1 was elongated up to 363 % of its initial length, much more than those of PK and other nanocomposites. Although the elongation at a break values decreased from 363 to 221 % as the content of PA 6-GO2-1 increased from 0.01 to 0.10 wt%, we found that the addition of PA 6-GO2-1 to PK could improve the toughness of PK significantly. This dramatic increase of the toughness can be explained by the excellent dispersion and good interfacial adhesion of PA 6-GO2-1 because PA6-GO2-1 has a higher PA 6 grafting density and more residual oxygen functional groups than other PA 6-GO, then strong interfacial specific interactions between ketone groups in PK with amide and oxygen functional groups in PA 6-GOs are possible. This could be proved by the IR results shown in a later part of this manuscript. Comparing the PA 6-GO1 0.01/PK and PA 6-GO2-2 0.01/PK composites, PA 6-GO2-2/PK having larger content of PA 6 on GO shows larger tensile strength and Young's modulus values. DMA results also

showed that PA 6-GO2-1 is much more effective in increasing the storage modulus (G') than PA 6-GO1 (Fig. 7).

Thermal properties

The thermal stability of the PK nanocomposites was analyzed by TGA. The thermal decomposition temperatures for 5 wt% loss ($T_{d,5\%}$) from the TGA measurements are listed in Table 2, and TGA curves of the PK nanocomposites are shown in Fig. 8. The decomposition temperatures of the PK nanocomposites are always larger than that of PK (288 ^{o}C). These results indicate that the incorporation of PA 6-GOs into the PK increase the thermal stabilities of the PK nanocomposites. Previously, it was reported that graphene-based fillers can increase the thermal stability of polymer nanocomposites, because radicals generated by thermal decomposition of the polymer matrix can be captured by the graphene [50].

The enhanced thermal stability of PA 6-GO1/PK was further studied by measuring the isothermal TGA curves shown in Fig. 9. The samples were heated from 50 to 250 ºC at a heating rate of 10 ^{o}C/min and maintained at 250 ºC for 2 h under nitrogen. As the content of PA 6-GO1 increased from 0 to 0.05 wt%, the

residual weight % after isothermal treatment increased from 85.0 to 96.9 %. And as the content of PA 6-GO1 increased further from 0.05 to 0.10 wt%, the residual weight % decreased slightly possibly due to the aggregation of PA 6-GO1. These results indicate that thermal stability of the PK nanocomposites was increased by the addition of small amount of PA 6-GO1 to the PK and it can be explained by the radical capture of the graphene in PA 6-GO.

Morphology of nanocomposite films

SEM images of fractured surfaces of PK and PK nanocomposite film shown in Fig. 10 could be correlated with the mechanical properties of the samples. The fractured surfaces of PK, PA 6-GO1/PK, and PA 6-GO2-2/PK show typical brittle fracture morphology, while that for PA 6-GO2-1/PK film shows ductile fracture morphology with plastic deformation, showing the roughest surface morphology. The plastic deformation behavior should arise from the larger interfacial interactions between the fillers and the polymer matrix [14]. Since PA 6-GO2-1 contains more oxygen functional groups and larger content of grafted PA 6 than the other PA 6-GOs, larger interfacial interactions between PA 6-GO2-1 and the PK matrix could be expected. The very rough fractured surface of PA 6-GO2-1/PK nanocomposites should be strongly related to the very large values of

elongation at break (> 200 %).

The mechanism of toughening

GO alone could not improve the mechanical properties of PK, because phase-separated domains of GOs are formed in the mixture of PK with GOs. However, when PA 6-GOs containing PA 6 chain was mixed with PK, much improved mechanical properties were observed, which was possibly due to the specific interactions between ketone groups in PK with amide and oxygen functional groups in PA 6-GOs. Similarly, remarkable improvements in the mechanical properties of the polymer nanocomposites having GO-based fillers were reported by others recently [51-53]. The improvements of the tensile strength and toughness of the GO nanocomposites were explained by a bio-inspired toughening mechanism, in that when a load is applied to the composites, the rupturing of sacrificial bonds (such as hydrogen bonds, ionic bonds, Van der Waals interaction, and hydrophobic interaction) and the stretching of hidden lengths occur at the interface of composites, and as a result, a balance of strength and toughness is obtained. The bio-inspired toughening mechanism could be applied to the PA 6-GO/PK nanocomposites. PA 6 grafting chains of PA 6-GOs have a strong interaction with PK chains via hydrogen bonding between ketone (C=O) groups

of PK and amide (CONH) groups of PA 6. In addition, there is further interfacial interaction for the PA 6-GO2-1/PK nanocomposites: PK chains can be physically adsorbed on the surface of PA 6-GO2-1 sheets by forming dipole-dipole interaction and/or hydrogen bonds at multiple points with oxygen functional groups on the surface of PA 6-GO2-1. When a load is applied to the PA 6-GO2-1/PK nanocomposites having various kinds of interactions at the interface between PA 6-GO2-1 and the PK, the dissociation of bonds (sacrificial bond rupture) can occur at the interface, and then the hidden length can be released. As a result, the nanocomposite films of PA 6-GO2-1/PK show much tougher ductile fracture behavior than PA 6-GO1/PK and PA 6-GO2-2/PK films. The incorporation of filler materials into polymer generally increase the tensile strength, while it can decrease the elongation property of the polymer nanocomposites [11,54,55]. However, when graphene derivatives having organic functional groups which have a specific interaction with polymer matrix were used as fillers, they could have increased the tensile strength without the loss of the elongation property by the formation of polymer-bridged graphene network structures [56-59]. Similarly, individual PA 6-GOs containing more oxygen functional groups such as PA 6-GO 2-1 can be entangled more with PK chains due to the multi contact on the graphene sheets in addition to the hydrogen bonding between PA 6 and PK chains, resulting in a continuous polymer-bridged graphene

network structure throughout the PK matrix even at extremely low graphene loading [56-57]. Therefore, these much improved mechanical properties of PA 6-GO2-1/PK nanocomposites could be attributed to the formation of the polymer-bridged graphene networks structure and/or the sacrificial bond and hidden length from various kinds of interactions at the interface between PA 6-GO2-1 and the PK on the molecular-scale. This proposed toughening mechanism for PA 6-GO2-1/PK nanocomposites is shown in Fig. 11.

The existence of the additional hydrogen bonding in PA 6-GO2-1/PK nanocomposites compared to PA 6-GO1/PK and PA 6-GO2-2/PK nanocomposites could be explained to some degree by the FT-IR spectra: a small shift of absorption at 1698 cm^{-1} corresponding to the C=O of PK was observed in the PA 6-GO1/PK nanocomposite due to the hydrogen bonding between C=O of PK and CONH of PA 6 (Fig. 12a), while the shift in absorption of C=O of PA 6-GO2-1/PK nanocomposites is larger than that of PA 6-GO1/PK nanocomposites (Fig. 12b). This might explain the evidence of further interaction between C=O of PK and residual oxygen functional groups on the surface of PA 6-GO2-1. The increased hydrogen bondings in the polymer nanocomposites systems using such peak shifts were also explained by others [16].

It is very noteworthy that the mechanical properties of the PK nanocomposites are remarkably improved by the addition of just a very small amount of the

graphene-based fillers. Since the PA 6-GOs also contain the grafted PA 6 chain, the 0.01 wt% of PA 6-GOs in PK corresponds to 0.0063, 0.0052, and 0.0042 wt% of graphene in PA 6-GO1/PK, PA 6-GO2-1/PK, and PA 6-GO2-2/PK nanocomposites, respectively. Furthermore, it was reported that PK/PA 6 alloys exhibited high impact resistance, high strength, and high modulus when the content of PA 6 was larger than 30 wt% [32]. We believe that this is the smallest amount used as graphene-based filler materials in the polymer nanocomposites showing improved mechanical properties to the best of our knowledge. The minimum amounts of graphene-based filler used by others are in the range of 0.05 to 0.10 wt% [15,16]. Recently, Yu *et al.* reported polyacrylamide/GO nanocomposite hydrogel, which exhibited a high elongation at break when the content of GO was 0.0079 wt% [16]. Therefore, the amount of PA 6-GO that we used as a graphene-based filler is still smaller than those of others. We do not have a very clear explanation in the current stage for why such a small amount of PA 6-GO could improve the mechanical properties of PK tremendously. Interestingly when the contents of PA 6-GO are larger than 0.1 wt%, the mechanical properties of the PK nanocomposites further decrease, although those of other polymer composites improve with such amounts. To elucidate the reasons for the mechanical property improvement using such an extremely small amount, further investigations using various GOs with different sizes containing different amounts

of oxygen or other types of functional groups and different types of polymers having various functional groups are needed to systematically correlate the relationship between the mechanical properties and the interactions between the polymer with the fillers. Such works are in progress by preparing various types of graphene-based nanocomposites using other polymers.

It is also possible that further improvements in the mechanical properties could be observed with even less than 0.01 wt% of PA 6-GOs. However, we could not prepare PA 6-GO/PK nanocomposites films containing less than 0.01 wt% of PA 6-GOs reproducibly and systematically with the experimental system used in this study (the solution casting method using HFIP as a solvent). We only used 0.1 mg of GOs, even for the preparation of PA 6-GO/PK nanocomposite films containing 0.01 wt% of PA 6-GOs. We can possibly prepare PA 6-GO/PK nanocomposites containing less than 0.01 wt% of PA 6-GOs by a melt blending system using a larger amount of filler materials and polymers. Such works are also under way, in addition to the preparation of other types of GO filler materials, in order to further elucidate the effect of graphene-based fillers on the mechanical properties. Although we need much more further works to more clearly elucidate the effect of graphene-based fillers on the mechanical properties of PK and other polymers, it is still very clear that the PA 6-GOs prepared in this work are very effective filler materials to improve the mechanical properties of PK due to the much larger

surface area of the graphene materials and the specific interactions between the filler and the polymer matrix.

2.4. Conclusion

The mechanical properties of PK were found to be much improved by adding an extremely small amount of PA 6 grafted GO (0.01 wt%). The PK nanocomposite containing PA 6 grafted GO with less oxygen functional groups on the graphene shows brittle fracture behavior without significant deformation. It was also found that the larger content of PA 6 in the PA 6 grafted GO can further improve the mechanical properties of the PK nanocomposite. When PA 6 grafted GO with more oxygen functional groups were used, ductile fracture behavior with a large amount of plastic deformation was observed due to the further specific interaction between PK and the oxygen functional groups on the GOs. Therefore, PA 6 grafted GOs could be used to manipulate the mechanical properties of PK as filler materials by changing the oxidation state of GO and the grafting density of PA 6 chains. We believe that this work provides an effective method for load transfer and toughening of the polymer nanocomposites using the graphene-based filler materials and will contribute to the efforts to develop a strategy for the fabrication of the polymer nanocomposites in a wide range of applications in polymer science and engineering.

2.5. References

[1] Fu SY, Feng XQ, Lauke B, Mai YW. Effects of particle size, particle/matrix interface adhesion and particle loading on mechanical properties of particulate-polymer composites. Compos Part B-Eng. 2008;39(6):933-61.

[2] Paul DR, Robeson LM. Polymer nanotechnology: Nanocomposites. Polymer. 2008;49(15):3187-204.

[3] Ning NY, Fu SR, Zhang W, Chen F, Wang K, Deng H, et al. Realizing the enhancement of interfacial interaction in semicrystalline polymer/filler composites via interfacial crystallization. Prog Polym Sci. 2012;37(10):1425-55.

[4] Jin J, Rafiq R, Gill YQ, Song M. Preparation and characterization of high performance of graphene/nylon nanocomposites. Eur Polym J. 2013;49(9):2617-26.

[5] Ma J, Meng QS, Michelmore A, Kawashima N, Izzuddin Z, Bengtsson C, et al. Covalently bonded interfaces for polymer/graphene composites. J Mater Chem A. 2013;1(13):4255-64.

[6] Bhattacharya M, Bhowmick AK. Polymer–filler interaction in nanocomposites: New interface area function to investigate swelling behavior and Young's modulus. Polymer. 2008;49(22):4808-18.

[7] Sikdar D, Katti DR, Katti KS, Bhowmik R. Insight into molecular interactions

between constituents in polymer clay nanocomposites. Polymer. 2006;47(14):5196-205.

[8] Kim HJ, Choi K, Baek Y, Kim D-G, Shim J, Yoon J, et al. High-Performance Reverse Osmosis CNT/Polyamide Nanocomposite Membrane by Controlled Interfacial Interactions. ACS Appl Mater Interfaces. 2014. http://dx.doi.org/10.1021/am405398f

[9] Sengupta R, Bhattacharya M, Bandyopadhyay S, Bhowmick AK. A review on the mechanical and electrical properties of graphite and modified graphite reinforced polymer composites. Prog Polym Sci. 2011;36(5):638-70.

[10] Moniruzzaman M, Winey KI. Polymer nanocomposites containing carbon nanotubes. Macromolecules. 2006;39(16):5194-205.

[11] Potts JR, Dreyer DR, Bielawski CW, Ruoff RS. Graphene-based polymer nanocomposites. Polymer. 2011;52(1):5-25.

[12] Kim H, Abdala AA, Macosko CW. Graphene/Polymer Nanocomposites. Macromolecules. 2010;43(16):6515-30.

[13] Spitalsky Z, Tasis D, Papagelis K, Galiotis C. Carbon nanotube–polymer composites: Chemistry, processing, mechanical and electrical properties. Prog Polym Sci. 2010;35(3):357-401.

[14] Liao WH, Yang SY, Wang JY, Tien HW, Hsiao ST, Wang YS, et al. Effect of molecular chain length on the mechanical and thermal properties of amine-

functionalized graphene oxide/polyimide composite films prepared by in situ polymerization. ACS Appl Mater Interfaces. 2013;5(3):869-77.

[15] Cano M, Khan U, Sainsbury T, O'Neill A, Wang Z, McGovern IT, et al. Improving the mechanical properties of graphene oxide based materials by covalent attachment of polymer chains. Carbon. 2013;52:363-71.

[16] Liu R, Liang S, Tang X-Z, Yan D, Li X, Yu Z-Z. Tough and highly stretchable graphene oxide/polyacrylamide nanocomposite hydrogels. J Mater Chem. 2012;22(28):14160-7.

[17] Yang L, Phua SL, Toh CL, Zhang L, Ling H, Chang M, et al. Polydopamine-coated graphene as multifunctional nanofillers in polyurethane. RSC Adv. 2013;3(18):6377-85.

[18] Salavagione HJ, Martinez G, Ellis G. Recent advances in the covalent modification of graphene with polymers. Macromol Rapid Comm. 2011;32(22):1771-89.

[19] Chen D, Feng H, Li J. Graphene oxide: preparation, functionalization, and electrochemical applications. Chem Rev. 2012;112(11):6027-53.

[20] Drent E, Budzelaar PHM. Palladium-catalyzed alternating copolymerization of alkenes and carbon monoxide. Chem Rev. 1996;96(2):663-81.

[21] Sommazzi A, Garbassi F. Olefin carbon monoxide copolymers. Prog Polym Sci. 1997;22(8):1547-605.

[22] Garbassi F, Sommazzi A, Meda L, Mestroni G, Sciutto A. Surface properties of alternated aliphatic polyketones. Polymer. 1998;39(6-7):1503-6.

[23] Cho H-S, Chung J-S, Baek SJ, Choi WJ, Kim J-J, Yoon SK, et al. Preparation and properties of glass fiber-reinforced poly(olefin ketone) composites. Appl Chem Eng. 2012;23(3):339-43.

[24] Pérez-Foullerat D, Hild S, Mücke A, Rieger B. Synthesis and Properties of Poly(ketone-co-alcohol) Materials: Shape Memory Thermoplastic Elastomers by Control of the Glass Transition Process. Macromol Chem Physic. 2004;205(3):374-82.

[25] Cho H-S, Chung J-S, Shim J, Kim J-J, Choi WJ, Lee J-C. Poly(1-oxotrimethylene) fibers prepared by different draw ratios for the tire cord application. Macromol Res. 2012;20(7):732-8.

[26] Lee J, Lee KH, Kim D, Lim S, Lee SS. Layered nanofiller-reinforced polyketone composites. Macromol Res. 2013;21(11):1270-3.

[27] Zhang Y, Broekhuis AA, Picchioni F. Thermally Self-Healing Polymeric Materials: The Next Step to Recycling Thermoset Polymers? Macromolecules. 2009;42(6):1906-12.

[28] Zehetmaier PC, Vagin SI, Rieger B. Functionalization of aliphatic polyketones. MRS Bulletin. 2013;38(03):239-44.

[29] Zuiderduin WCJ, Huétink J, Gaymans RJ. Rigid particle toughening of

aliphatic polyketone. Polymer. 2006;47(16):5880-7.

[30] Zuiderduin WCJ, Westzaan C, Huetink J, Gaymans RJ. Toughening of polypropylene with calcium carbonate particles. Polymer. 2003;44(1):261-75.

[31] Semeril D, Passaglia E, Bianchini C, Davies M, Miller H, Ciardelli F. Reactive blending of polyamides with different carbonyl containing olefin polymers. Macromol Mater Eng. 2003;288(6):475-83.

[32] Asano A, Nishioka M, Takahashi Y, Kato A, Hikasa S, Iwabuki H, et al. High Impact Properties of Polyketone/Polyamide-6 Alloys Induced by Characteristic Morphology and Water Absorption. Macromolecules. 2009;42(24):9506-14.

[33] Kato A, Nishioka M, Takahashi Y, Suda T, Sawabe H, Isoda A, et al. Phase Separation and Mechanical Properties of Polyketone/Polyamide Polymer Alloys. J Appl Polym Sci. 2010;116(5):3056-69.

[34] Hummers WS, Offeman RE. Preparation of Graphitic Oxide. J Am Chem Soc. 1958;80(6):1339.

[35] Kim T-H, Kim S-K, Lim T-W, Lee J-C. Synthesis and properties of poly(aryl ether benzimidazole) copolymers for high-temperature fuel cell membranes. J Membrane Sci. 2008;323(2):362-70.

[36] Kim T-H, Lim T-W, Lee J-C. High-temperature fuel cell membranes based on mechanically stable para-ordered polybenzimidazole prepared by direct casting. J Power Sources. 2007;172(1):172-9.

[37] Kim S-K, Kim T-H, Jung J-W, Lee J-C. Copolymers of Poly(2,5-benzimidazole) and Poly[2,2′-(p-phenylene)-5,5′-bibenzimidazole] for High-Temperature Fuel Cell Applications. Macromol Mater Eng. 2008;293(11):914-21.

[38] van Rijswijk K, Bersee HEN, Beukers A, Picken SJ, van Geenen AA. Optimisation of anionic polyamide-6 for vacuum infusion of thermoplastic composites: Influence of polymerisation temperature on matrix properties. Polym Test. 2006;25(3):392-404.

[39] Xu Z, Gao C. In situPolymerization Approach to Graphene-Reinforced Nylon-6 Composites. Macromolecules. 2010;43(16):6716-23.

[40] Krishnamoorthy K, Veerapandian M, Yun K, Kim SJ. The chemical and structural analysis of graphene oxide with different degrees of oxidation. Carbon. 2013;53:38-49.

[41] Marcano DC, Kosynkin DV, Berlin JM, Sinitskii A, Sun ZZ, Slesarev A, et al. Improved Synthesis of Graphene Oxide. ACS Nano. 2010;4(8):4806-14.

[42] Zhang XQ, Fan XY, Li HZ, Yan C. Facile preparation route for graphene oxide reinforced polyamide 6 composites via in situ anionic ring-opening polymerization. J Mater Chem. 2012;22(45):24081-91.

[43] Gao JB, Itkis ME, Yu AP, Bekyarova E, Zhao B, Haddon RC. Continuous spinning of a single-walled carbon nanotube-nylon composite fiber. J Am Chem Soc. 2005;127(11):3847-54.

[44] Kricheldorf HR, Al Masri M, Schwarz G. Cyclic polyamide-6 by thermal polycondensation of epsilon-caprolactam and epsilon-aminocaproic acid. Macromolecules. 2003;36(23):8648-51.

[45] Fang M, Wang K, Lu H, Yang Y, Nutt S. Single-layer graphene nanosheets with controlled grafting of polymer chains. J Mater Chem. 2010;20(10):1982-92.

[46] Stankovich S, Dikin DA, Piner RD, Kohlhaas KA, Kleinhammes A, Jia Y, et al. Synthesis of graphene-based nanosheets via chemical reduction of exfoliated graphite oxide. Carbon. 2007;45(7):1558-65.

[47] Botas C, Alvarez P, Blanco C, Santamaria R, Granda M, Gutierrez MD, et al. Critical temperatures in the synthesis of graphene-like materials by thermal exfoliation-reduction of graphite oxide. Carbon. 2013;52:476-85.

[48] Zhang C, Lv W, Xie XY, Tang DM, Liu C, Yang QH. Towards low temperature thermal exfoliation of graphite oxide for graphene production. Carbon. 2013;62:11-24.

[49] Young RJ, Kinloch IA, Gong L, Novoselov KS. The mechanics of graphene nanocomposites: A review. Compos Sci Technol. 2012;72(12):1459-76.

[50] Goncalves G, Marques PAAP, Barros-Timmons A, Bdkin I, Singh MK, Emami N, et al. Graphene oxide modified with PMMA via ATRP as a reinforcement filler. J Mater Chem. 2010;20(44):9927-34.

[51] Fantner GE, Oroudjev E, Schitter G, Golde LS, Thurner P, Finch MM, et al.

Sacrificial bonds and hidden length: Unraveling molecular mesostructures in tough materials. Biophys J. 2006;90(4):1411-8.

[52] Chen Z, Lu H. Constructing sacrificial bonds and hidden lengths for ductile graphene/polyurethane elastomers with improved strength and toughness. J Mater Chem. 2012;22(25):12479-90.

[53] Lu H, Chen Z, Ma C. Bioinspired approaches for optimizing the strength and toughness of graphene-based polymer nanocomposites. J Mater Chem. 2012;22(32):16182-90.

[54] Du J, Cheng H. The fabrication, properties, and uses of graphene/polymer composites. Macromol Chem Physic. 2012;213:1060-77.

[55] Kuilla T, Bhadra S, Yao D, Kim NH, Bose S, Lee JH. Recent advances in graphene based polymer composites. Prog Polym Sci. 2010;35:1350-75.

[56] Sabzi M, Jiang L, Liu F, Ghasemi I, Atai M. Graphene nanoplatelets as poly(lactic acid) modifier: linear rheological behavior and electrical conductivity. J Mater Chem A. 2013;1:8253-61.

[57] Chen P, Wang Y, Wei T, Meng Z, Jia X, Xi K. Greatly enhanced mechanical properties and heat distortion resistance of poly(l-lactic acid) upon compositing with functionalized reduced graphene oxide. J Mater Chem A. 2013;1:9028-32.

[58] Wang X, Song M. Toughening f polymers by graphene. Nanomaterials and energy. 2013;2:265-78.

[59] Knight GW. Polyethylene. In: Arends CB, editor. Polymer toughening, New York: Marcel Dekker Inc; 1996, p. 189–236.

Table 2.1 Feed ratios and mechanical properties of PA 6-GO/PK nanocomposites and the PK

Sample	Feed ratio (wt%)		Tensile strength (MPa)	Young's modulus (MPa)	Elongation at break (%)	$T_{d,5\%}$ (ºC)[d]
	PK	PA 6-GO				
PK	100	0	68.6±1.5	4090±380	3.7±0.1	288
PA 6-GO1 0.01/PK[a]	99.99	0.01	86.0±1.4	5570±270	6.4±0.2	301
PA 6-GO1 0.02/PK[a]	99.98	0.02	82.3±0.7	5420±310	7.1±0.4	305
PA 6-GO1 0.05/PK[a]	99.95	0.05	81.4±0.4	5280±540	7.2±0.4	324
PA 6-GO1 0.10/PK[a]	99.90	0.10	51.3±1.1	3580±350	5.5±0.2	299
PA 6-GO2-1 0.01/PK[b]	99.99	0.01	94.1±2.9	2360±320	363±13	301
PA 6-GO2-1 0.02/PK[b]	99.98	0.02	79.3±2.4	2560±300	314±12	331
PA 6-GO2-1 0.05/PK[b]	99.95	0.05	81.0±2.4	2510±67	297±11	326
PA 6-GO2-1 0.10/PK[b]	99.90	0.10	80.0±1.0	2820±330	221±22	311
PA 6-GO2-2 0.01/PK[c]	99.99	0.01	92.9±2.5	5170±120	6.5±0.1	298
PA 6-GO2-2 0.02/PK[c]	99.98	0.02	81.3±0.2	5120±280	8.3±0.6	296
PA 6-GO2-2 0.05/PK[c]	99.95	0.05	75.8±0.2	5240±230	6.3±0.1	302
PA 6-GO2-2 0.10/PK[c]	99.90	0.10	54.4±1.3	3410±280	4.1±0.2	295

[a]PA 6-GO1, [b]PA 6-GO2-1, and [c]PA 6-GO2-2 were used as the fillers. [d]The decomposition temperature ($T_{d,5\%}$) is defined as 5 wt % loss.

Table 2.2 Inherent viscosity, molecular weight and melting temperature of separated PA 6 from PA 6-GOs

Samples	PA 6 from PA 6-GO1	PA 6 from PA 6-GO2-1	PA 6 from PA 6-GO2-2
η_{inh} [a]	0.364	0.391	0.447
M_{η} [b]	8200	8900	10500
T_m (ºC) [c]	215	216	220

[a]Inherent viscosity of separated PA 6 of PA 6-GOs was measured at 25 ºC in formic acid solution by Ubbelohde viscometer. [b]The molecular weight of free PA 6 was calculated from Mark-Houwink equation, where K = 2.26 X10^{-4} and α = 0.82. [c]The melting temperature was measured by DSC.

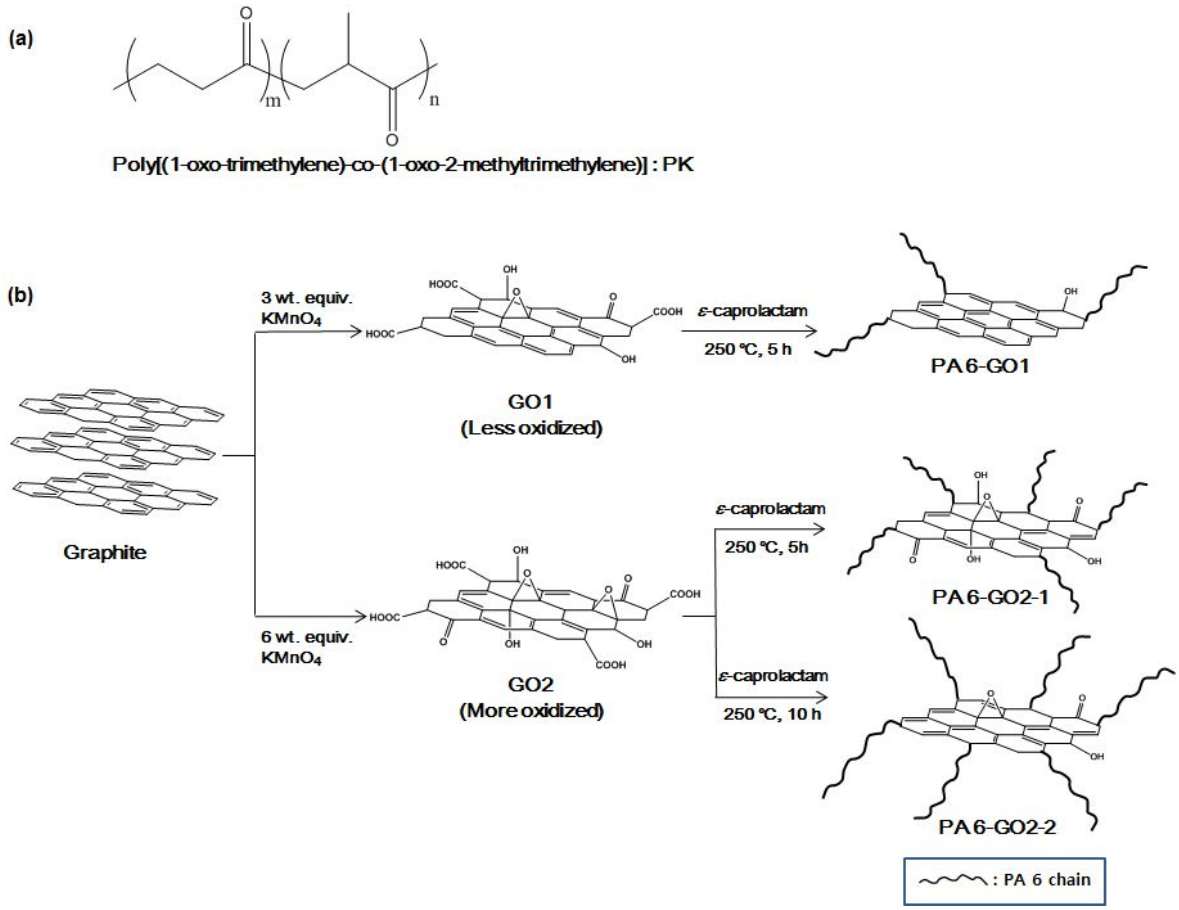

Fig. 2.1 (a) Chemical structure of PK and (b) schematic of the preparation PA 6-GO1, PA 6-GO2-1, and PA 6-GO2-2

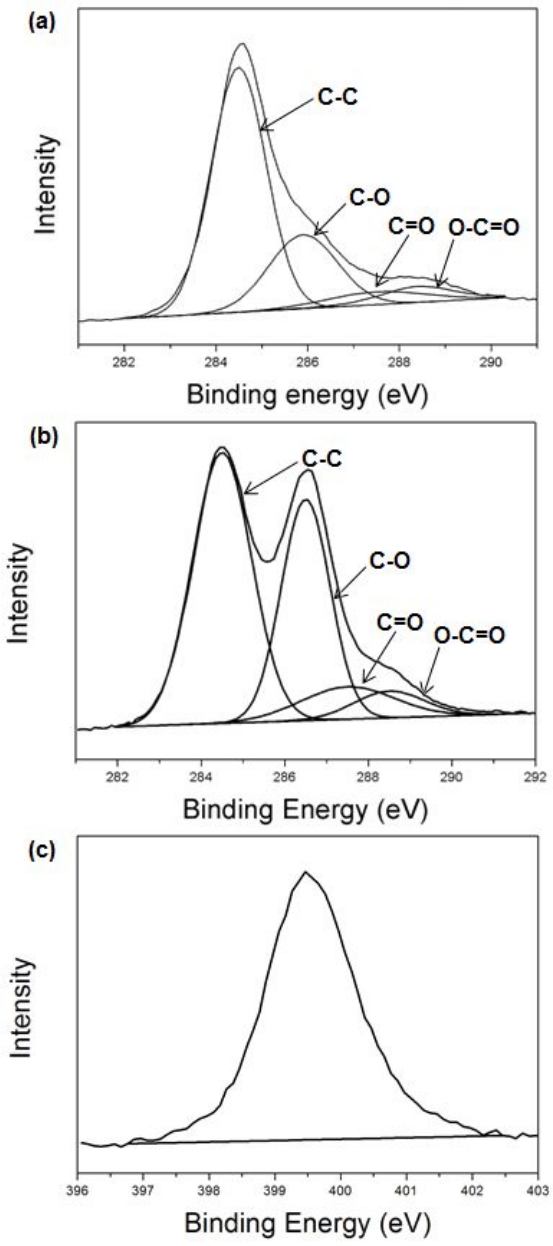

Fig. 2.2 XPS C1s spectra of (a) GO 1, (b) GO 2, and N1s spectrum of (c) PA 6-GO1

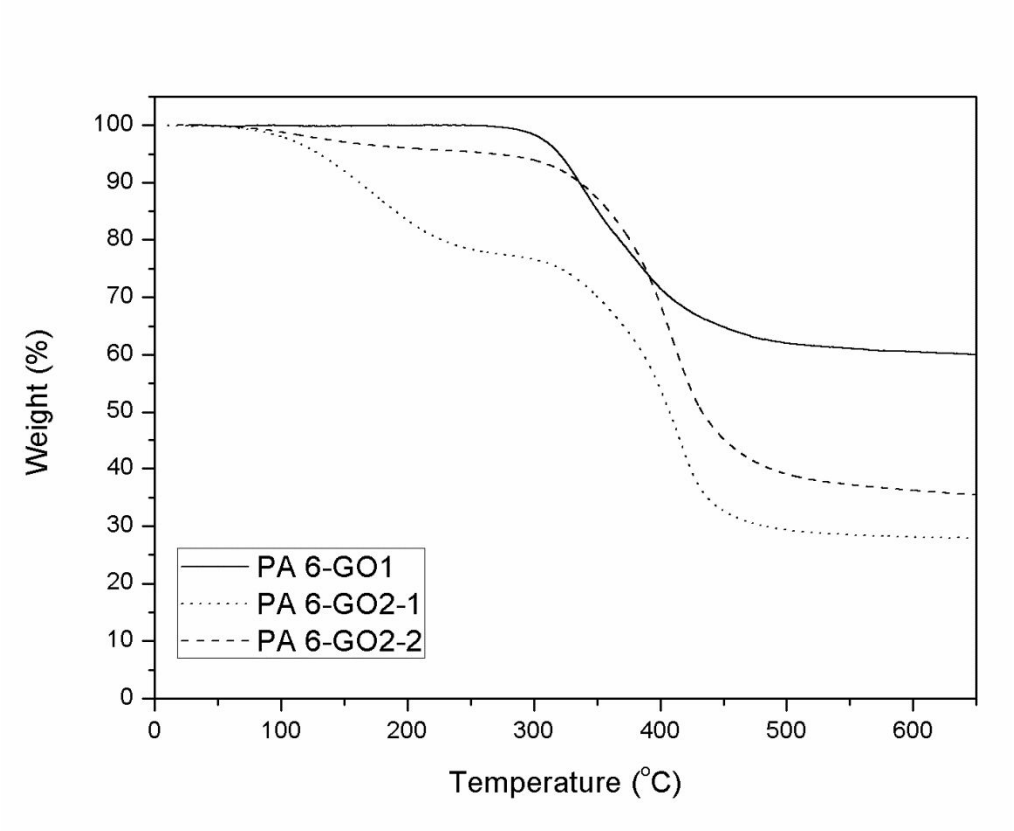

Fig. 2.3 TGA curves for PA 6-GO1, PA 6-GO2-1, and PA 6-GO2-2

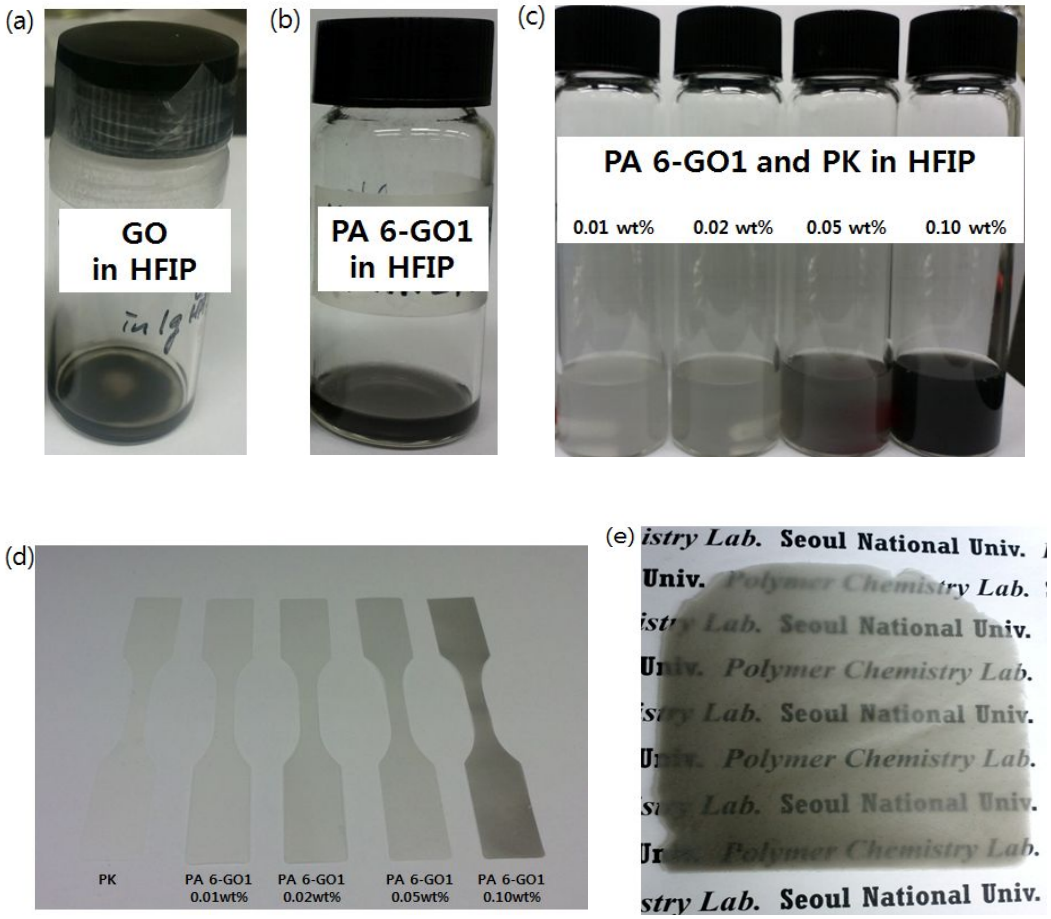

Fig. 2.4 Photographs of (a) GO dispersion, (b) PA 6-GO1 dispersion in HFIP, (c) the mixtures of PA 6-GO1 and PK in HFIP, (d) PK nanocomposite films containing PA 6-GO1, and (e) PA 6-GO1 0.15/PK film

(a)

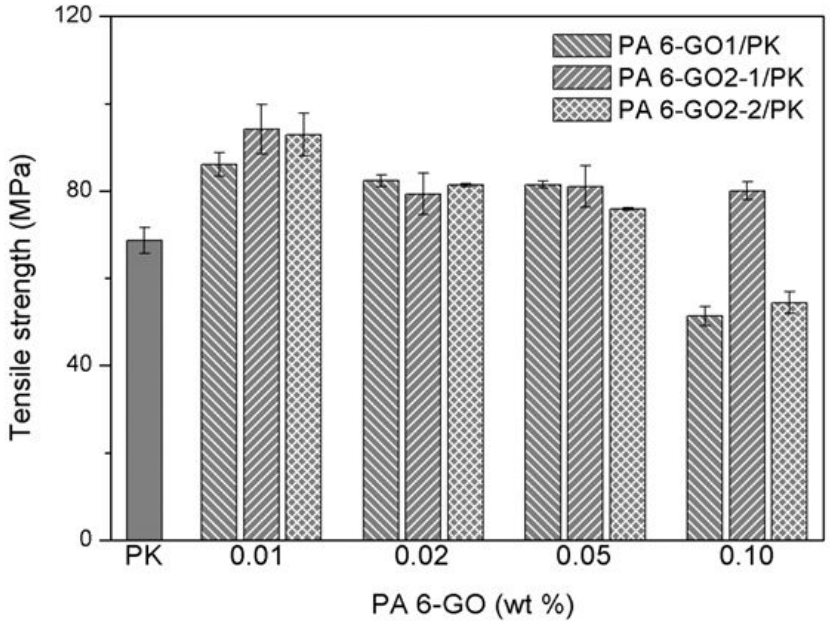
120
80
40
0
Tensile strength (MPa)
PA 6-GO1/PK
PA 6-GO2-1/PK
PA 6-GO2-2/PK
PK
0.01
0.02
0.05
0.10
PA 6-GO (wt %)

(b)

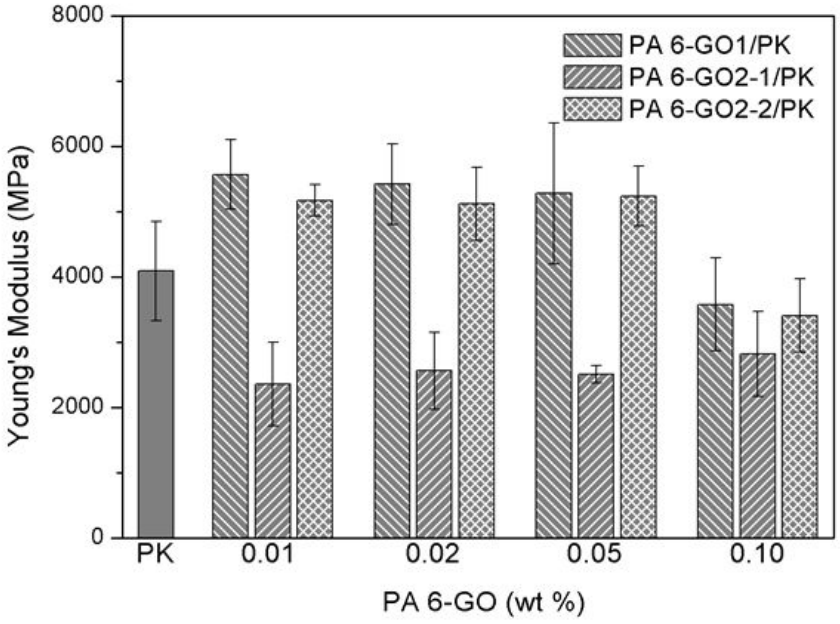
8000
6000
4000
2000
0
Young's Modulus (MPa)
PA 6-GO1/PK
PA 6-GO2-1/PK
PA 6-GO2-2/PK
PK
0.01
0.02
0.05
0.10
PA 6-GO (wt %)

(c)

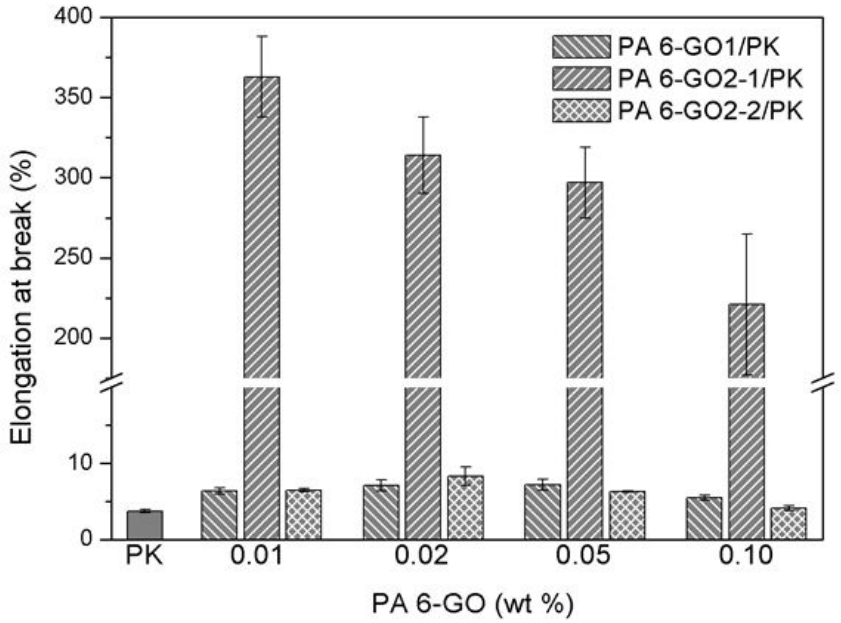

Fig. 2.5 Mechanical properties of PK nanocomposites containing PA 6-GOs and the PK. (a) tensile strength, (b) Young's modulus, and (c) elongation at break

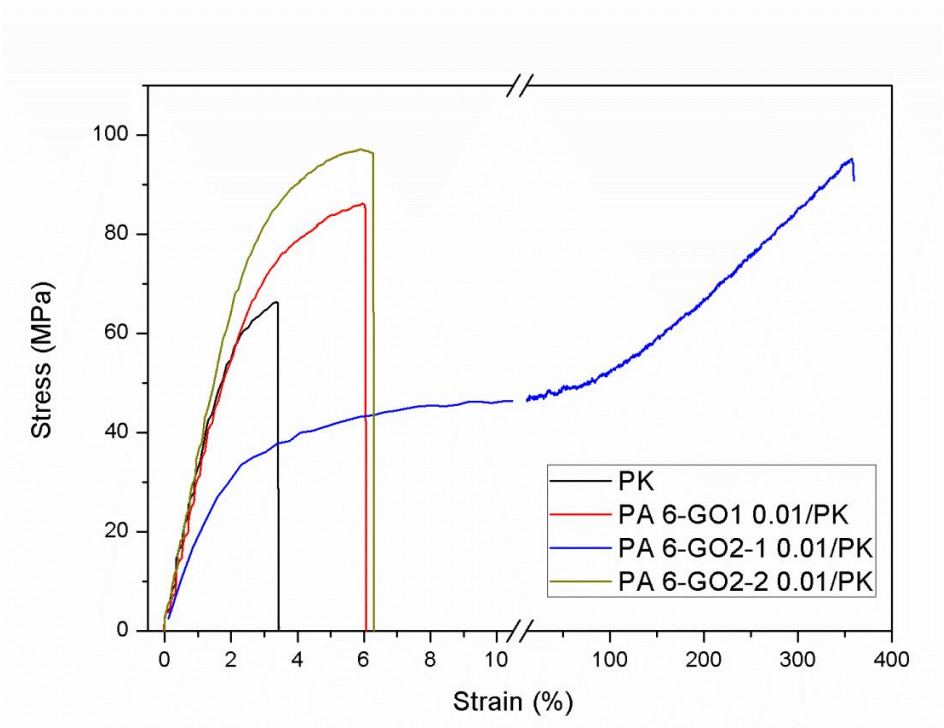

Fig. 2.6 Stress-strain curves for the pristine PK, PA 6-GO1 0.01/PK, PA 6-GO2-1 0.01/PK, and PA 6-GO2-2 0.01/PK

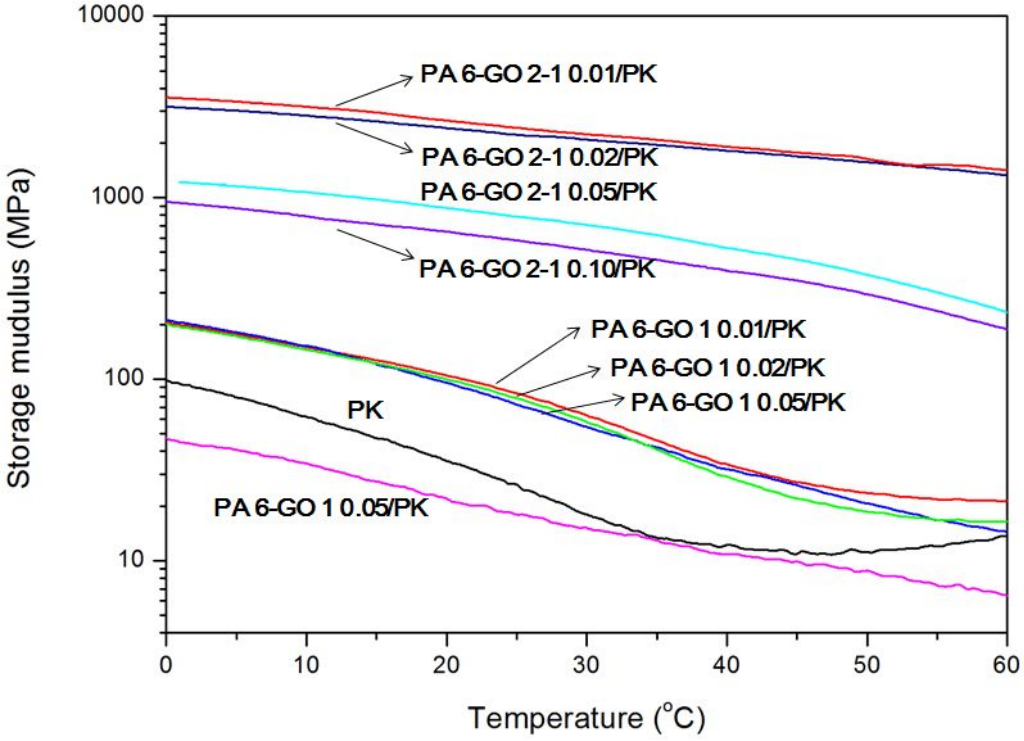

Fig. 2.7 Storage modulus versus temperature for PK and PK composites as measured by DMA

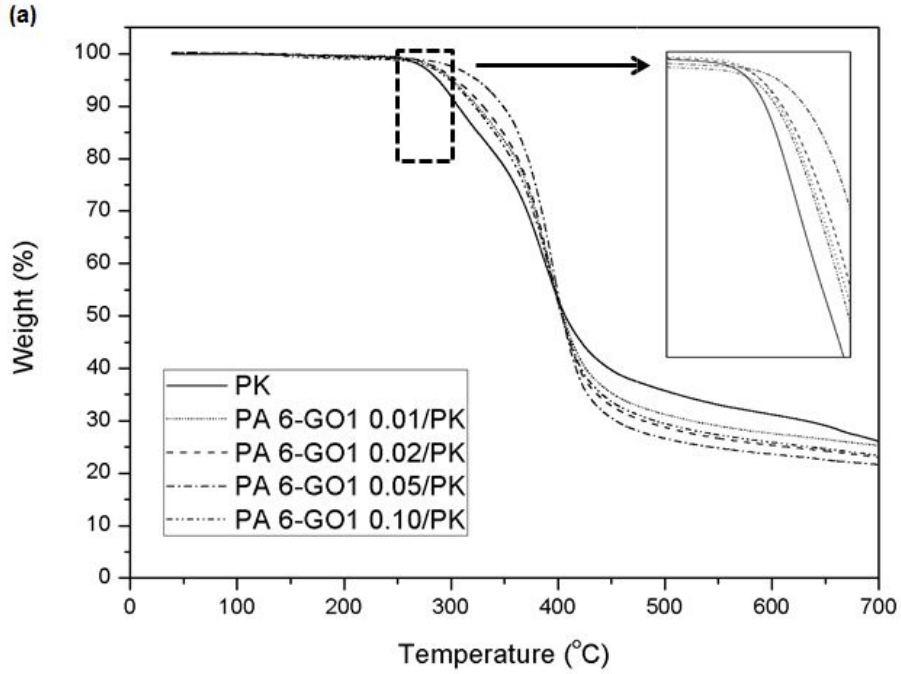
(a)
Weight (%)
Temperature (°C)
PK
PA 6-GO1 0.01/PK
PA 6-GO1 0.02/PK
PA 6-GO1 0.05/PK
PA 6-GO1 0.10/PK

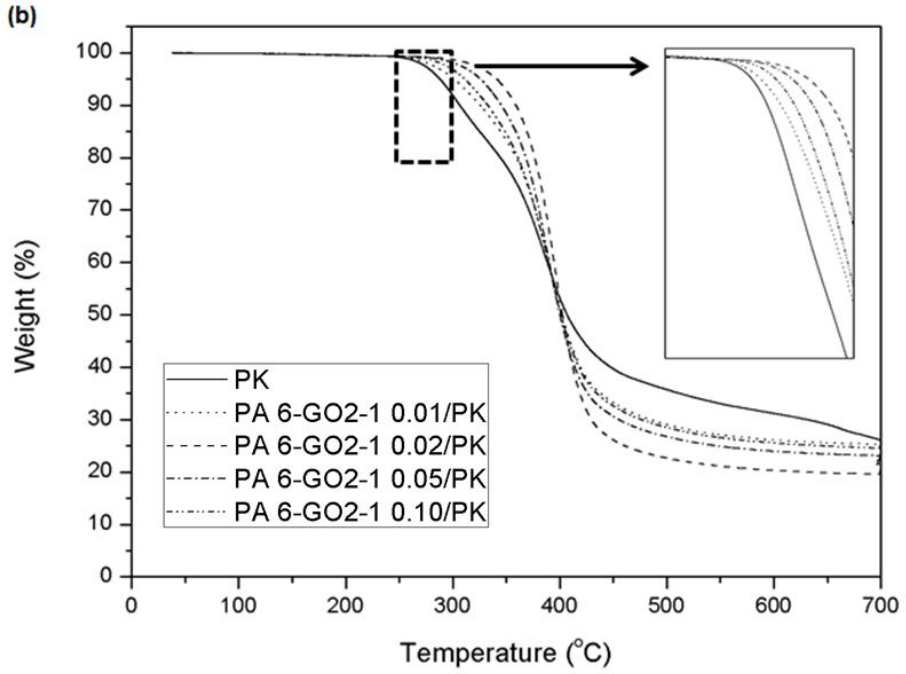
(b)
Weight (%)
Temperature (°C)
PK
PA 6-GO2-1 0.01/PK
PA 6-GO2-1 0.02/PK
PA 6-GO2-1 0.05/PK
PA 6-GO2-1 0.10/PK

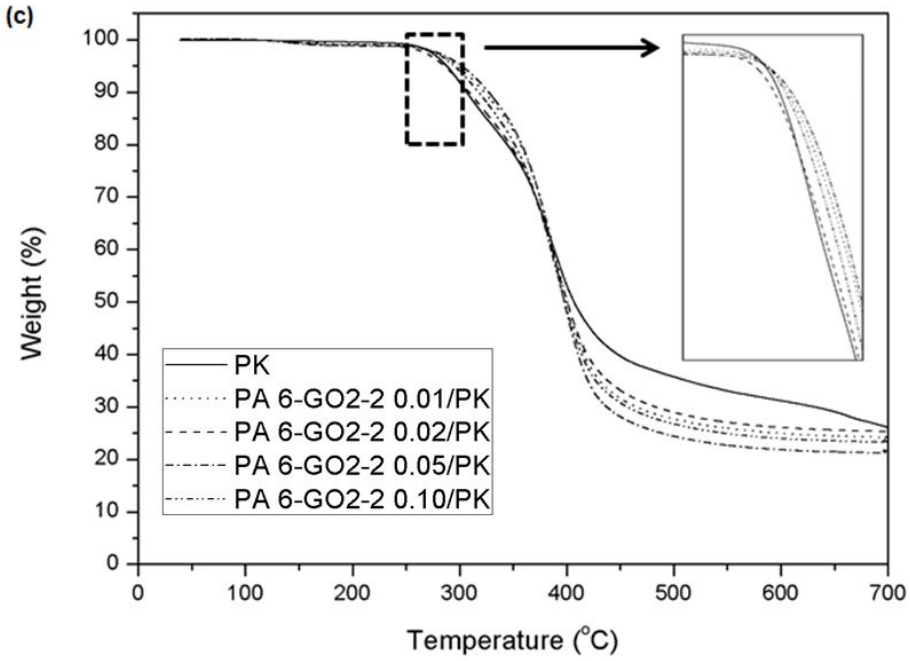

Fig. 2.8 TGA curves of (a) PA 6-GO1/PK nanocomposites, (b) PA 6-GO2-1/PK nanocomposites, and (c) PA 6-GO2-2/PK nanocomposites

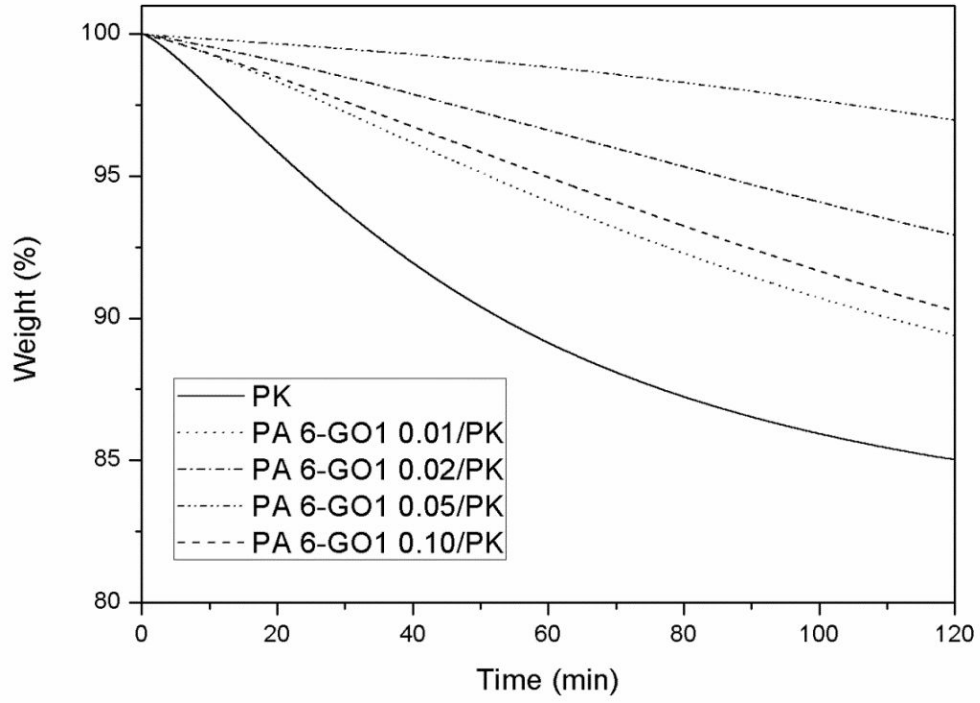

Fig. 2.9 Isothermal TGA curves (at 250 ºC) of PA 6-GO1/PK nanocomposites and the pristine PK

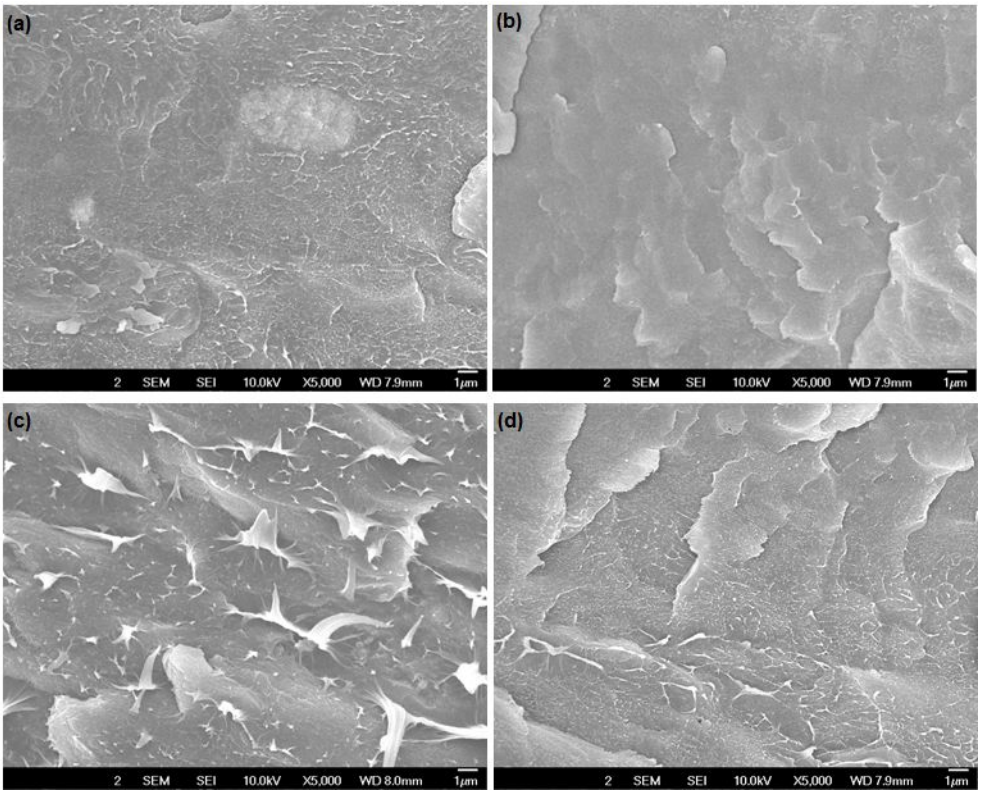

Fig. 2.10 SEM images of fractured surfaces of films. (a) PK, (b) PA 6-GO1 0.02/PK, (c) PA 6-GO2-1 0.02/PK, and (d) PA 6-GO2-2 0.02/PK

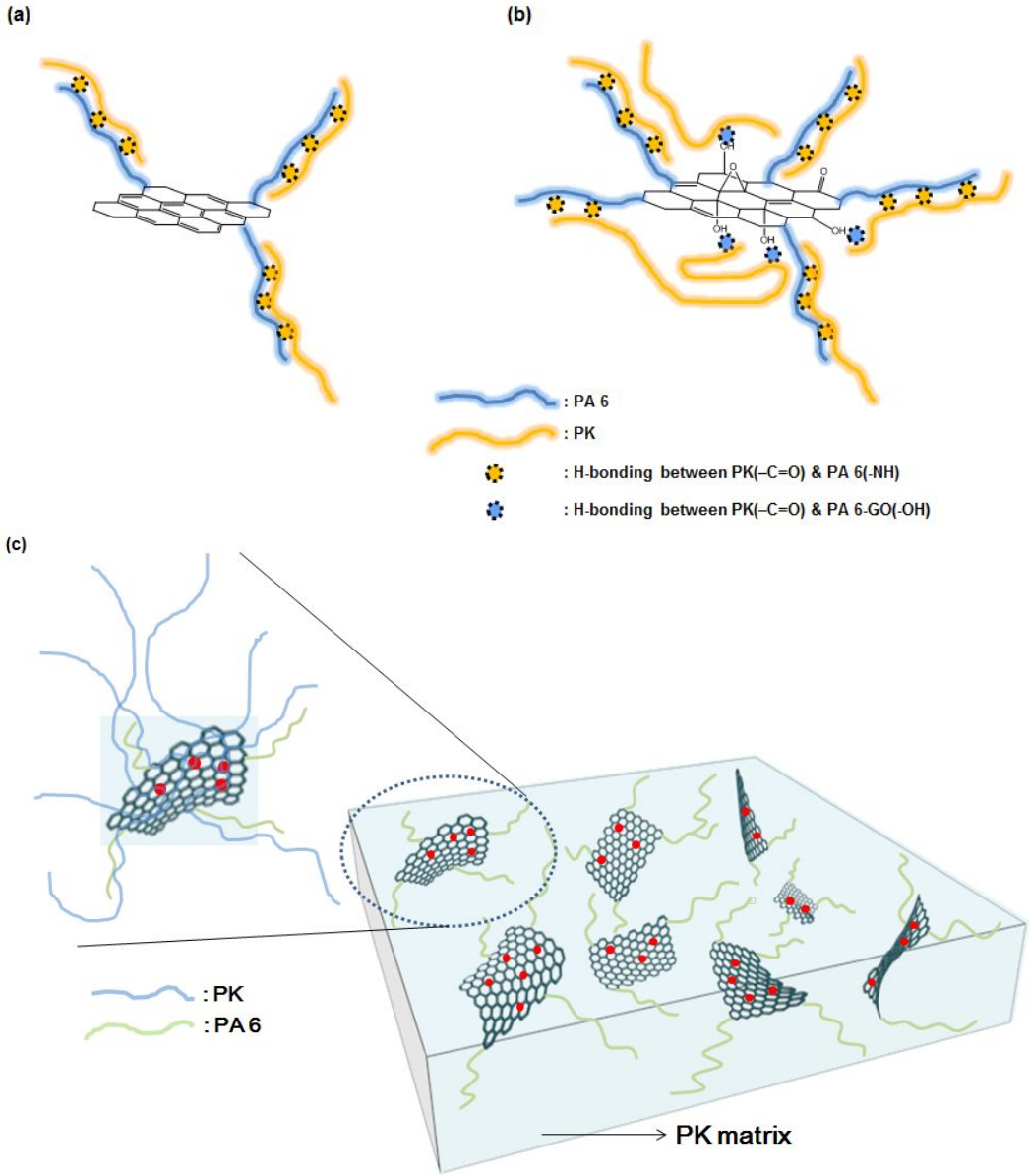

Fig. 2.11 Schematic of the toughening mechanism: formation of sacrificial bond and hidden length (a) PA 6-GO1or PA 6-GO2-2 and PK, (b) PA 6-GO2-1 and PK, and polymer-bridged graphene network (c) PA 6-GO2-1/PK nanocomposite

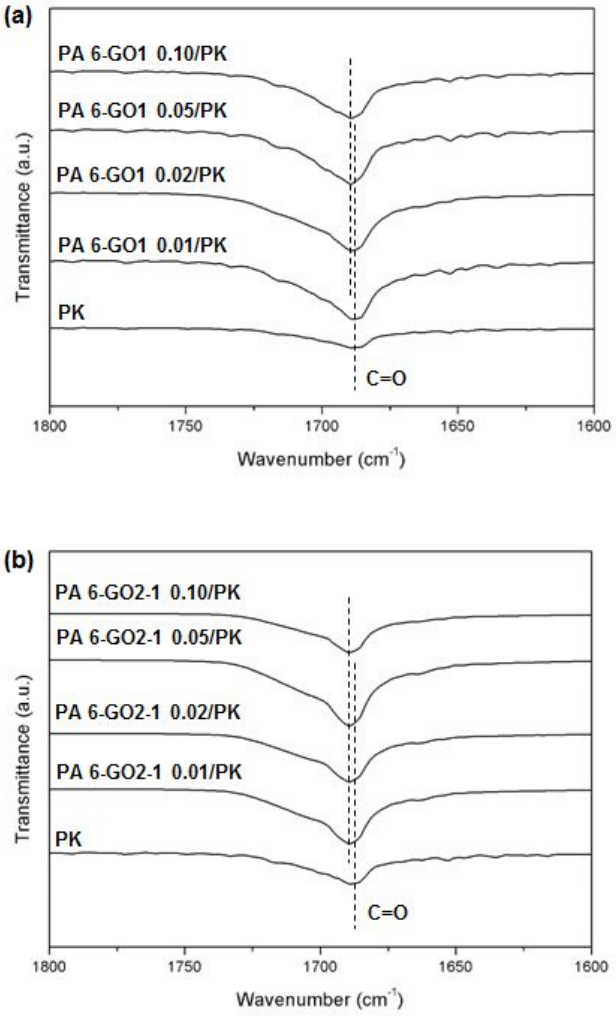

Fig. 2.12 FT-IR spectra of (a) PA 6-GO1/PK nanocomposites, and (b) PA 6-GO2-1/PK nanocomposites

Chapter 3

Effect of antioxidant grafted graphene oxides on the mechanical and thermal properties of polyketone nanocomposites

3.1. Introduction

Carbon nanomaterials, such as carbon nanotube (CNT), graphene, and graphene oxide (GO), have been widely used to improve the performance of polymer nanocomposites as filler materials due to their outstanding mechanical, thermal, and electrical properties [1-8]. Especially, the antioxidant behavior of the carbon nanomaterials in the polymer matrix and their effect on the thermal properties of polymer nanocomposites have drawn much attention for scientific interests and industrial purposes [9-11]. The remarkable improvement in thermal stability by the carbon nanomaterials has been known to be closely related to their inherent radical scavenging ability because they contain lattice defects, such as lattice vacancies, phenol, and other oxygen functional groups that can stabilize the radicals [10-12]. For example, when 5 wt% of CNT containing hindered phenol moieties was added to polyethylene (PE), the thermal oxidative stability of PE was found to be improved [13].

However, the application of CNT derivatives for the antioxidant has been limited due to the poor chemical compatibility with polymers forming non-uniform domains, and the effective improvement of the thermal stability could not be easily obtained [9, 10]. On the contrary, GO derivatives have been known to have

better compatibility with polymers because various kinds of oxygen functional groups, such as carboxylic acid, hydroxide, epoxide, and ketone groups, in the GO can increase the interactions with polymers. Furthermore, when the oxygen functional groups in the GO were modified with various kinds of chemical moieties including polymers, the compatibility with the polymer matrix was found to be considerably improved and the polymer nanocomposites containing such GO derivatives showed much enhanced mechanical strength and thermal stability. For example, when only 0.01 wt% of the GO derivatives containing polyamide 6 chains were mixed with aliphatic polyketone (PK), the elongation at break was increased by about 100 times and the thermal stability was found to be much improved [14].

PK is an alternating olefin/carbon monoxide (CO) copolymer having various advantageous properties such as good chemical resistance, mechanical properties, and low gas permeability [15-17]. Accordingly, it has a great potential to use in a wide range of possible applications, while further works on the synthesis, characterization, and process are required for practical applications in the engineering field. In particular, although PK is chemically and physically stable under inert conditions at room temperature, when it is exposed to heat and air, extensive thermal degradation was observed [18-20]. Therefore, the preparation of PK samples from extrusion or injection molding without deterioration of

properties has been known to be very difficult due to the poor thermal stability of PK [19, 21].

In this work, we tried to improve the physical properties including thermal stability of PK by adding CNT, GO, and GO derivatives containing antioxidant groups. The GO derivatives containing hindered phenol moiety as the antioxidant showed most improved mechanical strength and thermal stability. The synthesis of the GO derivatives and the characterization of the PK nanocomposites are discussed in this manuscript.

3.2. Experimental

Materials

Multi-walled carbon nanotubes (CNTs) were purchased from Nanocyl (Belgium). The purity, outer diameter, and length of CNT are ≥ 95 %, 10-20 nm, and 10-20 μm, respectively. Graphite powders were received from BASF (Germany). Aliphatic polyketone (PK, glass transition temperature = 10 ºC, melting temperature = 225 ^{o}C, melt index = 60 g/10 min) was kindly provided by Hyosung (Korea) and used as received. The PK used in this study is an alternating olefin/carbon monoxide copolymer prepared by olefins (ethylene and propylene) and carbon monoxide (CO) as monomers using palladium catalysts. The molar contents of 1-oxo-trimethylene and 1-oxo-2-methyltrimethylene in PK are 94 mol% and 6 mol%, respectively (Fig. 1a). Phosphorus (V) oxide (P_2O_5), sodium nitrate ($NaNO_3$), potassium permanganate ($KMnO_4$), and hydrogen peroxide (H_2O_2), all from Aldrich, were used as received. 3, 5-*di*-*tert*-butyl-4-hydroxyphenylpropionic acid (hindered phenolic compound, HP) was purchased from Alfar aesar and used as received. 4-amino-2,2,6,6-tetramethylpiperidine (hindered amine compound, HA) was purchased from TCI and used as received. All other reagents and solvents were used as received from standard vendors.

Preparation of GO

GO was prepared according to the modified Hummers method [14, 22, 23]. Graphite powders (1.0 g) and P_2O_5 (0.5 g) were added to concentrated sulfuric acid (98%, 6.0 mL). The mixture was heated at 85 ºC for 5 h and deionized water (200 mL) was added to the mixture. Then the mixture was filtered through anode aluminum oxide (AAO) membrane filter with 0.2 μm pore size and washed with water several times. The solid was dried in vacuum oven at 35 ºC for 24 h. The dried product (pre-oxidized graphite, 1.0 g) and $NaNO_3$ (0.5 g) were added to sulfuric acid (98%, 23.0 mL) in an ice bath and kept the temperature below 5 ºC for 40 min without stirring. Then $KMnO_4$ (3.0 g) was added slowly with stirring at 0-5 ^oC. The mixture was heated to 35 ºC and stirred for 2 h and then 140 mL of deionized water and 10 mL of 30 % H_2O_2 were added. Then the mixture was filtered through 0.2 μm AAO membrane filter. The solid was washed with 250 mL of 10 % HCl followed by water until the pH was 7. The solid was dried overnight at 35 ºC.

Preparation of hindered phenol grafted GO (HP-GO)

3,5-*di-tert*-butyl-4-hydroxyphenylpropionic acid (hindered phenolic compound, HP, 0.7 g, 2.5 mmol) was added into 50 mL of anhydrous chloroform. Then 2 mL of thionyl chloride was added into the solution and the solution was refluxed under N_2 for 12 h with stirring. After the mixture was cooled to room temperature, residual thionyl chloride and chloroform were removed under reduced pressure. The product (3,5-*di-tert*-butyl-4-hydroxyphenylpropionyl chloride, HP-Cl) was dried in vacuum overnight. Hindered phenol grafted GO (HP-GO) was obtained by the reaction of HP-Cl with GO as follows. 25 mL of anhydrous DMF solution containing 52.5 mg of GO was sonicated for 30 min and was poured into a vacuumed flask containing HP-Cl. The DMF solution was heated at 80 ºC for 30min and then 1 mL of anhydrous triethylamine was added. The reaction mixture was stirred for 3 days and the product was obtained by filtering through PTFE membrane filter with 0.2 μm pore size followed by washing with ethanol several times. Then the product was further purified by dissolving in DMF, filtering, and washing using ethanol. The synthetic route to prepare HP-GO is shown in Fig. 1b.

Preparation of hindered amine grafted GO (HA-GO)

0.1 g of GO was added into 30 mL of anhydrous DMF and the mixture was sonicated for 30 min. 0.2 g of 4-amino-2,2,6,6-tetramethylpiperidine (hindered

amine compound, HA) was slowly added to the GO solution with stirring. The mixture was heated to 80 ºC and stirred for 12 h and the product was filtered and washed with DMF several times. Then the product was purified by dissolving in DMF, filtering, and washing using DMF to obtain hindered amine grafted GO (HA-GO). The synthetic route to prepare HA-GO is shown in Fig. 1c.

Preparation of PK nanocomposites

PK nanocomposites were prepared by the polymer powder coating method reported by others before [24, 25]. 10 mg of HP-GO was added to 5.0 g of ethanol and then sonicated for 30 min to make a homogeneous dispersion. 10 g of PK powders were added to 100g of ethanol and then the HP-GO dispersed in ethanol was added into the PK powder in ethanol with stirring. PK powders coated by HP-GOs homogeneously (PK nanocomposites) were obtained by evaporating ethanol at 110 ºC. The obtained PK nanocomposite with 0.1 wt% of HP-GO was noted as HP-GO/PK. Other nanocomposites containing 0.1 wt% of CNT, GO, and HA-GO named as CNT/PK, GO/PK, and HA-GO/PK, respectively, were also prepared by the same procedure except the filler materials. The resulting composite powders were used for injection molding to measure tensile properties of the PK nanocomposites.

Characterization

Thermal gravimetric analysis (TGA) was performed in a Q-5000 IR from TA Instruments to study the thermal stability of the PK nanocomposites. The samples were heated from 25 ºC to 600 ºC using a heating rate of 5 ^{o}C/min under a nitrogen atmosphere. For isothermal TGA measurements, the samples were heated from 50 ºC to 250 ºC at a heating rate of 10 ^{o}C/min and maintained at 250 ^{o}C for 2 hr under nitrogen. The isothermal weight loss was calculated using the weight of the sample after thermal degradation. Samples for universal testing machine (UTM) test were prepared by injection molding using MINIMAX molder (Bautech). The mechanical properties were measured using UTM (Instron-5567). The dumbbell specimens were prepared using the ASTM standard D638-V (Type V specimen dog-bone shaped samples) by injection molding at 235 ^{o}C. The tensile properties of the samples were measured in air at 23 ^{o}C under a 45% relative humidity (RH) with a gauge length and cross head speed of 15 mm and 5 mm/min, respectively. At least 5 samples were tested for each composite material. X-ray photoelectron spectroscopy (XPS) was recorded on a KRATOS AXIS-His using MgKα (1254.0 eV) as the radiation source. Spectra were collected over a range of 0-1200 eV, followed by high resolution scan of the C 1s, O 1s, and N 1s regions.

Fourier-transform infrared (FT-IR) spectra of films were recorded on a Cary 660 FT-IR spectrometer (Agilent Technology) at ambient temperature. Data were collected over 30 scans at 4 cm^{-1} resolution.

3.3. Results and Discussion

Preparation of GO grafted with hindered phenol (HP-GO) and GO grafted with hindered amine (HA-GO)

GOs grafted with hindered phenol and hindered amine group, named as HP-GO and HA-GO, respectively, were prepared by the reactions of GOs with hindered phenol or hindered amine, respectively, as shown in Fig.1. These antioxidant grafted GOs were used as fillers to impart the antioxidant property to the PK composites. HP-GO was synthesized by the esterification between the acyl chloride group in hindered phenol and the hydroxyl groups in GO. HA-GO was prepared by the ring-opening reaction between the epoxide groups in GO and the amine groups in hindered amine.

Fig. 2a shows the FT-IR spectra of GO, HP, and HP-GO. In the spectrum of GO, a broad O-H stretching peak from the hydroxyl groups and the water molecules absorbed on the GO sheets at 3450 cm^{-1} and a C=O peak from the carboxyl groups on the GO sheets at 1740 cm^{-1} are observed [26-28]. On the contrary, HP-GO shows sp^3 C-H stretching peaks at 2916 and 2846 cm^{-1}, which are associated with methyl groups from the hindered phenol, indicating that the hindered phenol

groups are successfully grafted on the GO sheets [13]. For HA-GO, characteristic absorption peaks of the piperidine ring from the hindered amine compound are clearly observed at 2900-3000 cm^{-1} and a new weak absorption peak is also observed at 1440 cm^{-1} corresponding to C-N stretching, indicating the successful grafting of hindered amine onto the GO surface. XPS results of HP-GO and HA-GO shown in Fig. 3 also indicate the successful incorporation of the hindered phenol group and hindered amine group into GOs to form HP-GO and HA-GO, respectively [26, 29].

The content of the grafted antioxidant moieties on the GO sheets were estimated from the TGA curves for GO, HP-GO, and HA-GO as shown in Fig. 4. It is well-known that the weight changes below 300 ºC of the GO derivatives are due to the thermal decomposition of the labile oxygen functional groups such as carboxylic acid, hydroxyl, epoxide, and ketone in the GO and those between 300-500 ºC are due to the thermal decomposition of the other organic moieties bonded on the GO [29-31]. Therefore, 12 and 13 wt% of the weight loss between 300 and 500 ºC for HP-GO and HA-GO, respectively, can be ascribed to the amounts of antioxidant functional groups on the GO. The smaller weight loss of HP-GO below 300 ºC than that of HA-GO indicates that HP-GO contains smaller amount of oxygen functional groups than HA-GO. Since HP-GO was prepared by a longer reaction time (3 days) than HA-GO (12 h), it is possible that more oxygen

functional groups in HP-GO could be reduced. Raman spectroscopy results also indicate that HP-GO is more reduced; the G band of HP-GO is more shifted than that of HA-GO (Fig. 5) [32].

PK nanocomposites with carbon nanomaterials

Preparation of PK nanocomposites

PK nanocomposites were prepared by the polymer powder coating method instead of using the general process such as the melt and solution blending methods [24, 25, 33]. Previously, we found that PK nanocomposites containing polyamide grafted GO prepared by the solution blending method show much improved mechanical properties by adding only a very small amount of GO derivatives such as less than 0.1 wt% because the polymer and the nanofillers are mixed homogeneously in the molecular level in the solution state [14]. In this study, we prepared PK nanocomposites with a small amount of the carbon nanomaterials such as 0.1 wt% by the cost-efficient and manufacturing-friendly polymer powder coating method. The reason why 0.1 wt% was used will be discussed in a later part of this manuscript. First, we had tried to prepare the PK nanocomposites containing the carbon nanomaterials as the fillers using a melt blender by simply mixing PK with carbon nanomaterials in the melted state, while

homogeneous polymer mixture could not be obtained and poor dispersion and agglomeration of the carbon nanomaterials were observed in the PK matrix. Therefore, the agglomerated carbon nanomaterials could not increase the thermal and mechanical properties of PK. While we could have prepared the PK nanocomposites by the solution casting method, PK is only soluble in *m*-cresol and 1,1,1,3,3,3-hexafluoro-2-propanol, which are either toxic (and high boiling point) or very expensive. On the contrary, in the polymer powder coating method used in this work, environmentally friendly ethanol could be used as the solvent and very homogeneous polymer nanocomposites samples could be prepared by mixing the polymer powders and carbon nanomaterials in ethanol followed by the drying process and the compression or injection molding process.

Thermal properties

The thermal stability of the PK nanocomposites was evaluated by TGA. The thermal decomposition temperatures for 5 wt% mass loss ($T_{d,5\%}$) and char yields at 600 ^{o}C from the TGA measurements are listed in Table 1, and TGA curves of the PK composites are shown in Fig. 6. The decomposition temperature of PK was found to increase from 301.7 ^{o}C ($T_{d,5\%}$ of PK) to 308.6, 318.0, and 340.5 ^{o}C by adding 0.1 wt% of GO, HP-GO, and HA-GO, respectively. These results

indicate that the incorporation of the graphene-based nanofillers into the PK increases the thermal stabilities of the PK nanocomposites due to their good dispersion in the PK matrix and the heat and mass barrier effect of GO [34]. On the contrary, the decomposition temperature (301.7 ^{o}C) of the PK nanocomposite with 0.1 wt% of CNT (CNT/PK) was slightly lower than that of the PK, possibly due to the aggregation of CNTs in the polymer matrix.

The char yields of the PK nanocomposites were found to be irrelevant to their initial decomposition temperature; the initial decomposition temperatures of the PK nanocomposites containing GO and GO derivatives are higher than that of PK, while the char yields of the PK nanocomposites at 600 ^{o}C were found to be smaller than that of PK. The char yield of PK at 600 ^{o}C was 27.9 wt%, indicating that PK has an excellent char-forming capacity, while those of the PK nanocomposites were found to be smaller and they are 26.1, 25.6, 23.6, and 20.6 wt% for CNT/PK, GO/PK, HP-GO/PK, and HA-GO/PK, respectively, indicating that the addition of the carbon nanomaterials to the PK disrupts the char-formation in the polymer upon heating. Similar disruptions on the char-formation by the addition of the fillers were reported by others and are explained by the physical barrier effect of the fillers on the aromatization for the generation of char [35, 36].

The effect of the different carbon nanomaterials on the thermal properties of PK was further studied by observing the weight changes at the initial degradation

temperature of PK (250 ^{o}C) known as the isothermal TGA [14, 37]. Similar isothermal TGA studies at the initial degradation temperature for the thermal-oxidative stability behavior of the polymers were also previously reported by others [10, 37-39]. The content of fillers such as 0.1 wt% used in this work, was also determined by the isothermal TGA results of the PK nanocomposites because the PK nanocomposites containing 0.1 wt% of HP-GO showed larger residual weight % than other PK nanocomposites containing 0.05, 0.2, and 0.5 wt% of HP-GOs when they were isothermally treated at 250 ^{o}C for 2 h, as shown in Fig. 7. Since 0.1 wt% of HP-GO was found to be the most effective filler content to impart the thermal stability of PK, the PK nanocomposites from other carbon nanomaterials were also prepared using 0.1 wt%. Although the other PK nanocomposite having different carbon materials has a different optimum content showing the largest char yield, the PK nanocomposites having the larger char yield values in the isothermal TGA always exhibit the larger char yield behavior when they have the same filler content. For example, the PK nanocomposites containing HA-GO and HP-GO showed larger char yield than the PK nanocomposites containing CNT if they have the same filler content. Since the main focus of this study is the effect of the chemical structures of carbon nanomaterials as the fillers in the PK nanocomposites, all the samples were prepared using 0.1 wt% of fillers, the content in which the PK nanocomposites

containing HP-GO show maximum thermal stability.

From the isothermal TGA results, we found that the amounts of residue of the PK nanocomposites containing the carbon nanomaterials are larger than that of PK, as shown in Fig. 8. For example, the residual weight % after isothermal treatment for PK is 89.0 % and those for the PK nanocomposites containing 0.1 wt% of CNT, GO, HP-GO, and HA-GO are 90.2, 96.8, 97.9, and 98.2 %, respectively. Therefore, the carbon nanomaterials can increase the thermal-oxidative stability of the PK nanocomposites, and it is also quite obvious that carbon nanomaterials based on graphene, such as GO, HP-GO, and HA-GO, are much more effective in increasing the thermal stability of PK than CNT. Since CNTs cannot be well-dispersed in ethanol, the solvent used to prepare PK nanocomposites from the powder coating method, they cannot be effectively incorporated on the surface of PK powders, then CNTs should be agglomerated in the matrix polymer. On the contrary, GO-based nanomaterials are well-dispersed in ethanol, then the nanomaterials can be also well-dispersed in the polymer matrix. The poor and good dispersions of the CNTs and the GO-based nanomaterials, respectively, in ethanol are shown in Fig. 9. It was also found that the color of PK nanocomposite containing CNT is much darker than those containing GO-based nanomaterials, although the same amount of fillers are included, which indicates that the GO-based fillers are more well-dispersed in the

polymer matrix (Fig. 10). Therefore, the more well-dispersed GO-based nanomaterials in the polymer matrix were found to be more effective in increasing the thermal stability than the poorly dispersed CNTs. The effect of the dispersion state of the nanofillers on the physical properties, including the thermal stabilities, has also been reported previously [40-42].

In addition to the better dispersion state of GO-based nanomaterials than CNTs, the better antioxidative and barrier properties of GO than CNTs should be related to the improved thermal stabilities [34]. The antioxidant property of GO has been known to be superior to that of CNTs because GO contains abundant oxygen functional groups such as hydroxide on the surface, which can be used as additional radical scavengers in the polymer matrix. Moreover, since GO has a sheet-like structure, it can be used as barriers to heat and mass transfer in the polymer matrix and then the thermal stability of the polymer nanocomposites can be further increased [43]. The isothermal TGA curves of HP/PK and HA/PK (the PK nanocomposites containing HP and HA, respectively) in the Supporting Information further indicates the increase of the thermal stabilities of the PK nanocomposites with GO-based nanomaterials due to the barrier property of GO units with thin film shapes (Fig. 11).

Among the GO-based nanomaterials, HA-GO and HP-GO were found to be more effective heat stabilizers than GO. These results can be attributed to the

combined effect of the grafted antioxidants (hindered phenol and hindered amine) and the GO units. Although GOs have antioxidant ability by a free radical scavenging mechanism, the radical scavenging efficiency could be increased by the introduction of antioxidant groups to GO due to the formation of the excellent dispersion of GOs in the polymer matrix and the addition of other radical scavengers such as hindered phenol and hindered amine, which can react with various kinds of free radicals generated in the polymer matrix [9, 11, 13, 43]. A schematic illustration of the antioxidant mechanism for the PK nanocomposites containing the antioxidant grafted GOs is shown in Fig. 12.

Mechanical properties

The mechanical properties of PK were found to be improved by the addition of the carbon nanomaterials, as shown in Fig. 13; tensile strength, Young's modulus, and elongation at break values of the PK nanocomposites are always larger than those of PK. For example, the tensile strength value of PK was found to increase from 56.1 MPa to 59.9, 62.4, 67.8, and 67.6 MPa and Young's modulus of the PK was also found to increase from 1022 MPa to 1059, 1138, 1213, and 1214 MPa by adding 0.1 wt% of HA-GO, CNT, GO, and HP-GO, respectively. Therefore, it was also found that the tensile strength and Young's modulus values of CNT/PK,

GO/PK, and HP-GO/PK are larger than those of HA-GO/PK. As mentioned above, HA-GO contains larger contents of the flexible organic moieties than HP-GO, and CNT and GO do not have any flexible organic moieties [44]. Therefore, the smallest increase of the tensile strength and Young's modulus values of HA-GO/PK could be ascribed to the largest amount of flexible organic moieties in the matrix. Although the content difference of the organic moieties between HA-GO and HP-GO is only 1 wt%, the mechanical strength values of HP-GO/PK are quite larger than those of HA-GO/PK because HP-GO contains larger content of rigid conjugated carbon units; more oxygen functional groups in HP-GO could be reduced because HP-GO is prepared using a longer reaction time (3 days) than HA-GO (12 h). Others also reported that the polymer nanocomposites containing more oxidized GOs have the smaller mechanical strength values [45-47]. Therefore, the carbon nanomaterials can increase the mechanical strength of the PK, while CNT, GO, and HP-GO having a relatively larger content of rigid conjugated carbon units are more effective than HA-GO in increasing the mechanical strength of PK. In addition, the reinforcing efficiency of GO and HP-GO is higher than that of CNT due to the better dispersion state of GO and HP-GO than CNT, indicating that both the rigidity and dispersion state of fillers are related to the improved mechanical strength of polymer nanocomposites.

The elongation at break value of the PK nanocomposite with HA-GO was

found to be larger than the other PK nanocomposites; the elongation at break values of PK, CNT/PK, GO/PK, HP-GO/PK, and HA-GO/PK are 17.5, 18.5, 21.2, 21.4, and 23.3 %, respectively. Obviously, HA-GO/PK and HP-GO/PK having the flexible organic moieties show the larger elongation at break values than the other GO/PK and CNT/PK. The modulus of toughness was calculated using the area under the stress-strain curve to further study the effect of the carbon nanomaterials on the physical property (Table 2). Similar to the elongation at break, the PK nanocomposites have larger modulus of toughness values than PK, and HA-GO/PK and HP-GO/PK show larger modulus of toughness than GO/PK and CNT/PK. For example, the modulus toughness of PK was also found to increase from 780 MJ/m^3 to 900, 1050, 1140, and 1120 MJ/m^3 by adding 0.1 wt% of CNT, GO, HP-GO, and HA-GO, respectively. Similar to the thermal stability behavior, it is obvious that GO-based nanomaterials are more effective than CNT to increase the toughness of PK. Since GO-based filler materials are more well-dispersed in the matrix polymer than CNT, the effective load transfer and energy dissipation at the interface between the fillers and the PK matrix are possible, which can lead to improve the toughness of PK. The better dispersion state of the GO-based filler materials was also confirmed by the SEM images. The agglomerates of CNTs in the PK matrix are clearly observed in the CNT/PK, while any obvious aggregates of the GO-based fillers could not be observed, which might explain the larger

elongation at break values of the PK nanocomposites with GO-based fillers than that of CNT/PK (Fig. 14). Among the GO-based nanomaterials, HA-GO and HP-GO were found to be the more effective fillers for increasing the toughness of PK (Fig. 15). This can be explained by the strong interfacial interactions between the ketone groups in PK and organic functional groups, such as hindered amine and hindered phenol, in HA-GO and HP-GO, respectively. Although GO has good interfacial interaction with PK due to the oxygen functional groups in GO, since HA-GO and HP-GO contain additional surface functional groups, larger interfacial interactions between HA-GO or HP-GO and the PK matrix could be expected. Similarly, it was reported that when GO derivatives containing organic functional groups that have a specific interaction with the polymer matrix were used as fillers for polymer nanocomposites, they could increase the toughness of polymers [14, 46].

Since HP-GO and HA-GO were found to be very effective nanofiller materials to improve both of the thermal stability and the mechanical property, further studies on observing the changes of the mechanical properties by heat treatment were carried out. Fig. 16 shows the strain-stress curves of PK and HP-GO/PK before and after the thermal treatment at 200 ^{o}C for 24 h. Large decreases in tensile strength, Young's modulus, and the elongation at break were observed from PK. On the contrary, HP-GO/PK shows a smaller decrease of the elongation at break

value, and the tensile strength and Young's modulus do not change significantly after the thermal treatment. Therefore, the antioxidant grafted GOs can also improve the mechanical properties of PK after exposure at the high temperature condition.

3.4. Conclusion

The thermal stabilities and mechanical properties of PK were found to be much improved by adding a small amount of antioxidant (hindered amine and hindered phenol) grafted GOs. The antioxidant grafted GOs in the PK nanocomposites can increase the mechanical properties because organic functional groups in the GOs can increase the interfacial interactions between the fillers and the polymer matrix, then the homogeneously dispersed rigid conjugated carbon units in GOs can increase the mechanical strength of the polymers. The remarkably enhanced thermal stability of the PK nanocomposites could be ascribed to the antioxidant properties of the grafted antioxidants and the barrier property of GOs having ultrathin sheet shapes. Therefore, the antioxidant grafted GOs were found to be very effective filler materials for increasing the interactions with the polymeric material to improve the mechanical and thermal properties simultaneously.

3.5. References

[1] Ma J, Meng QS, Michelmore A, Kawashima N, Izzuddin Z, Bengtsson C, et al. Covalently bonded interfaces for polymer/graphene composites. J Mater Chem A. 2013;1(13):4255-64.

[2] Young RJ, Kinloch IA, Gong L, Novoselov KS. The mechanics of graphene nanocomposites: A review. Compos Sci Technol. 2012;72(12):1459-76.

[3] Sengupta R, Bhattacharya M, Bandyopadhyay S, Bhowmick AK. A review on the mechanical and electrical properties of graphite and modified graphite reinforced polymer composites. Prog Polym Sci. 2011;36(5):638-70.

[4] Salavagione HJ, Martinez G, Ellis G. Recent advances in the covalent modification of graphene with polymers. Macromol rapid comm. 2011;32(22):1771-89.

[5] Potts JR, Dreyer DR, Bielawski CW, Ruoff RS. Graphene-based polymer nanocomposites. Polymer. 2011;52(1):5-25.

[6] Spitalsky Z, Tasis D, Papagelis K, Galiotis C. Carbon nanotube–polymer composites: Chemistry, processing, mechanical and electrical properties. Prog Polym Sci. 2010;35(3):357-401.

[7] Kim H, Abdala AA, Macosko CW. Graphene/Polymer Nanocomposites.

Macromolecules. 2010;43(16):6515-30.

[8] Moniruzzaman M, Winey KI. Polymer nanocomposites containing carbon nanotubes. Macromolecules. 2006;39(16):5194-205.

[9] Watts PCP, Fearon PK, Hsu WK, Billingham NC, Kroto HW, Walton DRM. Carbon nanotubes as polymer antioxidants. J Mater Chem. 2003;13(3):491-5.

[10] Shi X, Jiang B, Wang J, Yang Y. Influence of wall number and surface functionalization of carbon nanotubes on their antioxidant behavior in high density polyethylene. Carbon. 2012;50(3):1005-13.

[11] Goncalves G, Marques PAAP, Barros-Timmons A, Bdkin I, Singh MK, Emami N, et al. Graphene oxide modified with PMMA via ATRP as a reinforcement filler. J Mater Chem. 2010;20(44):9927-34.

[12] Dintcheva NT, Arrigo R, Gambarotti C, Carroccio S, Filippone G, Cicogna F, et al. α-Tocopherol-induced radical scavenging activity in carbon nanotubes for thermo-oxidation resistant ultra-high molecular weight polyethylene-based nanocomposites. Carbon. 2014;74:14-21.

[13] Shi X, Wang J, Jiang B, Yang Y. Hindered phenol grafted carbon nanotubes for enhanced thermal oxidative stability of polyethylene. Polymer. 2013;54(3):1167-76.

[14] Lim M-Y, Kim HJ, Baek SJ, Kim KY, Lee S-S, Lee J-C. Improved

strength and toughness of polyketone composites using extremely small amount of polyamide 6 grafted graphene oxides. Carbon. 2014;77:366-78.

[15] Zehetmaier PC, Vagin SI, Rieger B. Functionalization of aliphatic polyketones. MRS Bull. 2013;38(03):239-44.

[16] Sommazzi A, Garbassi F. Olefin carbon monoxide copolymers. Prog Polym Sci. 1997;22(8):1547-605.

[17] Drent E, Budzelaar PHM. Palladium-catalyzed alternating copolymerization of alkenes and carbon monoxide. Chem rev. 1996;96(2):663-81.

[18] Garbassi F, Sommazzi A, Meda L, Mestroni G, Sciutto A. Surface properties of alternated aliphatic polyketones. Polymer. 1998;39(6-7):1503-6.

[19] Chien JCW, Zhao AX. Thermolysis of alternating ethylene-carbon monoxide copolymer. Polym Degrad Stabil. 1993;40(2):257-61.

[20] De Vito S, Ciardelli F, Ruggeri G, Chiantore O, Moro A. Thermal degradation of ethylene carbon monoxide alternating copolymer under inert atmosphere. Polym Int. 1998;45(4):353-65.

[21] Conti G, Sommazzi A. Thermal-Degradation of Polyketones - Vibrational Spectroscopy Studies. J Mol Struct. 1993;294:275-8.

[22] Hummers WS, Offeman RE. Preparation of Graphitic Oxide. J Am Chem Soc. 1958;80(6):1339-.

[23] Shim J, Kim, D.-G., Kim, H.J., Lee, J.H., Baik, J.-H., Lee, J.-C. . Novel

composite polymer electrolytes containing poly(ethyelene glycol)-grafted graphene oxide for all-solid-sate lithium-ion battery applications. J Mater Chem A. 2014;2:13873.

[24] Yoonessi M GJR. Highly conductive multifunctional graphene polycarbonate nanocomposites. Acs Nano. 2010;4(12):7211-20.

[25] Kalaitzidou K, Fukushima H, Drzal LT. A new compounding method for exfoliated graphite–polypropylene nanocomposites with enhanced flexural properties and lower percolation threshold. Compos Sci Technol. 2007;67(10):2045-51.

[26] Dong J, Weng J, Dai L. The effect of graphene on the lower critical solution temperature of poly(N-isopropylacrylamide). Carbon. 2013;52:326-36.

[27] Chen Z, Lu H. Constructing sacrificial bonds and hidden lengths for ductile graphene/polyurethane elastomers with improved strength and toughness. J Mater Chem. 2012;22(25):12479.

[28] Cano M, Khan U, Sainsbury T, O'Neill A, Wang Z, McGovern IT, et al. Improving the mechanical properties of graphene oxide based materials by covalent attachment of polymer chains. Carbon. 2013;52:363-71.

[29] Xu Z, Gao C. In situPolymerization Approach to Graphene-Reinforced Nylon-6 Composites. Macromolecules. 2010;43(16):6716-23.

[30] Zhang XQ, Fan XY, Li HZ, Yan C. Facile preparation route for graphene

oxide reinforced polyamide 6 composites via in situ anionic ring-opening polymerization. J Mater Chem. 2012;22(45):24081-91.

[31] Stankovich S, Dikin DA, Piner RD, Kohlhaas KA, Kleinhammes A, Jia Y, et al. Synthesis of graphene-based nanosheets via chemical reduction of exfoliated graphite oxide. Carbon. 2007;45(7):1558-65.

[32] Li J, Xiao GY, Chen CB, Li R, Yan DY. Superior dispersions of reduced graphene oxide synthesized by using gallic acid as a reductant and stabilizer. J Mater Chem A. 2013;1(4):1481-7.

[33] Jiang X, Drzal LT. Exploring the potential of exfoliated graphene nanoplatelets as the conductive filler in polymeric nanocomposites for bipolar plates. J Power Sources. 2012;218:297-306.

[34] Hu W, Zhan J, Wang X, Hong N, Wang B, Song L, et al. Effect of Functionalized Graphene Oxide with Hyper-Branched Flame Retardant on Flammability and Thermal Stability of Cross-Linked Polyethylene. Ind Eng Chem. 2014;53(8):3073-83.

[35] Du BX, Ma HY, Fang ZP. How nano-fillers affect thermal stability and flame retardancy of intumescent flame retarded polypropylene. Polym Advan Technol. 2011;22(7):1139-46.

[36] Du BX, Fang ZP. Effects of carbon nanotubes on the thermal stability and flame retardancy of intumescent flame-retarded polypropylene. Polym Degrad

Stabil. 2011;96(10):1725-31.

[37] Xie W, Heltsley R, Cai XH, Deng FQ, Liu JM, Lee C, et al. Study of stability of high-temperature polyimides using TG/MS technique. J Appl Polym Sci. 2002;83(6):1219-27.

[38] Hu WZ, Zhan J, Wang X, Hong NN, Wang BB, Song L, et al. Effect of Functionalized Graphene Oxide with Hyper-Branched Flame Retardant on Flammability and Thermal Stability of Cross-Linked Polyethylene (vol 53, pg 3073, 2014). Ind Eng Chem. 2014;53(13):5622-.

[39] Schmid M, Affolter S. Interlaboratory tests on polymers by differential scanning calorimetry (DSC): determination and comparison of oxidation induction time (OIT) and oxidation induction temperature (OIT). Polym Test. 2003;22(4):419-28.

[40] Cao Y, Feng J, Wu P. Alkyl-functionalized graphene nanosheets with improved lipophilicity. Carbon. 2010;48(5):1683-5.

[41] Cao Y, Lai Z, Feng J, Wu P. Graphene oxide sheets covalently functionalized with block copolymersvia click chemistry as reinforcing fillers. J Mater Chem. 2011;21(25):9271-8.

[42] Verdejo R, Bernal MM, Romasanta LJ, Lopez-Manchado MA. Graphene filled polymer nanocomposites. J Mater Chem. 2011;21(10):3301-10.

[43] Gensler R, Plummer CJG, Kausch HH, Kramer E, Pauquet JR, Zweifel H.

Thermo-oxidative degradation of isotactic polypropylene at high temperatures: phenolic antioxidants versus HAS. Polym Degrad Stabil. 2000;67(2):195-208.

[44] Chen L, Chai S, Liu K, Ning N, Gao J, Liu Q, et al. Enhanced epoxy/silica composites mechanical properties by introducing graphene oxide to the interface. ACS Appl Mater Interfaces. 2012;4(8):4398-404.

[45] Shen X, Lin XY, Yousefi N, Jia JJ, Kim JK. Wrinkling in graphene sheets and graphene oxide papers. Carbon. 2014;66:84-92.

[46] X. W, M. S. Toughening of polymers by graphene. Nanomaterials and energy. 2013;2:265.

[47] Wang X, Jin J, Song M. An investigation of the mechanism of graphene toughening epoxy. Carbon. 2013;65:324-33.

Table 3.1 Thermal properties of PK nanocomposites

Sample	$T_{d,5\%}$ (ºC)[a]	Char yield at 600 ^{o}C (%)
PK	301.7	27.9
HP-GO/PK	318.0	23.6
HA-GO/PK	340.5	20.6
GO/PK	308.6	25.6
CNT/PK	301.1	26.1

[a]The decomposition temperature ($T_{d,5\%}$) is defined as 5 wt % loss.

Table 3.2 Mechanical properties of PK nanocomposites and the pristine PK

Sample	Tensile strength (MPa)	Young's modulus (MPa)	Elongation at break (%)	Modulus of toughness (MJ/m^3)
PK	56.1±0.6	1022±42	17.5±0.7	780±25
HP-GO/PK	67.6±0.4	1214±35	21.4±1.2	1140±27
HA-GO/PK	59.9±0.4	1059±37	23.3±0.9	1120±38
GO/PK	67.8±1.3	1213±20	21.2±2.5	1050±56
CNT/PK	62.4±1.4	1138±39	18.5±3.3	900±39

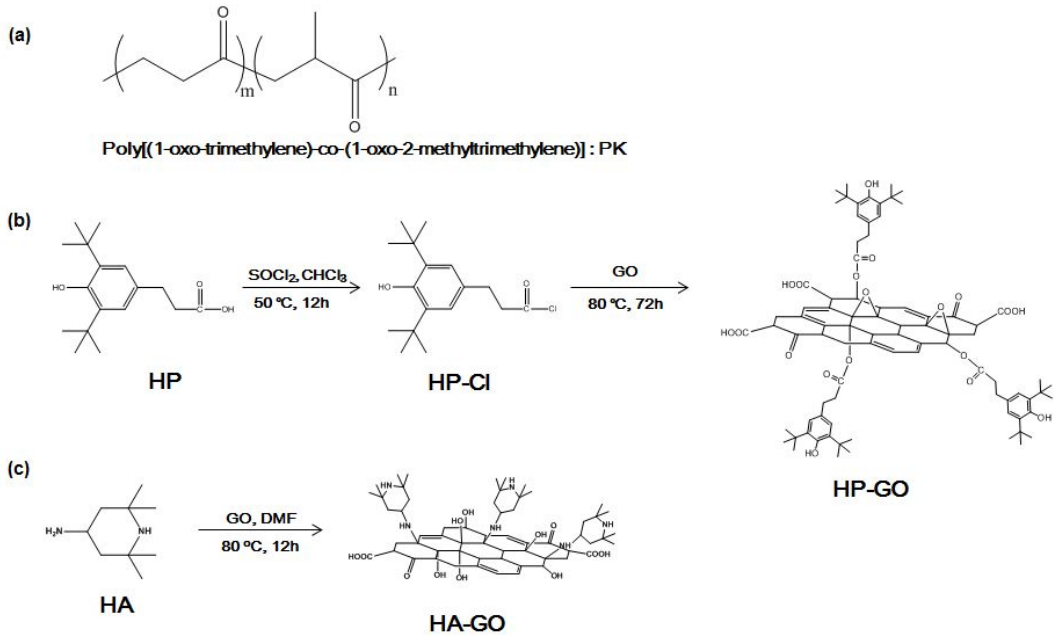

Fig. 3.1 Chemical structure of (a) PK and schematic of (b) the preparation HP-GO and (c) HA-GO

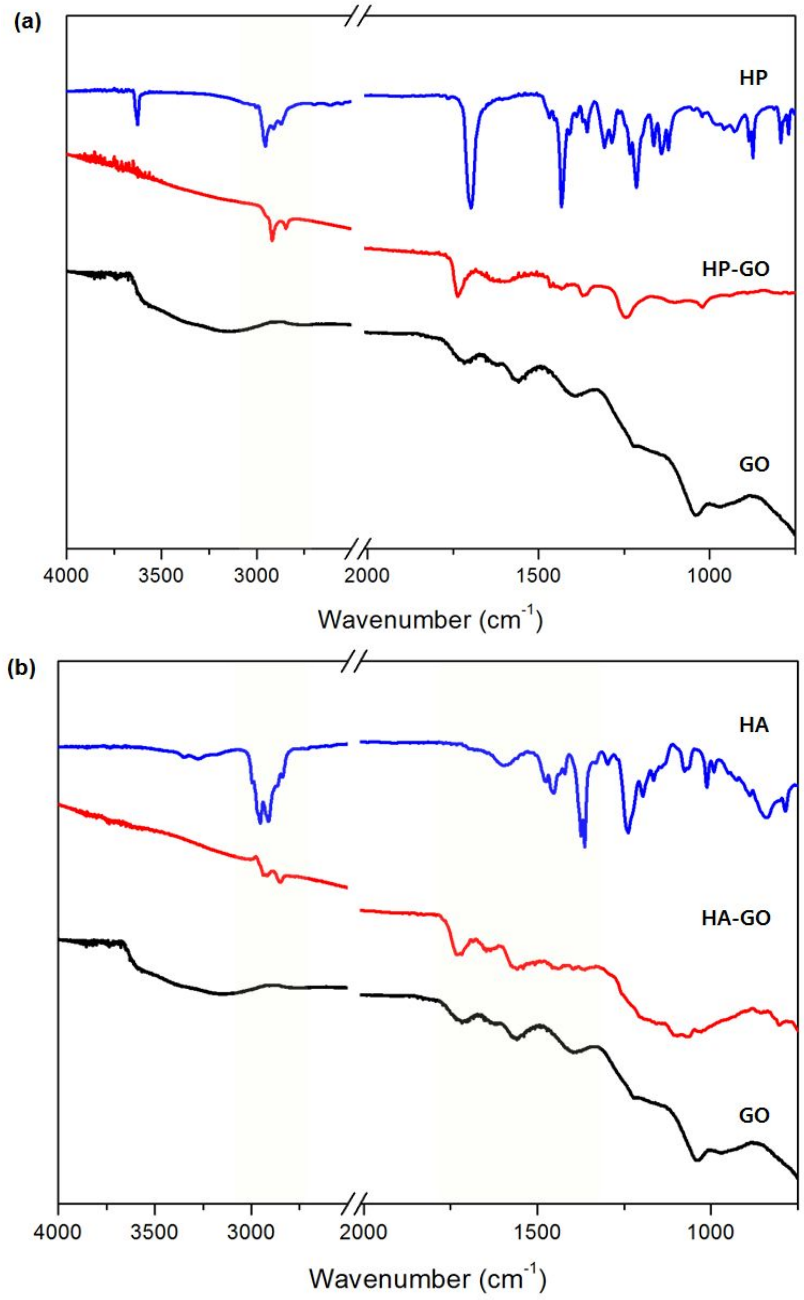

Fig. 3.2 FT-IR spectra of (a) GO, HP, and HP-GO, and (b) GO, HA, and HA-GO

(a)

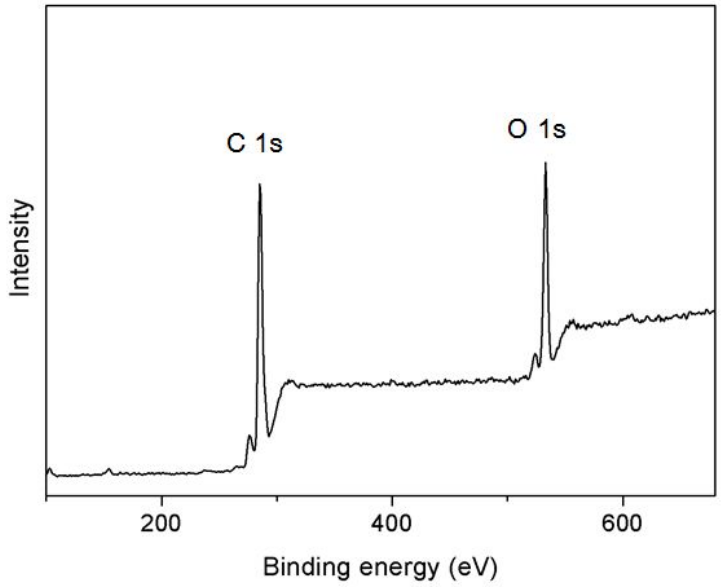

(b)

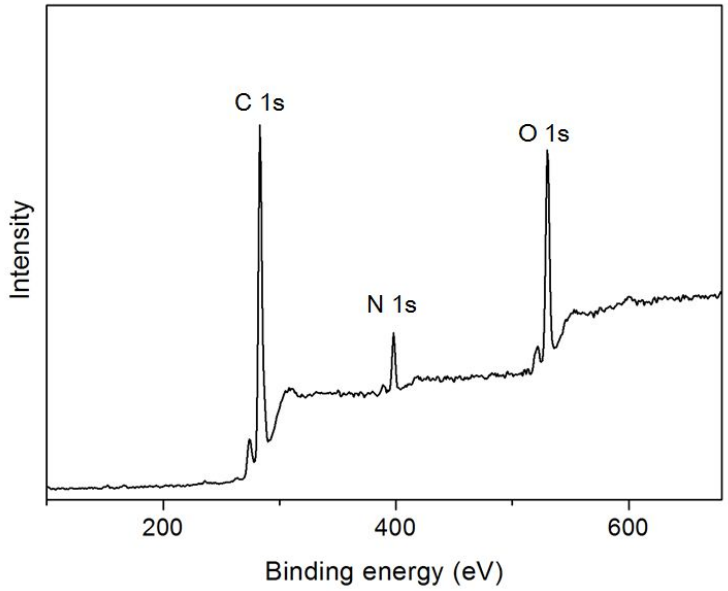

Fig. 3.3 XPS spectra of (a) HP-GO and (b) HA-GO

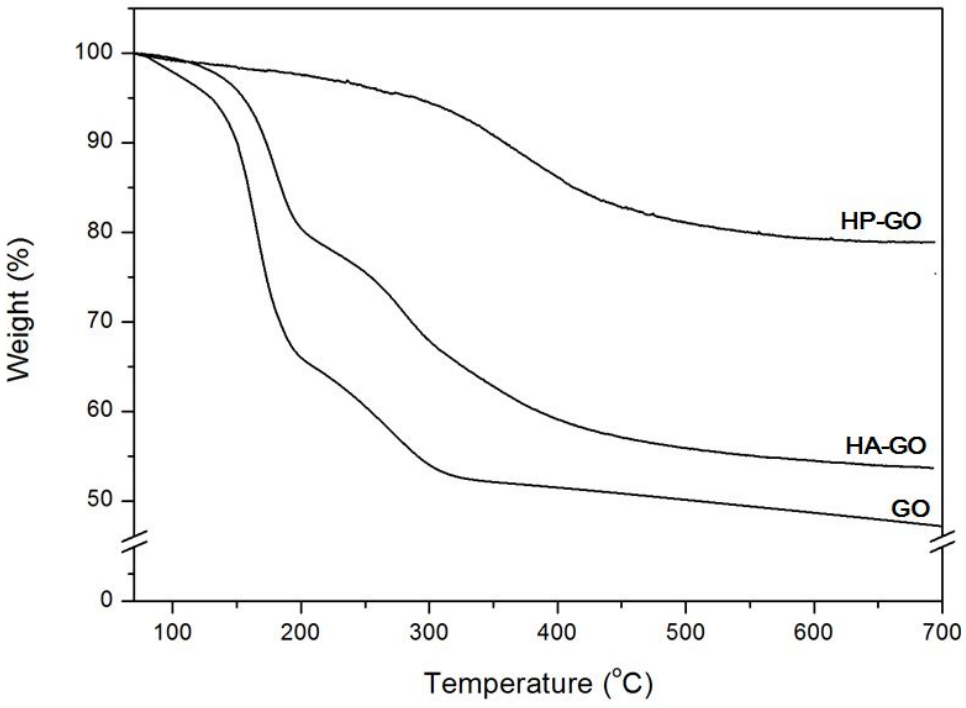

Fig. 3.4 TGA curves of GO, HP-GO, and HA-GO

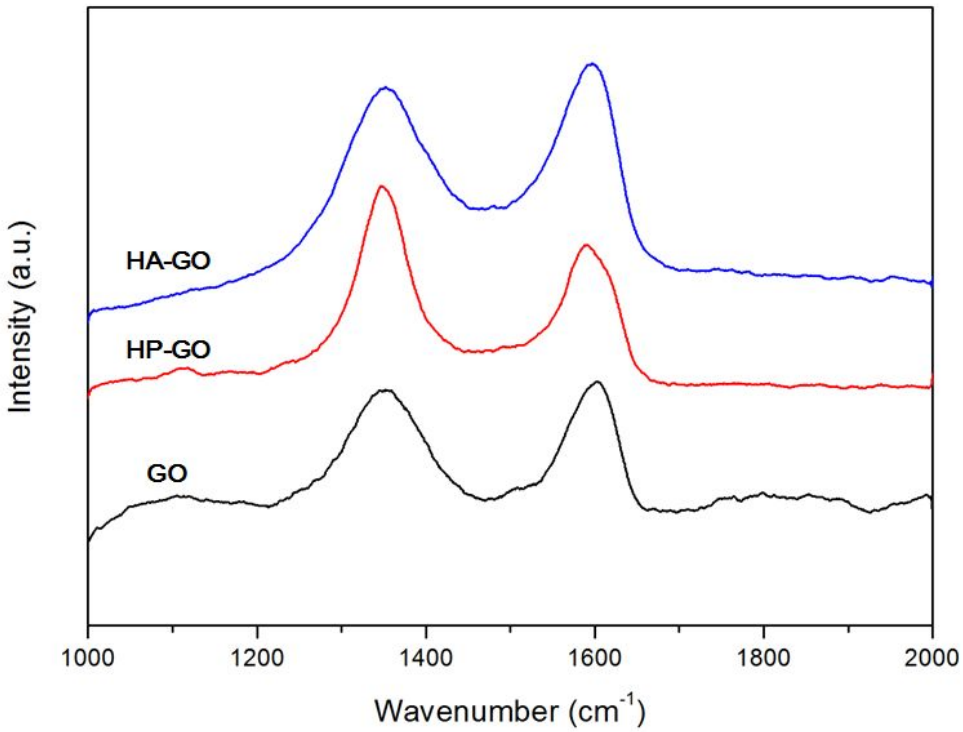

Fig. 3.5 Raman spectra of GO, HA-GO, and HP-GO

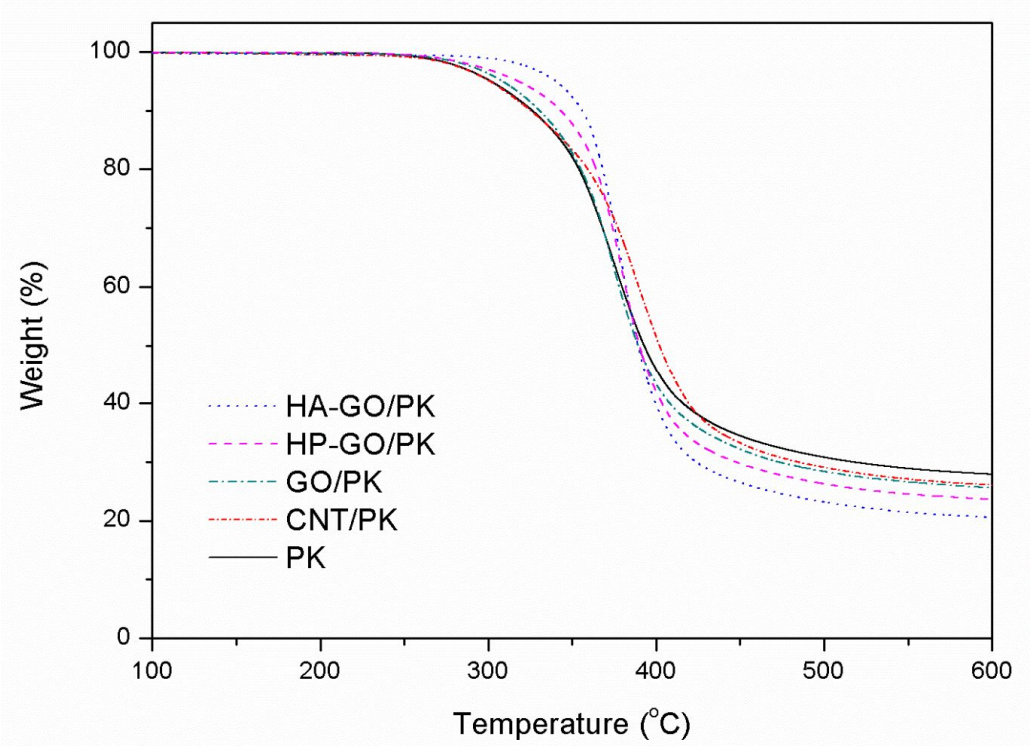

Fig. 3.6 TGA curves of the PK nanocomposites

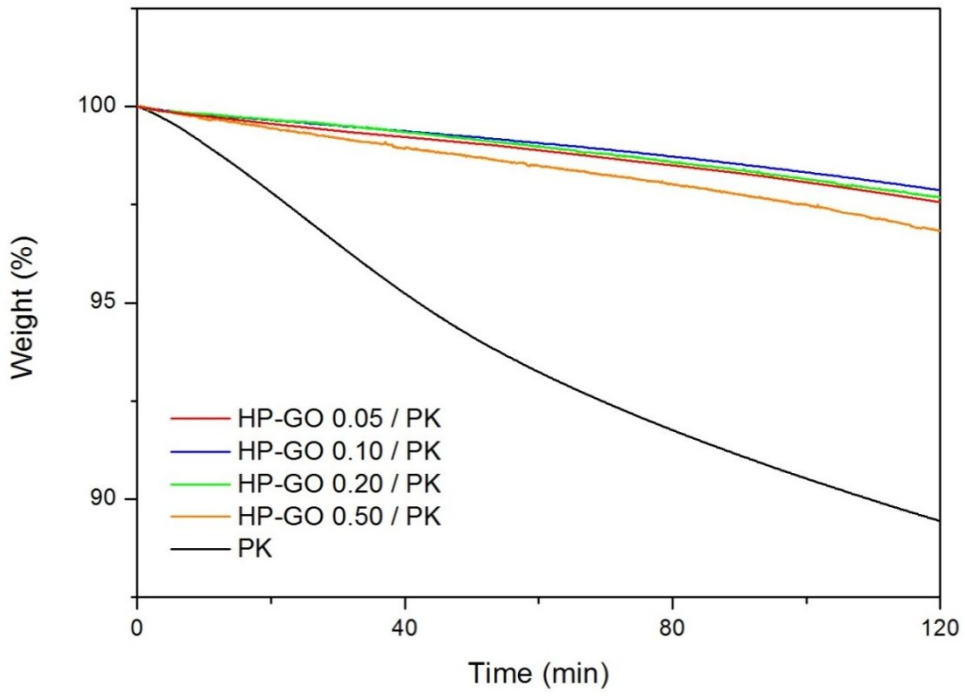

Fig. 3.7 Isothermal TGA curves (at 250 °C) of PK nanocomposite with HP-GO and the pristine PK

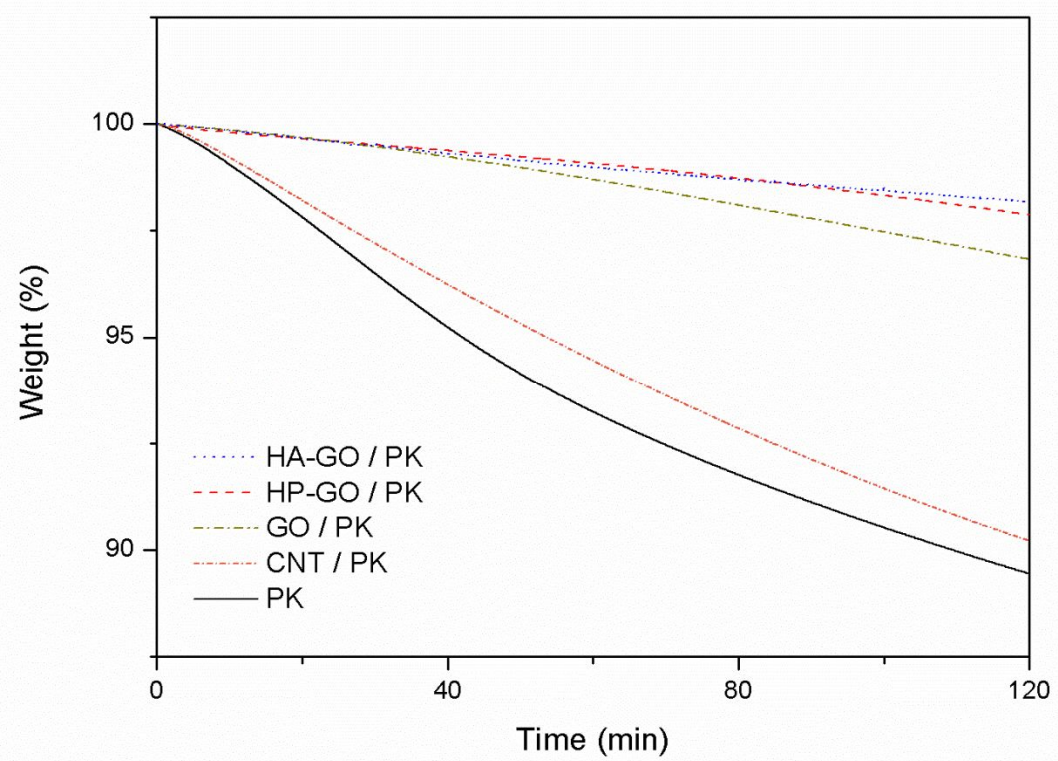

Fig. 3.8 Isothermal TGA curves (at 250 °C) of PK nanocomposites and the pristine PK

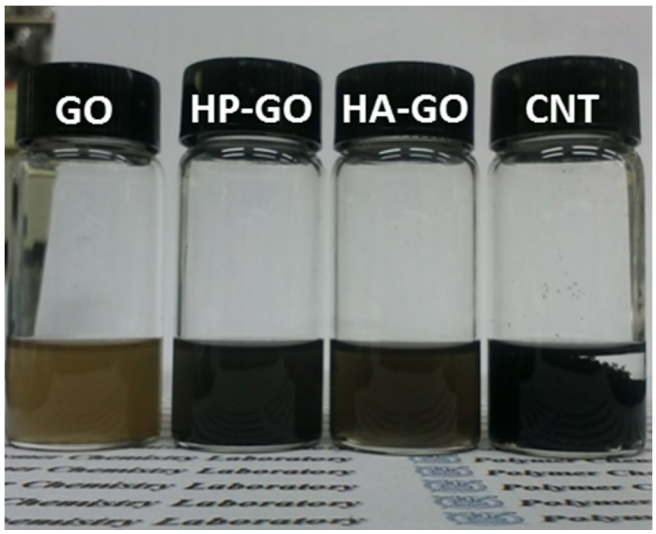

Fig. 3.9 Photographs of dispersions of the carbon nanomaterials in ethanol

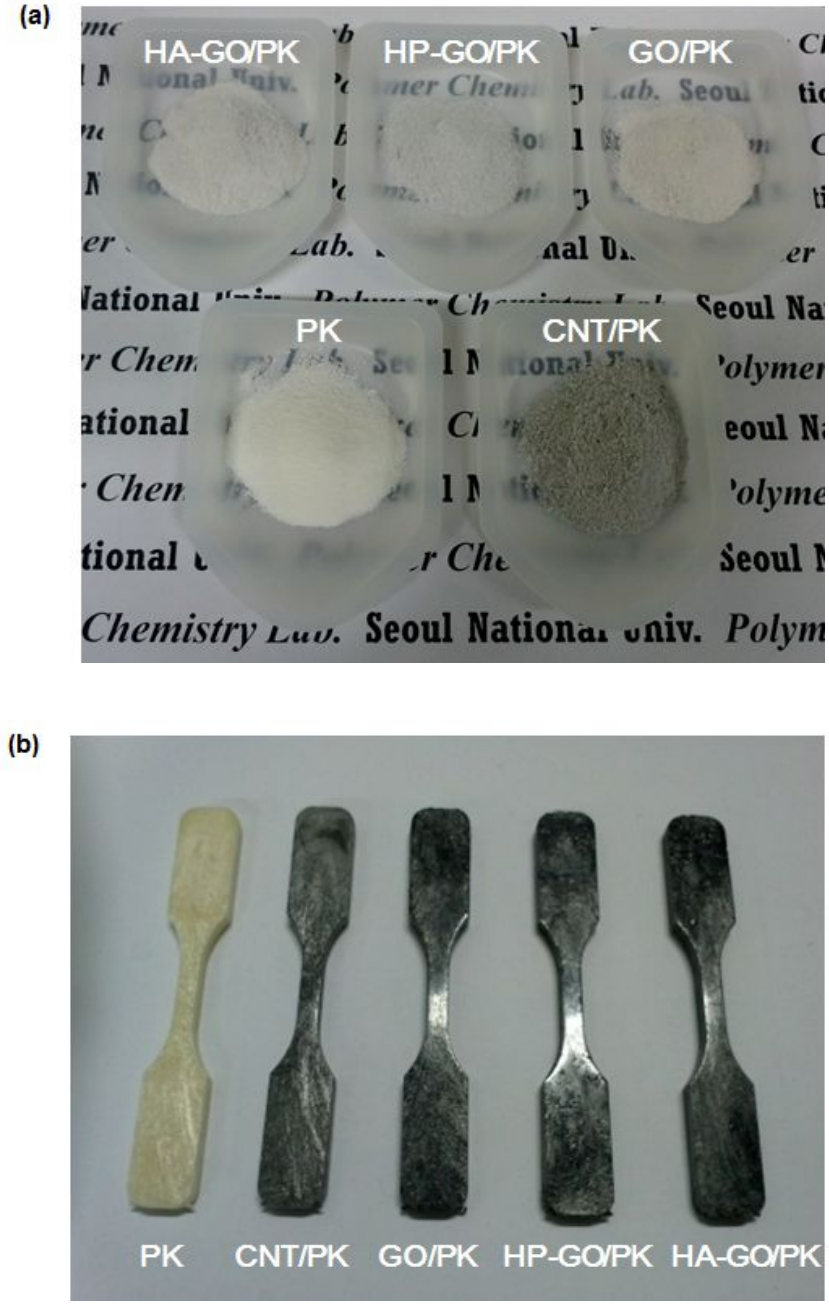

Fig. 3.10 Photographs of (a) PK nanocomposites and (b) the samples for UTM test

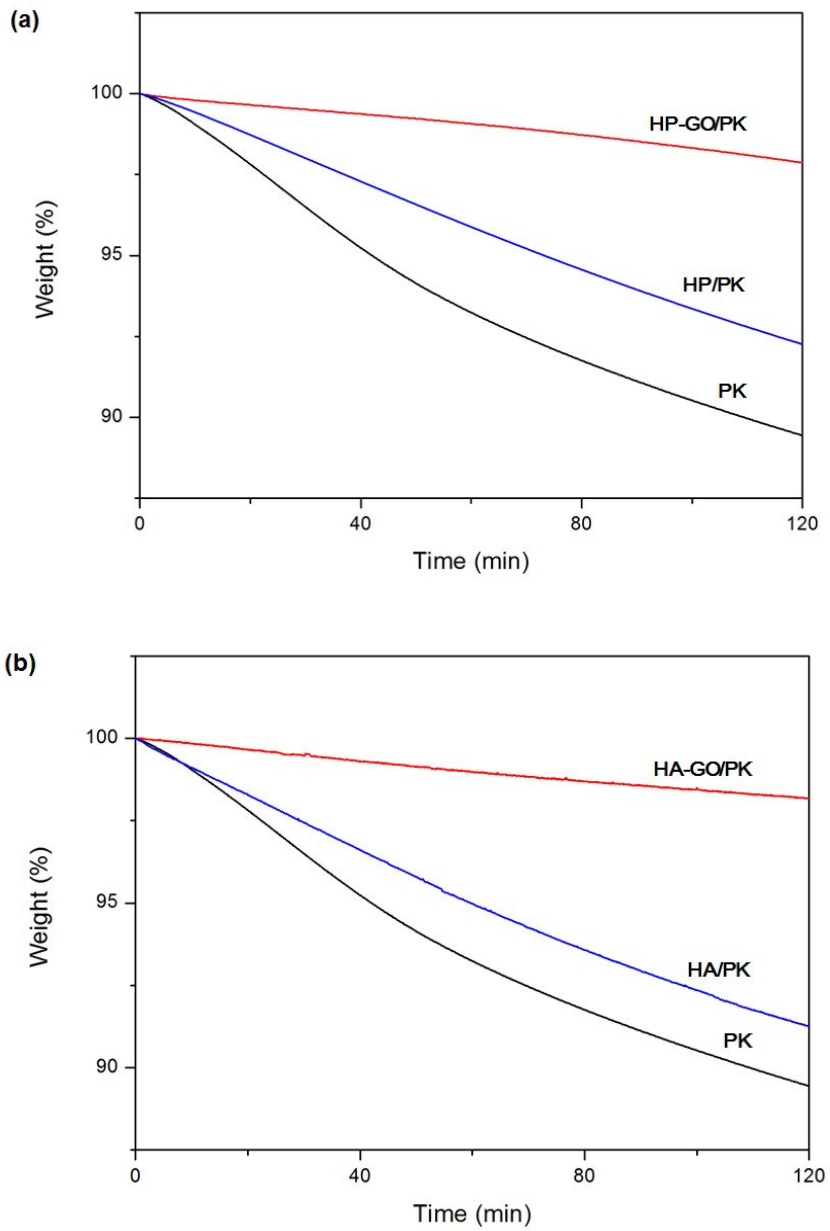

Fig. 3.11 Isothermal TGA curves (at 250 ºC) of (a) PK and PK nanocomposites with HP-GO and HP, and (b) PK and PK nanocomposite with HA-GO and HA

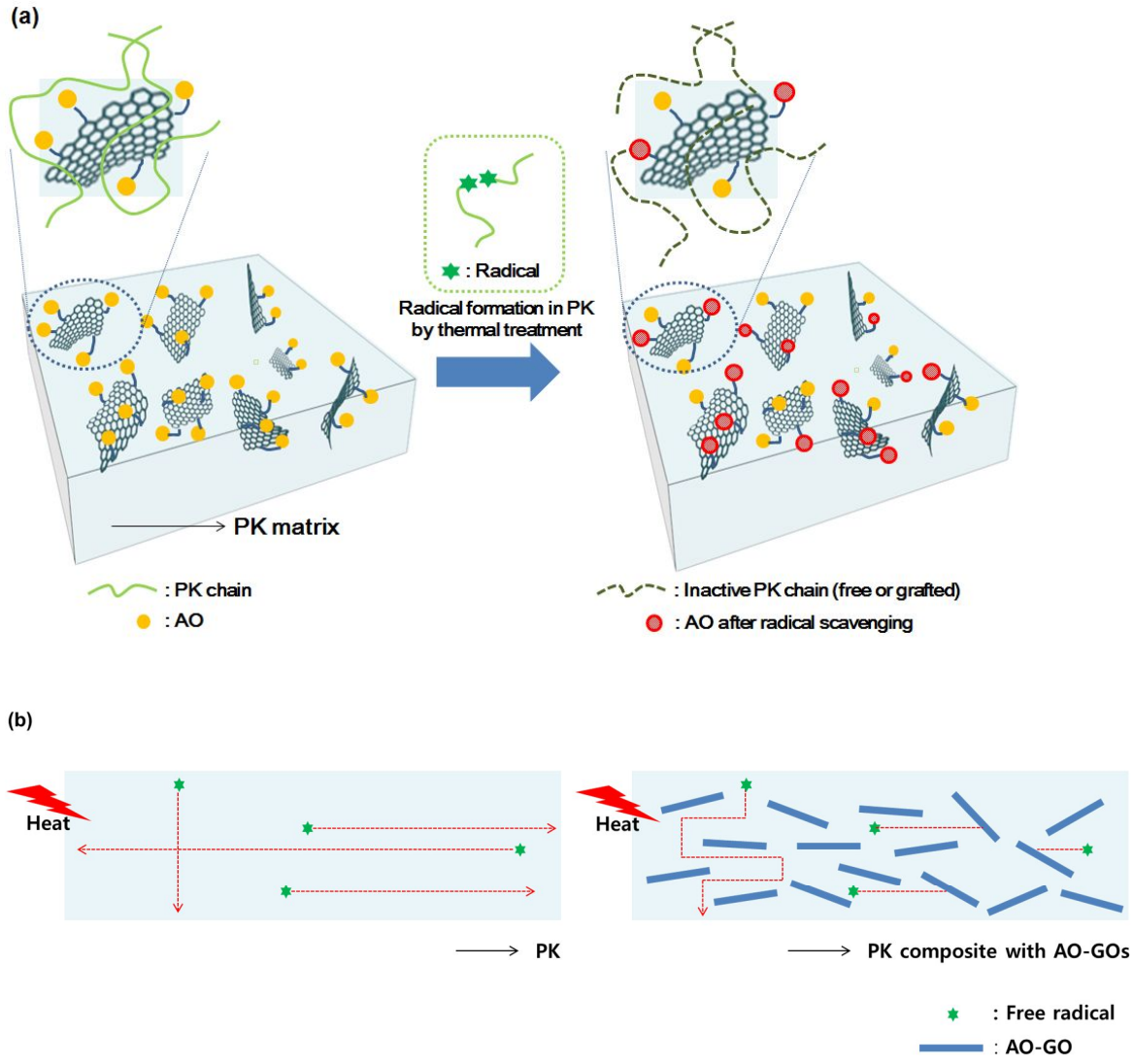

Fig. 3.12 Schematic illustration of the antioxidant mechanism of AO-GOs: (a) formation of inactive polymer chains by radical scavenging of GO and the antioxidant and (b) barrier effect of AO-GOs in PK matrix

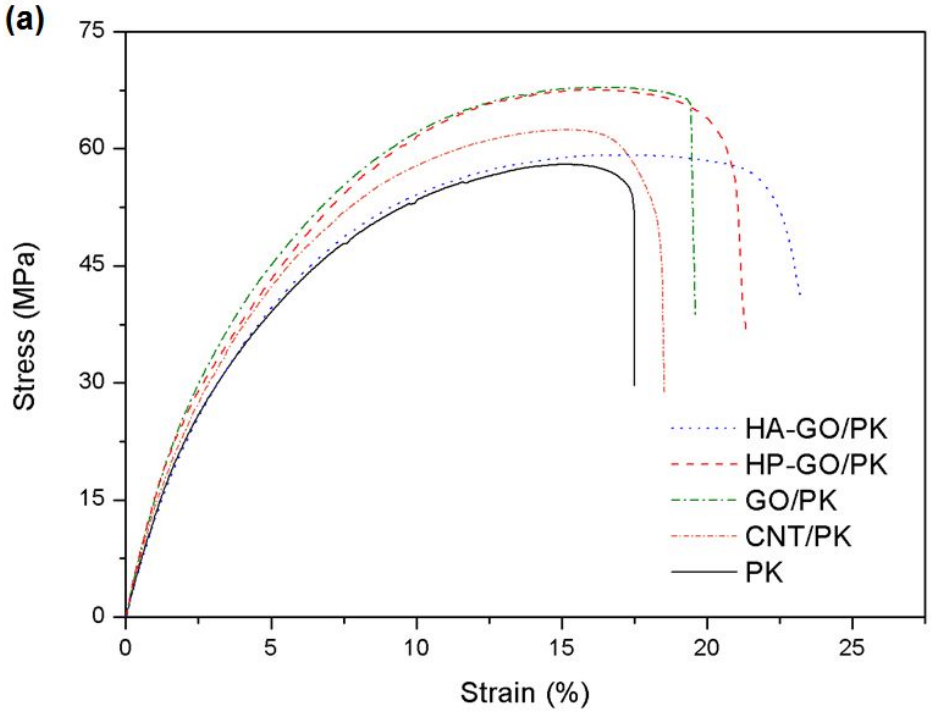
(a)
Stress (MPa)
Strain (%)
0
15
30
45
60
75
0
5
10
15
20
25
HA-GO/PK
HP-GO/PK
GO/PK
CNT/PK
PK

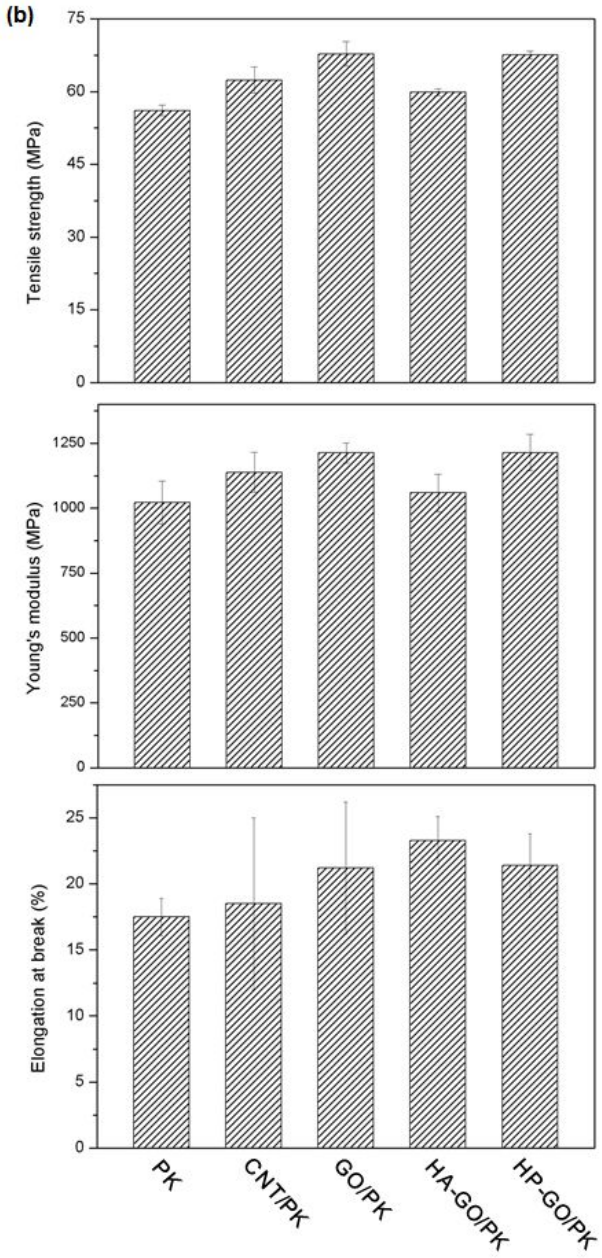

Fig. 3.13 (a) Stress-strain curves and (b) mechanical properties of PK nanocomposites and the pristine PK

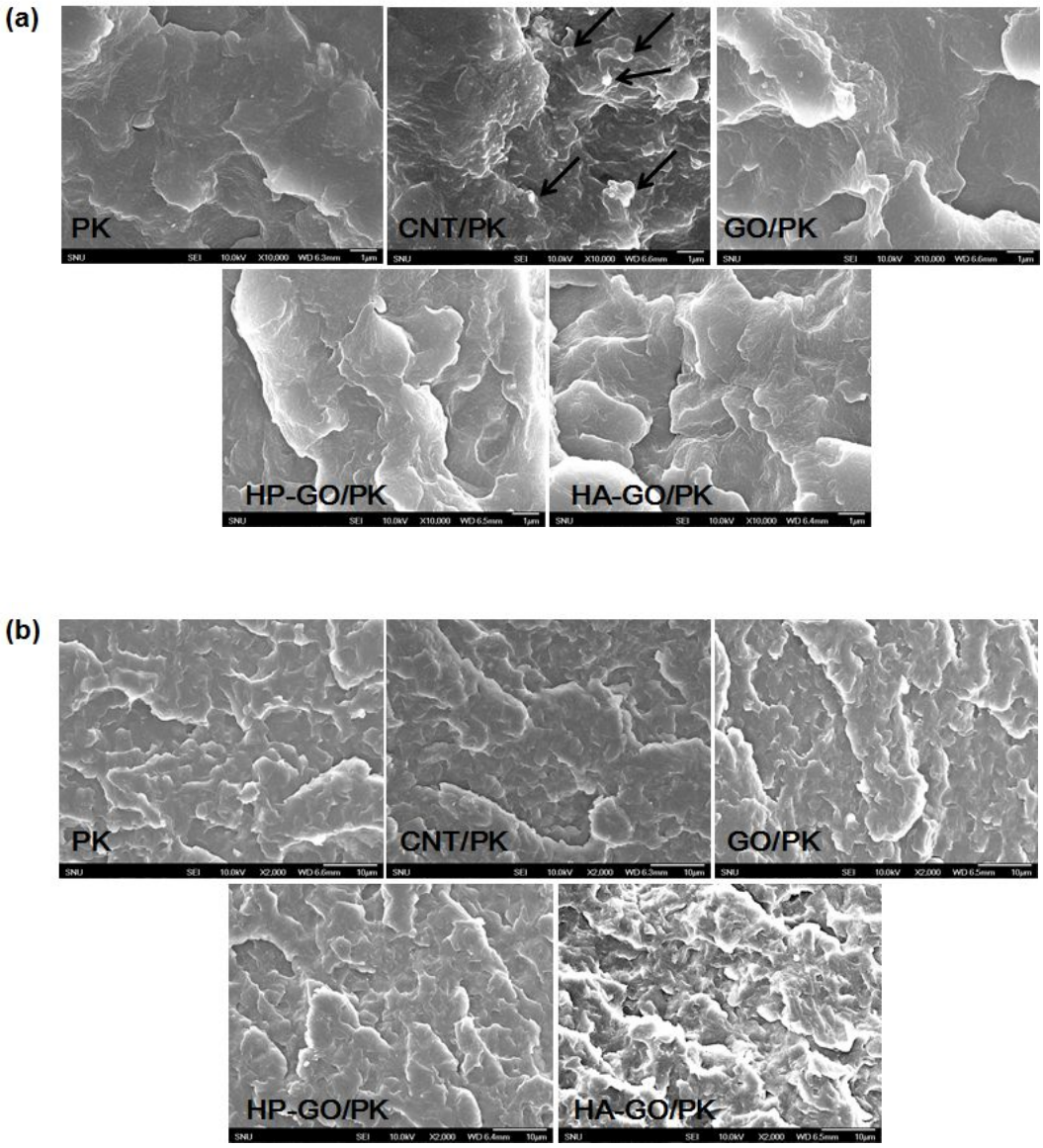

Fig. 3.14 SEM images of fractured surface of PK and PK nanocomposites (a) at high and (b) low magnification

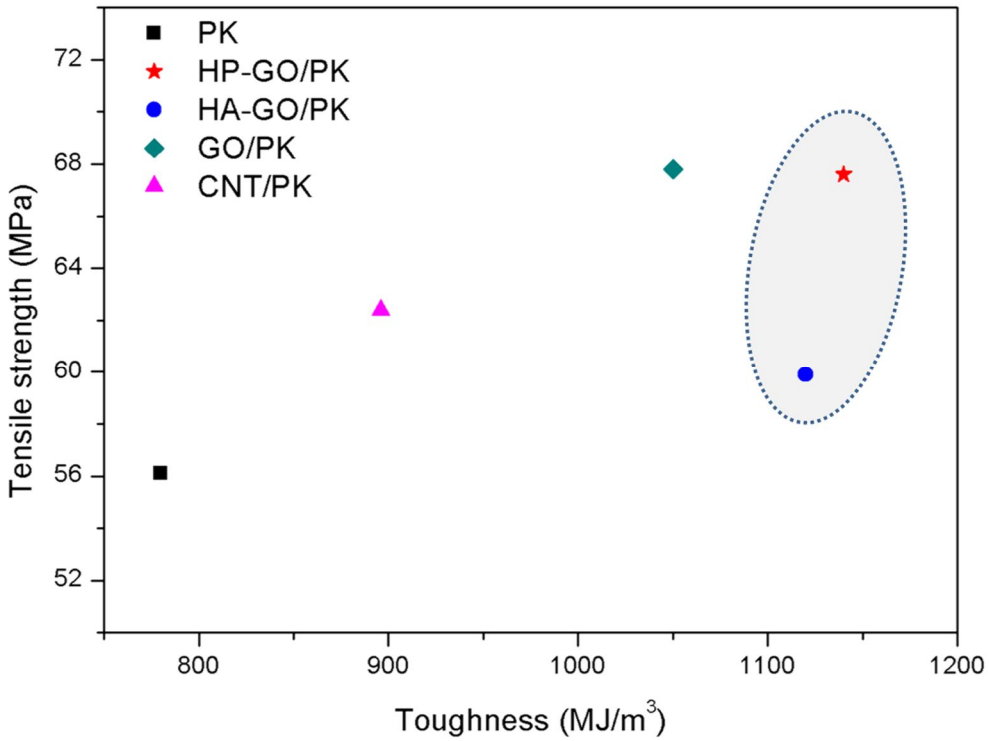

Fig. 3.15 Comparison of tensile strength and toughness of PK nanocomposites and the pristine PK

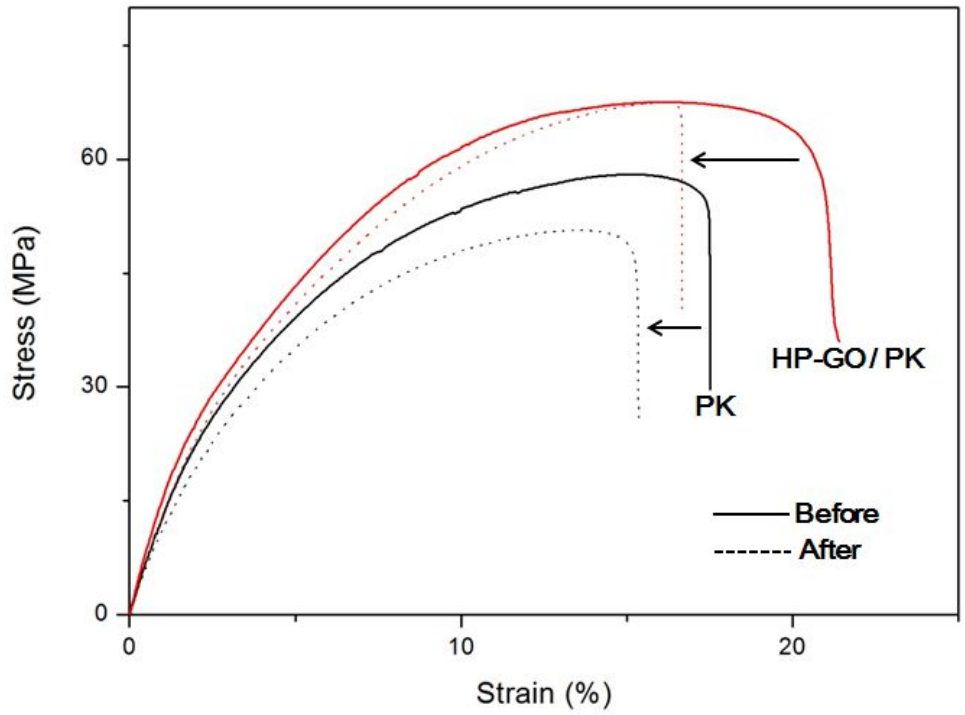

Fig. 3.16 Stress-strain curves of PK nanocomposites and the pristine PK before and after the heat exposure

Chapter 4

Poly(vinyl alcohol) nanocomposites containing reduced graphene oxide coated with tannic acid for humidity sensor

4.1. Introduction

Graphene, a single layered two-dimensional atomic carbon sheet, has drawn much attention for scientific interests and industrial applications because it has outstanding mechanical, thermal, and electrical properties [1-6]. Accordingly, it has great potential for use in a wide range of possible applications such as sensors, energy storage, nanoelectronics, and polymer nanocomposites [2, 3, 7-15]. In particular, polymer nanocomposites containing graphene or graphene derivatives have been widely studied over the past few years because the addition of only a very small amount of graphene derivatives as fillers can improve the performances of the polymers very much [7, 8, 10, 11, 14]. However, the poor dispersion of graphene in the polymer limits its practical application for the polymer nanocomposites; most of the polymers having polar functional groups are not practically miscible with the strongly non-polar graphene [16, 17]. Therefore, graphene was modified to increase the miscibility with the polymers using various approaches. For example, graphene oxide (GO) having oxygen functional groups was reacted with organic molecules followed by the reduction of the GO to produce functionalized graphene or functionalized reduced GO [1, 4, 5]. Recently, functionalized graphene was also prepared by a one-step modification and

reduction process using natural compounds such as dopamine, gallic acid, tannic acid, and tea polyphenol [18-25]. Especially, tannic acid (TA), a low-cost plant polyphenol consisting of a central glucose and gallic acid groups, has been known to be very useful as a reducing and stabilizing agent to modify GO [21]. In addition, TA was found to be very useful as a surface coating material for forming TA polymeric layers on various substrates by pH-induced oxidative polymerization [26, 27]. Therefore, we believe that GO functionalized, reduced, and/or coated by TA can be a very useful nanofiller for the preparation of polymer nanocomposites with improved performance, while such polymer nanocomposites using TA functionalized GO have not yet been reported.

In this work, reduced graphene oxide coated with TA (rGO-TA) was prepared by a one-step reduction and surface coating process using GO and TA in an aqueous solution. The rGO-TA was used as a filler for the polymer nanocomposites having poly(vinyl alcohol) (PVA) as a polymer matrix. The mechanical strength and toughness of PVA were much improved using rGO-TA as the filler of PVA nanocomposites. The PVA nanocomposites furthermore showed excellent humidity sensing properties over a wide relative humidity range and the long-term stability. The synthesis of rGO-TA and the characterization of the PVA nanocomposites containing rGO-TA are fully discussed in this manuscript.

4.2. Experimental

Materials.

Tannic acid (TA), tris(hydroxymethyl)aminomethane (Trizma® base), and tris(hydroxymethyl)aminomethane hydrochloride (Trizma® hydrochloride) were purchased from Aldrich and used as received. Poly(vinyl alcohol) (PVA) (Mw = 89,000 ~ 98,000 and 99% hydrolyzed) was purchased from Aldrich and used without further purification. Graphite powders (Graphite UF 99.5) were purchased from BASF (Germany). All other reagents and solvents were used as received from standard vendors.

Preparation of reduced graphene oxide coated with tannic acid (rGO-TA)

Graphene oxide (GO) was synthesized according to the modified Hummers method [28]. 0.1 M Trizma-buffer solution (pH = 8.5) was prepared by dissolving 8.72 g of Trizma® base in 1 L of DI water and adjusting the pH to 8.5 with Trizma® hydrochloride. 50 mg of GO was added to 100 mL of 0.1 M Trizma-

buffer solution (pH = 8.5) and sonicated for 30 min. 200 mg of TA was added to the Trizma-buffer solution containing GO and the reaction mixture was stirred at room temperature for 1 day. The product was obtained by filtering through an anode aluminum oxide (AAO) membrane filter with 0.2 μm pore size followed by washing with deionized water several times. Then the product was further purified by dissolving in dimethylsulfoxide (DMSO), filtering, and washing using ethanol. The resulting solid (reduced graphene oxide coated with tannic acid, rGO-TA) was dried overnight in a vacuum oven at 35 ºC.

Preparation of polymerized TA (pTA) and reduced graphene oxide (rGO)

During the purification process of rGO-TA, the free TA polymer was separated from the filtered solution by removing the water followed by a washing process using ethanol [21, 29]. This separated TA polymer is called “polymerized TA (pTA)” in this paper. Reduced graphene oxide without TA layers was also prepared using the same process as that used for the preparation of rGO-TA except using the Trizma-buffer solution. The reduced graphene oxide without the TA layers is called as “rGO”. pTA and rGO were also used as fillers to

systematically observe the effect of rGO-TA on the properties of the PVA nanocomposites.

Preparation of PVA nanocomposites with rGO-TA (PVA/rGO-TA)

PVA nanocomposites were prepared by a solution blending method using DMSO as a solvent and rGO-TA as a filler. 10 mg of TA-rGO was added to 5.0 g of DMSO and then sonicated for 30 min to make a homogeneously dispersed solution. 1.0 g of PVA powder was dissolved in 10 g of DMSO. The TA-rGO dispersed solution was added to the PVA solution and sonicated for 30 min. The mixture solution was poured on a Teflon plate and dried at room temperature overnight. It was then heated at 80 ºC for 3 days under vacuum to remove any possible remaining solvent in the composite film, and the dried film was peeled off from the substrate. The obtained PVA nanocomposite with 1.0 wt% of rGO-TA was noted as PVA/rGO-TA 1.0. Other nanocomposites containing 3.0 and 5.0 wt% of rGO-TA were also prepared using the same procedure and were named as PVA/rGO-TA 3.0 and PVA/rGO-TA 5.0, respectively.

Characterization

Thermal gravimetric analysis (TGA) was performed in a Q-5000 IR from TA Instruments to study the thermal property of rGO-TA. The sample was heated from 25 to 700 ºC using a heating rate of 10 ºC/min under a nitrogen atmosphere. Raman spectra were collected on a T64000 Triple Raman spectrometer (HORIBA) equipped with a 514.5 nm Ar laser source. X-ray diffraction (XRD) patterns were recorded with RIGAKU MODE 1 SMARTLAB. Monochromatic CuKα radiation from a rotating anode X-ray generator operating at 40 kV and 30 mA was used. X-ray photoelectron spectroscopy (XPS) was recorded on a KRATOS AXIS-His using MgKα (1254.0 eV) as the radiation source. XPS spectra were collected over a range of 0-1200 eV, followed by high resolution scan of the C 1s and O 1s regions. Tapping-mode atomic force microscopy (AFM) measurements were performed using scanning probe microscopy (MFP-3D Classic, Asylum Research, Oxford Instruments). Silicon cantilevers with the normal resonance frequency of 330 kHz (PPP-NCHR, Nanosensors) were used. The mechanical properties were measured using a universal testing machine (LS1SC, LLOYD Instruments). The dumbbell specimens were prepared using the ASTM standard D638 (Type V specimens dog-bone shaped samples). Type V specimens were prepared using die cutting to the dimensions of W = 3.18 ± 0.03 mm, L = 9.53 ± 0.08 mm, G = 7.62 ± 0.02 mm, and R = 12.7 ± 0.08 mm. The tensile properties of the nanocomposite samples were measured in air at 23 ºC under a 45% relative humidity (RH) with a

gauge length and cross head speed of 15 mm and 10 mm/min, respectively. At least 5 samples were tested for each nanocomposite. The storage modulus (E') values of the PVA nanocomposites are measured using a dynamic mechanical analyzer (DMA) (model DMA/SDTA861e, Mettler Toledo). The film samples are heated from -40 to 100 ºC at the heating rate of 5 ºC/min. The G' values are measured at a constant frequency of 1 Hz with a static force of 1 N. The fractured surface morphologies of the nanocomposite films were inspected by scanning electron microscopy (SEM) using a field emission scanning electron microscope (FESEM, JEOL JSM-6701F). The weight swelling ratio of the samples was calculated using the following formula (1):

$$\text{Weight swelling ratio (\%)} = (W\text{-}W_0)/W_0 \times 100(\%) \quad (1)$$

where W0 and W are the weights before and after dipping the samples in water for 24 hours at room temperature, respectively [30]. The weight loss of the samples was calculated using following formula (2):

$$\text{Weight loss (\%)} = (W_0\text{-}W_d)/W_0 \times 100(\%) \quad (2)$$

where Wd is the weight of the sample dried at 35 ºC for 3 days under vacuum after the water dipping test [31, 32]. The electrical resistivity of the rGO-TA films prepared on AAO filters by vacuum filtration method was measured using four points probe system (Cresbox, Napson Corporation) and those of the PVA

nanocomposite films prepared using solution casting technique were measured using ring type probe with high resistivity meter, Hiresta-UP (MCP-HT450). The impedance measurement was carried out using the IM-6ex impedance analyzer (ZAHNER-elektrik GmbH & Co. KG, Germany) in potentiostat mode with a perturbation amplitude of 1.0 V over a frequency range of 1 Hz to 1 MHz in the relative humidity range of 40 to 90% at 30 ºC. The PVA nanocomposites film was equilibrated for 30 min at each condition before measurement. The impedance was obtained from a Nyquist plot.

4.3. Results and Discussion

Preparation and characterization of rGO-TA

Reduced graphene oxide coated with tannic acid (rGO-TA) was prepared by the reaction of GO with TA in a basic aqueous solution, as shown in Fig. 1. The yellow-brown color of the reactant mixture in the beginning changed to a dark-brown color after the reaction, indicating that GO was reduced, because the color of reduced GO is darker than that of GO [22]. As schematically described in Figure 1a, the reduction of GO starts with the reaction between the epoxy groups in GO and the hydroxyl groups in TA. The additional reaction between the hydroxyl groups in TA and the carbon atoms in GO can form additional ether linkages accompanied by the elimination of water, and finally the elimination reaction of the intermediate results in the formation of *o*-quinone in TA and the reduced GO (rGO) [21, 22].

The reduction of GO by TA was confirmed by the TGA curves of GO and rGO-TA as shown in Fig. 2a. The weight decrease below 300 ºC for GO was ascribed to the thermal decomposition of the oxygen functional groups in GO [29, 33, 34]. The TGA curve of rGO-TA shows much smaller weight change below 300 ºC, indicating that the content of the oxygen functional groups in rGO-TA is much

decreased by the reduction process. The content of the TA layers on the reduced GO sheet could be estimated by comparing the TGA curve between rGO and rGO-TA (Fig. 2a). Since the weight change between 320 and 500 ºC is due to the thermal decomposition of the polymerized TA (pTA) (Fig. 3), the weight change difference between for rGO-TA and rGO in this temperature range could be ascribed to the content of the TA layers on the GO sheets; the weight change difference was found to be about 7 wt% [5, 29, 35]. The reduction could be further confirmed by Raman spectra as shown in Fig. 2b. The G band of GO was observed at 1603 cm^{-1}, while those of rGO and rGO-TA were shifted to lower frequencies (1596 and 1595 cm^{-1}, respectively). Therefore, the red shift of 8 cm^{-1} from 1603 cm^{-1} of the G band for GO to 1595 cm^{-1} indicates the reduction as reported by others [21, 22].

The XRD patterns of GO and rGO-TA shown in Fig. 4a indicate sharp peaks at 10.3^{o} and 10.4^{o}, respectively, corresponding to the d-spacing values of 8.58 Å and 8.50 Å, respectively. The *d*-spacing of 8.58 Å of GO is close to those of other GOs reported previously [4, 19, 21, 36], while that of 8.50 Å for rGO-TA is much larger than those of other reduced GOs; about 3.35 Å is the commonly known *d*-spacing value of the distance of reduced GO sheets [5, 21, 37]. The larger *d*-spacing value of rGO-TA could be ascribed to the TA layers on the reduced GO, enlarging the distance between the reduced GO sheets. However, a weak and

broad peak observed at 26.4°, corresponding to the d-spacing of 3.37 Å, indicates that a small amount of reduced GO sheets are stacked.

Fig. 4b shows AFM images of GO and rGO-TA including the height profiles for the single sheets. The thickness of a single GO sheet measured from the height profile was found to be about 1.0 nm, which is consistent with the thickness of the other GO sheets reported previously [19, 21, 23]. However, it was found to be larger than the interlayer distance of about 8.58 Å observed from XRD. Such mismatch between the layer distance from XRD and the thickness of the single sheet from AFM of GO and GO derivatives was also observed in previous studies [38-40]. Although the mismatch has not been clearly explained, the oxygen functional groups on GO can affect the surface profile of the GO single sheets according to the tapping-mode AFM measurement. The thickness of rGO-TA was found to be about 1.6 nm, which is larger than that of GO by about 0.6 nm and larger than the interlayer distance from XRD by about 0.75 nm. Similarly, it is reported that the other functionalized rGOs had a thickness in the range of 1.0 to 1.6 nm and their layer distances were in the range of 0.43 to 1.2 nm (or 4.3 to 12 Å) [21-23]. Therefore, the organic moieties on the reduced GO enlarge the thickness of the reduced GO sheets. Since the thickness values of other reduced GO sheets reported previously are in the range of 0.8 to 1.0 nm [37, 41, 42], the difference of the thickness between rGO-TA and the other reduced GO sheets

would have originated from the TA layers. It is also noteworthy that rGO-TA sheets can be completely exfoliated forming one layer sheet as shown in the AFM image, although it is well-known that reduced GOs cannot be easily exfoliated due to the irreversible restacking of reduced GO sheets by the strong interactions between the sheets [5].

The existence of TA layers on reduced GO sheets was further confirmed by the C1s XPS spectra of GO and rGO-TA as shown in Fig. 5. The C1s XPS spectrum of GO shows four peaks, which can be assigned to the oxygen functional groups in GO: C-C (284.5 eV), C-O (286.5 eV), C=O (287.5 eV), and O-C=O (288.5 eV) [36, 43, 44]. Although the peak intensity of the C-O groups in C1s XPS spectrum of GO should be larger than that of the reduced GO as reported before [18, 21, 23, 37, 45], the C-O peak intensity in GO was found to be smaller than that in rGO-TA because the larger amount of oxygen functional groups in the TA layers are incorporated in the reduced GO.

The TA layers on reduced GO having about 0.6 ~ 0.8 nm thickness and 7 wt% as estimated from the AFM and TGA results, respectively, are not simple stacks of pristine TA, while it is very probable that they are formed by the polymerization of TA in the buffer solution used in this study. It is well-known that TA can be polymerized by the oxidative coupling reactions of the radicals

generated in the basic buffer solution; the polymerized TA can then be covalently bonded on the surface of the reduced GO to produce covalently-grafted TA layers on reduced GO sheets [26]. The formation of a TA polymeric layer on reduced GO was confirmed by the FT-IR spectra of GO, reduced graphene oxide (rGO) without the TA layer, rGO-TA, pTA, and TA (Fig. 6). The following were observed in the spectrum of GO: a broad O-H stretching peak from the hydroxyl groups and the water molecules absorbed on the GO sheets at 3450 cm^{-1}, a C=O peak from the ketone and carboxyl acid groups at 1740 cm^{-1}, aromatic C=C and O-H bending peaks from phenolic groups at 1620 cm^{-1}, a C-O peak from the epoxy groups at 1240 cm^{-1}, and a C-O in the alkoxy groups at 1050 cm^{-1} [46-48]. After reduction, the peak intensities from the oxygen functional groups of rGO became much smaller, while those from rGO-TA did not change significantly, if at all. Furthermore, the spectrum of rGO-TA is more similar to that of pTA than that of rGO, indicating that the TA polymeric layer is successfully incorporated into the reduced GO surface. Therefore, the simple mixing process using GO and TA under the basic condition was found to produce covalently-grafted TA layers having a polymeric structure on the reduced GO sheet.

PVA nanocomposites with rGO-TA

Mechanical properties and morphology of nanocomposite films

Fig. 7 shows the change of the mechanical properties of PVA by the addition of rGO-TA to PVA. It is obvious that the addition of rGO-TA increases the mechanical strength of PVA; the tensile strength and Young's modulus values of the PVA nanocomposites are always larger than those of PVA (Table 1). In particular, the Young's modulus value of PVA was found to increase with the increase of filler content from 0 to 3.0 wt%, while that of PVA/rGO-TA 5.0 having 5.0 wt% of rGO-TA was found to be slightly smaller than that of PVA/rGO-TA 3.0 having 3.0 wt% of rGO-TA (Fig. 8a). On the other hand, the Young's modulus value of PVA/rGO-TA 5.0 is much larger than that of PVA. The DMA results also indicate that the storage modulus (E') of PVA increases with the increase of the filler content, as shown in Fig. 9.

Interestingly, both the tensile strength and elongation at break values of PVA/rGO-TA 1.0 are larger than those of PVA, although other PVA/rGO-TAs with larger rGO-TA contents have larger tensile strength and smaller elongation break values than PVA (Table 1, Fig. 8b). Therefore, a larger amount of rGO-TA can only increase the mechanical strength of PVA, while an optimum amount such as 1.0 wt% can increase the toughness of PVA. The improved toughness of PVA/rGO-TA 1.0 can be explained by the bio-inspired toughening mechanism

involving the sacrificial bonds and hidden length [29, 49, 50]. Since TA contains various types of oxygen functional groups, PVA chains can be entangled and/or physically cross-linked on the surface of the rGO-TA sheets by forming sacrificial bonds, such as hydrogen bonds, at multiple points with the oxygen functional groups in the TA layers on the reduced GO sheets (Fig. 10). Accordingly, when stress is applied to the PVA nanocomposites, the dissociation of hydrogen bonds can occur at the interface between the rGO-TA and PVA matrix (sacrificial bond rupture). The entangled and/or physically cross-linked PVA chains can then be released (the hidden length release), which can dissipate large amounts of energy at the interface between the fillers and PVA matrix, leading to the toughening of PVA. When the content of rGO-TA is larger than 1.0 wt%, the Young's modulus values of PVA/rGO-TA 3.0 and PVA/rGO-TA 5.0 increase, while the elongation at break values decrease significantly, indicating that the incorporation of larger amounts of rGO-TA increases the degree of entanglement or physical cross-linking of PVA chains, which can restrict the dissociation of interfacial bondings between the fillers and PVA, leading to an increase of the mechanical strength and a decrease of the elongation property of PVA. The toughness of PVA calculated using the area under stress-strain curves was also found to much increase from 6462 MJ/m^3 to 12530 MJ/m^3 by adding 1.0 wt% of rGO-TA, and then decreased as the filler content further increased (Table 1). Unfortunately, the changes of the

mechanical properties could not be observed when rGO-TA content is larger than 5.0 wt%, because we were not able to prepare such PVA nanocomposite films; when the rGO-TA content is larger than 5.0 wt%, the films became too brittle and easily fractured due to the phase separation of the filler domains. Therefore, the smaller elongation break values of PVA/rGO-TA 3.0 and PVA/rGO-TA 5.0 than that of PVA could also have originated from the partially aggregated GO domains in the PVA nanocomposite films, as reported by others [17, 30, 51].

The fractured surfaces of PVA and PVA nanocomposites obtained after the tensile test were observed by SEM (Fig. 11). The PVA shows a relatively smooth surface image, while the PVA nanocomposites show much rougher surface images with fibrils and/or agglomerated domains. Especially, PVA/rGO-TA 1.0 shows longer fibrils without any agglomeration. Such images were often observed from the toughened polymeric materials with large tensile strength and elongation at break values [52]. Therefore, PVA/rGO-TA 1.0, having the strong interfacial interactions between the well-dispersed fillers and the polymer matrix, shows a typical fractured surface morphology for the toughened plastics [52, 53]. PVA/rGO-TA 3.0 and PVA/rGO-TA 5.0 having larger Young's modulus and smaller elongation at break values than PVA show some agglomerated domains that would have originated from the clusters of the filler, rGO-TA.

We also attempted to prepare PVA nanocomposites using GO, rGO, and pTA as fillers to observe the effect of rGO-TA on the PVA nanocomposite materials. As previously reported, GO can improve the mechanical properties of PVA; both the tensile strength and elongation values of PVA were increased by the addition of 1.0 wt% of GO due to the excellent dispersion of GOs in the PVA matrix and the strong interfacial interactions, such as hydrogen bonds, between GO and PVA (Fig. 12) [17, 30, 52, 54]. However, rGO could not improve the mechanical properties of PVA, because it is not miscible with PVA. As a result, phase-separated domains of the rGOs were formed in the PVA nanocomposite film containing 1.0 wt% of rGOs, as shown in Fig. 13 [45]. Similarly, it was reported that when reduced GO was incorporated in the PVA solution, it was not well-dispersed in the PVA due to the poor compatibility with the polymer matrix [17]. Although pTA is miscible with PVA, it could not considerably increase the mechanical properties of PVA because pTA composed of organic TA moieties is not as effective as the graphene derivatives composed of the sp^2 carbon sheets for the application of reinforcing filler (Fig. 12) [55-58]. Therefore, it is clear that rGO-TA is more effective for improving the mechanical properties of PVA than rGO and is more effective than pTA for increasing the mechanical strength due to the excellent dispersity of the graphene materials and the strong interfacial interactions between the fillers and the polymer matrix. Although GO was found

to be as effective as rGO-TA in increasing the mechanical strength, it is not as effective as rGO-TA in increasing the water resistance, as shown in the next section.

Water resistance properties

The water resistance properties of the PVA nanocomposites were evaluated by measuring the weight swelling ratio and the weight loss from a water-dipping test. After dipping the samples, the difference in the swelling behavior for neat PVA, PVA/GO, PVA/pTA, and PVA/rGO-TA could be clearly observed; the dimensions of PVA, PVA/GO 1.0 having 1.0 wt% of GO, and PVA/pTA 1.0 having 1.0 wt% of pTA increased much by the absorption of water molecules, while those of PVA/rGO-TAs did not change significantly (Fig. 14a and Fig. 15). Therefore, it is obvious that the introduction of rGO-TA into the PVA matrix effectively prevents the swelling of PVA. Furthermore, the weight swelling ratios of PVA/GO 1.0 and PVA/pTA 1.0 are close to that of PVA, while that of PVA/rGO-TA 1.0 is smaller than that of PVA (Fig. 16). In particular, the weight swelling ratio of PVA was found to decrease considerably from 110.5% to 64.7% and 75.6%, by adding 3.0 and 5.0 wt% of rGO-TA, respectively, indicating that the introduction of rGO-TA could effectively decrease the water permeability of

PVA because rGO-TA can work as a physical barrier to prevent the water transfer in the PVA matrix due to the ultrathin sheet-like structure of the graphene derivatives (Fig. 14b) [51, 59]. The smaller weight loss of the PVA nanocomposites compared with PVA further support the physical barrier effect of rGO-TA (Fig. 14c). On the contrary, when the content of rGO-TA is larger than 3.0 wt%, the weight swelling ratio and the weight loss of PVA/rGO-TA 5.0 slightly increase, indicating that the incorporation of amounts of rGO-TA larger than 3.0 wt% increases the agglomerated domains of rGO-TAs in the polymer matrix, which can lead to the decrease of the physical barrier effect of rGO-TA. Therefore, 3.0 wt% of rGO-TA was found to be the most effective filler content to impart the water resistance properties of PVA.

The contact angles of PVA nanocomposites films were measured to further investigate the water resistance properties of the PVA nanocomposites. The water contact angle of PVA was found to increase from 33.7^{o} to 51.2^{o}, 62.8^{o}, and 60.5^{o}, by adding 1.0, 3.0, and 5.0 wt% of rGO-TA, respectively, indicating that the hydrophilicity of PVA decreases by the addition of rGO-TA (Table 1). Previously, it was reported that the introduction of a small amount of graphene to a PVA matrix could improve the water resistance of PVA by decreasing the water affinity of PVA [17]. For example, when 1.0 wt% of graphene was incorporated into PVA, the water contact angle of PVA was much increased from 36^{o} to 97^{o}, indicating

that graphene can make PVA quite hydrophobic (> 90^{o}) [17]. On the contrary, the water contact angle values of PVA nanocomposites with various rGO-TA contents in the range of 51^{o} – 62^{o} are quite smaller than that of PVA with 1.0 wt% of graphene.

Therefore, PVA/rGO-TAs have physical stability in water because rGO-TA can work as a physical barrier to water molecules, while the surface PVA/rGO-TAs can still show hydrophilicity to some degree due to the relatively hydrophilic property of rGO-TA. This unique property of PVA/rGO-TAs should be advantageous for the application as a humidity sensor, which needs good humidity sensing ability and long-term stability [16, 51, 60, 61].

Humidity sensing properties

The humidity sensing ability of the PVA nanocomposites was evaluated by measuring the electrical resistances at different RH conditions using PVA/rGO-TA 3.0 and PVA/rGO-TA 5.0 having the smaller swelling ratio values, because the smaller volume change is beneficial for the humidity sensor materials for practical applications [16, 17, 51, 60, 61]. Very large decrease of the resistance with the increase of the RH from 40% to 90% were observed from the PVA

nanocomposites as shown in Fig. 17, indicating that they have excellent humidity sensing properties over the wide relative humidity range between 40% and 90% RH. The decrease of the resistance with the increased humidity can be ascribed to the increase of the proton concentration by the capillary condensation of water in the PVA matrix as reported previously [51]. Furthermore, PVA/rGO-TA 3.0 and PVA/rGO-TA 5.0 were found to have good resistance reversibility to 10 humidification-dehumidification cycles between 40% and 70% RH showing only a very small change in the resistance of less than 3% over 10 cycles (Fig. 18 and Fig.19). This indicates that the swelling of the PVA matrix could be effectively retarded by rGO-TA, because rGO-TA can work as an effective physical barrier to water molecules and the electrical conductive networks formed by rGO-TAs are not much damaged during the humidification-dehumidification process. Since PVA has the humidity sensing properties only in an extremely narrow sensing range of between 98% and 99% RH [62]. PVA composites having conductive fillers, such as carbon blacks, conducting polymers, and electrolytes, were used to increase the humidity sensing range [62-64]. However, to the best of our knowledge, there has been no report to show the long-term performance of PVA-based humidity sensors over a wide relative humidity range because the electrical conductive networks formed by the conductive fillers in the PVA matrix can be disconnected due to the poor physical stability of PVA to water molecules. On the

contrary, the excellent humidity sensing properties and long-term stability of PVA-based humidity sensors could be achieved by the introduction of rGO-TA having sheet-like structures and abundant oxygen functional groups on the surfaces.

4.4. Conclusion

Reduced graphene oxide coated with tannic acid (rGO-TA) could be prepared by a facile one-step method using a low-cost plant polyphenol, tannic acid, as a reducing agent and surface coating materials of GO in a basic buffer solution. The toughness of PVA was found to be much improved by adding 1.0 wt% of rGO-TA as the filler due to the formation of a bio-inspired structured interface between PVA and rGO-TA having the covalently-grafted TA polymeric layer on the surface. Furthermore, the PVA nanocomposite containing 3.0 wt% of rGO-TA showed excellent humidity sensing performance over the wide relative humidity range. It also showed long-term stability due to the unique structures and surface characteristics of rGO-TA, having a sheet-like structure and abundant oxygen functional groups on the surface. Therefore, we believe that the incorporation of rGO-TA into PVA is a very promising approach for the development of novel humidity sensor materials using water soluble polymer systems for practical applications.

4.5. References

[1] Novoselov KS, Fal'ko VI, Colombo L, Gellert PR, Schwab MG, Kim K. A roadmap for graphene. Nature. 2012;490(7419):192-200.

[2] Chen D, Feng H, Li J. Graphene oxide: preparation, functionalization, and electrochemical applications. Chem Rev. 2012;112(11):6027-53.

[3] Salavagione HJ, Martinez G, Ellis G. Recent advances in the covalent modification of graphene with polymers. Macromol Rapid Comm. 2011;32(22):1771-89.

[4] Dreyer DR, Park S, Bielawski CW, Ruoff RS. The chemistry of graphene oxide. Chem Soc Rev. 2010;39(1):228-40.

[5] Stankovich S, Dikin DA, Piner RD, Kohlhaas KA, Kleinhammes A, Jia Y, et al. Synthesis of graphene-based nanosheets via chemical reduction of exfoliated graphite oxide. Carbon. 2007;45(7):1558-65.

[6] Stankovich S, Piner RD, Nguyen ST, Ruoff RS. Synthesis and exfoliation of isocyanate-treated graphene oxide nanoplatelets. Carbon. 2006;44(15):3342-7.

[7] Sun Y, Shi G. Graphene/polymer composites for energy applications. J Polym Sci Part B: Polym Phys. 2013;51(4):231-53.

[8] Stankovich S, Dikin DA, Dommett GH, Kohlhaas KM, Zimney EJ, Stach EA, et al. Graphene-based composite materials. Nature. 2006;442(7100):282-6.

[9] Paul DR, Robeson LM. Polymer nanotechnology: Nanocomposites. Polymer. 2008;49(15):3187-204.

[10] Kim H, Abdala AA, Macosko CW. Graphene/Polymer Nanocomposites. Macromolecules. 2010;43(16):6515-30.

[11] Kuilla T, Bhadra S, Yao D, Kim NH, Bose S, Lee JH. Recent advances in graphene based polymer composites. Prog. Polym. Sci. 2010;35(11):1350-75.

[12] Potts JR, Dreyer DR, Bielawski CW, Ruoff RS. Graphene-based polymer nanocomposites. Polymer. 2011;52(1):5-25.

[13] Sengupta R, Bhattacharya M, Bandyopadhyay S, Bhowmick AK. A review on the mechanical and electrical properties of graphite and modified graphite reinforced polymer composites. Prog. Polym Sci. 2011;36(5):638-70.

[14] Verdejo R, Bernal MM, Romasanta LJ, Lopez-Manchado MA. Graphene filled polymer nanocomposites. J Mater Chem. 2011;21(10):3301-10.

[15] Young RJ, Kinloch IA, Gong L, Novoselov KS. The mechanics of graphene nanocomposites: A review. Compos Sci Technol. 2012;72(12):1459-76.

[16] Flores A, Salavagione HJ, Ania F, Martinez G, Ellis G, Gomez-Fatou MA. The overlooked role of reduced graphene oxide in the reinforcement of hydrophilic polymers. J Mater Chem C. 2015;3(6):1177-80.

[17] Wang JC, Wang XB, Xu CH, Zhang M, Shang XP. Preparation of graphene/poly(vinyl alcohol) nanocomposites with enhanced mechanical properties and water resistance. Polym Int. 2011;60(5):816-22.

[18] Bo Z, Shuai X, Mao S, Yang H, Qian J, Chen J, et al. Green preparation of reduced graphene oxide for sensing and energy storage applications. Sci Rep. 2014;4:4684.

[19] Cheng C, Nie SQ, Li S, Peng H, Yang H, Ma L, et al. Biopolymer functionalized reduced graphene oxide with enhanced biocompatibility via mussel inspired coatings/anchors. J Mater Chem B. 2013;1(3):265-75.

[20] Dintcheva NT, Arrigo R, Gambarotti C, Carroccio S, Filippone G, Cicogna F, et al. α-Tocopherol-induced radical scavenging activity in carbon nanotubes for thermo-oxidation resistant ultra-high molecular weight polyethylene-based nanocomposites. Carbon. 2014;74:14-21.

[21] Lei Y, Tang Z, Liao R, Guo B. Hydrolysable tannin as environmentally friendly reducer and stabilizer for graphene oxide. Green Chem. 2011;13(7):1655.

[22] Li J, Xiao G, Chen C, Li R, Yan D. Superior dispersions of reduced graphene oxide synthesized by using gallic acid as a reductant and stabilizer. J Mater Chem A. 2013;1(4):1481.

[23] Liao R, Tang Z, Lei Y, Guo B. Polyphenol-Reduced Graphene Oxide: Mechanism and Derivatization. J Phys Chem C. 2011;115(42):20740-6.

[24] Xu LQ, Yang WJ, Neoh KG, Kang ET, Fu GD. Dopamine-Induced Reduction and Functionalization of Graphene Oxide Nanosheets. Macromolecules. 2010;43(20):8336-9.

[25] Yang LP, Phua SL, Toh CL, Zhang LY, Ling H, Chang MC, et al. Polydopamine-coated graphene as multifunctional nanofillers in polyurethane. RSC Adv. 2013;3(18):6377-85.

[26] Sileika TS, Barrett DG, Zhang R, Lau KHA, Messersmith PB. Colorless Multifunctional Coatings Inspired by Polyphenols Found in Tea, Chocolate, and Wine. Angew Chem Int Edit. 2013;52(41):10766-70.

[27] Ejima H, Richardson JJ, Liang K, Best JP, van Koeverden MP, Such GK, et al. One-Step Assembly of Coordination Complexes for Versatile Film and Particle Engineering. Science. 2013;341(6142):154-7.

[28] Hummers WS, Offeman RE. Preparation of Graphitic Oxide. J Am Chem Soc. 1958;80(6):1339-.

[29] Lim M-Y, Kim HJ, Baek SJ, Kim KY, Lee S-S, Lee J-C. Improved strength and toughness of polyketone composites using extremely small amount of polyamide 6 grafted graphene oxides. Carbon. 2014;77:366-78.

[30] Zhang L, Wang ZP, Xu C, Li Y, Gao JP, Wang W, et al. High strength graphene oxide/polyvinyl alcohol composite hydrogels. J Mater Chem. 2011;21(28):10399-406.

[31] Kim K, Heo P, Ko T, Kim K-h, Kim S-K, Pak C, et al. Poly(arylene ether sulfone) based semi-interpenetrating polymer network membranes containing cross-linked poly(vinyl phosphonic acid) chains for fuel cell applications at high temperature and low humidity conditions. J Power Sources. 2015;293(0):539-47.

[32] Ko T, Kim K, Jung BK, Cha SH, Kim SK, Lee JC. Cross-Linked Sulfonated Poly(arylene ether sulfone) Membranes Formed by in Situ Casting and Click Reaction for Applications in Fuel Cells. Macromolecules. 2015;48(4):1104-14.

[33] Zhang C, Huang S, Tjiu WW, Fan W, Liu TX. Facile preparation of water-dispersible graphene sheets stabilized by acid-treated multi-walled carbon nanotubes and their poly(vinyl alcohol) composites. J Mater Chem. 2012;22(6):2427-34.

[34] Xu Z, Gao C. In situPolymerization Approach to Graphene-Reinforced Nylon-6 Composites. Macromolecules. 2010;43(16):6716-23.

[35] Zhang XQ, Fan XY, Li HZ, Yan C. Facile preparation route for graphene oxide reinforced polyamide 6 composites via in situ anionic ring-opening polymerization. J Mater Chem. 2012;22(45):24081-91.

[36] Hung W-S, Tsou C-H, De Guzman M, An Q-F, Liu Y-L, Zhang Y-M, et al. Cross-Linking with Diamine Monomers To Prepare Composite Graphene Oxide-Framework Membranes with Varying d-Spacing. Chem Mater. 2014;26(9):2983-90.

[37] Zhang JL, Yang HJ, Shen GX, Cheng P, Zhang JY, Guo SW. Reduction of graphene oxide via L-ascorbic acid. Chem Comm. 2010;46(7):1112-4.

[38] Chen CM, Yang QH, Yang YG, Lv W, Wen YF, Hou PX, et al. Self-Assembled Free-Standing Graphite Oxide Membrane. Adv Mater. 2009;21(29):3007.

[39] Shen JF, Hu YZ, Shi M, Lu X, Qin C, Li C, et al. Fast and Facile Preparation of Graphene Oxide and Reduced Graphene Oxide Nanoplatelets. Chem Mater. 2009;21(15):3514-20.

[40] Xu YX, Bai H, Lu GW, Li C, Shi GQ. Flexible graphene films via the filtration of water-soluble noncovalent functionalized graphene sheets. J Am Chem Soc. 2008;130(18):5856-+.

[41] Wang Y, Shi ZX, Yin J. Facile Synthesis of Soluble Graphene via a Green Reduction of Graphene Oxide in Tea Solution and Its Biocomposites. ACS Appl Mater Interfaces. 2011;3(4):1127-33.

[42] Zhu CZ, Guo SJ, Fang YX, Dong SJ. Reducing Sugar: New Functional Molecules for the Green Synthesis of Graphene Nanosheets. ACS Nano. 2010;4(4):2429-37.

[43] Marcano DC, Kosynkin DV, Berlin JM, Sinitskii A, Sun ZZ, Slesarev A, et al. Improved Synthesis of Graphene Oxide. ACS Nano. 2010;4(8):4806-14.

[44] Krishnamoorthy K, Veerapandian M, Yun K, Kim SJ. The chemical and structural analysis of graphene oxide with different degrees of oxidation. Carbon. 2013;53:38-49.

[45] Ai KL, Liu YL, Lu LH, Cheng XL, Huo LH. A novel strategy for making soluble reduced graphene oxide sheets cheaply by adopting an endogenous reducing agent. J Mater Chem. 2011;21(10):3365-70.

[46] Dong J, Weng J, Dai L. The effect of graphene on the lower critical solution temperature of poly(N-isopropylacrylamide). Carbon. 2013;52:326-36.

[47] Chen Z, Lu H. Constructing sacrificial bonds and hidden lengths for ductile graphene/polyurethane elastomers with improved strength and toughness. J Mater Chem. 2012;22(25):12479.

[48] Cano M, Khan U, Sainsbury T, O'Neill A, Wang Z, McGovern IT, et al. Improving the mechanical properties of graphene oxide based materials by covalent attachment of polymer chains. Carbon. 2013;52:363-71.

[49] Fantner GE, Oroudjev E, Schitter G, Golde LS, Thurner P, Finch MM, et al. Sacrificial bonds and hidden length: Unraveling molecular mesostructures in tough materials. Biophys J. 2006;90(4):1411-8.

[50] Lu H, Chen Z, Ma C. Bioinspired approaches for optimizing the strength and toughness of graphene-based polymer nanocomposites. J Mater Chem. 2012;22(32):16182.

[51] Hwang SH, Kang D, Ruoff RS, Shin HS, Park YB. Poly(vinyl alcohol) Reinforced and Toughened with Poly(dopamine)-Treated Graphene Oxide, and Its Use for Humidity Sensing. ACS Nano. 2014;8(7):6739-47.

[52] Qi XD, Yao XL, Deng S, Zhou TN, Fu Q. Water-induced shape memory effect of graphene oxide reinforced polyvinyl alcohol nanocomposites. J Mater Chem A. 2014;2(7):2240-9.

[53] Li YQ, Yang TY, Yu T, Zheng LX, Liao K. Synergistic effect of hybrid carbon nantube-graphene oxide as a nanofiller in enhancing the mechanical properties of PVA composites. J Mater Chem. 2011;21(29):10844-51.

[54] Shao L, Li J, Zhang Y, Gong S, Zhang H, Wang Y. The effect of the reduction extent on the performance of graphene/poly(vinyl alcohol) composites. J Mater Chem A. 2014;2(34):14173.

[55] Melo TJA, Araujo EM, Brito GF, Agrawal P. Development of nanocomposites from polymer blends: Effect of organoclay on the morphology and mechanical properties. J Alloy Compd. 2014;615:S389-S91.

[56] Crosby AJ, Lee JY. Polymer nanocomposites: The "nano" effect on mechanical properties. Polym Rev. 2007;47(2):217-29.

[57] Tang XZ, Alavi S. Recent advances in starch, polyvinyl alcohol based polymer blends, nanocomposites and their biodegradability. Carbohyd Polym. 2011;85(1):7-16.

[58] Mukhopadhyay P, Gupta RK. Trends and Frontiers in Graphene-Based Polymer Nanocomposites. Plast Eng. 2011;67(1):32-42.

[59] Hu W, Zhan J, Wang X, Hong N, Wang B, Song L, et al. Effect of Functionalized Graphene Oxide with Hyper-Branched Flame Retardant on Flammability and Thermal Stability of Cross-Linked Polyethylene. Ind Eng Chem Res. 2014;53(8):3073-83.

[60] Fei T, Jiang K, Jiang F, Mu R, Zhang T. Humidity Switching Properties of Sensors Based on Multiwalled Carbon Nanotubes/Polyvinyl Alcohol Composite Films. J Appl Polym Sci. 2014;131(1).

[61] Yang JH, Lee YD. Highly electrically conductive rGO/PVA composites with a network dispersive nanostructure. J Mater Chem. 2012;22(17):8512-7.

[62] Barkauskas J. Investigation of conductometric humidity sensors. Talanta. 1997;44(6):1107-12.

[63] Yang MR, Chen KS. Humidity sensors using polyvinyl alcohol mixed with electrolytes. Sensor Actuat B-Chem. 1998;49(3):240-7.

[64] Li Y, Ying BY, Hong LJ, Yang MJ. Water-soluble polyaniline and its composite with poly(vinyl alcohol) for humidity sensing. Synthetic Met. 2010;160(5-6):455-61.

Table 4.1 Mechanical properties, water contact angles, and weight swelling ratios of PVA and the PVA nanocomposites

Sample	Tensile strength (MPa)	Young's modulus (GPa)	Elongation at break (%)	Toughness (MJ/m^3)	Contact angle (^{o})	Weight swelling ratio (%)
PVA	58.8±1.1	4.15±0.09	124±5	6462±56	33.7	111
PVA/rGO-TA 1.0	77.3±2.7	5.56±0.07	195±7	12530±94	51.2	104
PVA/rGO-TA 3.0	65.3±2.5	6.60±0.05	75±7	4541±38	62.8	65
PVA/rGO-TA 5.0	60.4±2.9	6.50±0.07	64±10	3514±49	60.5	76

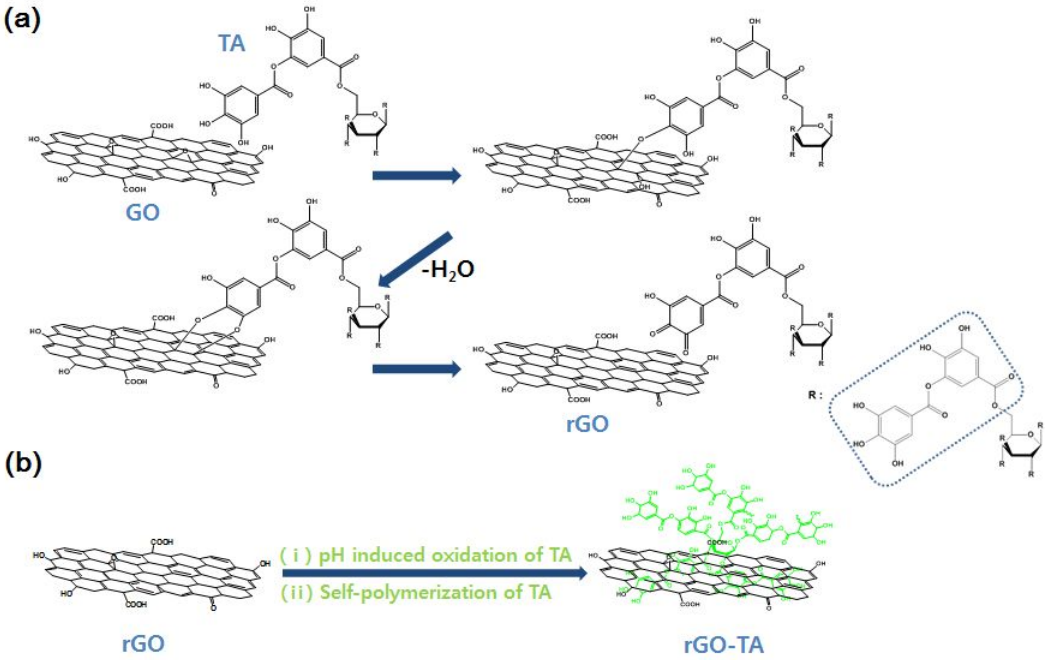

Fig. 4.1 Schematic diagrams for the preparation of rGO-TA: (a) reduction of GO by TA and (b) pH induced oxidation and self-polymerization of TA

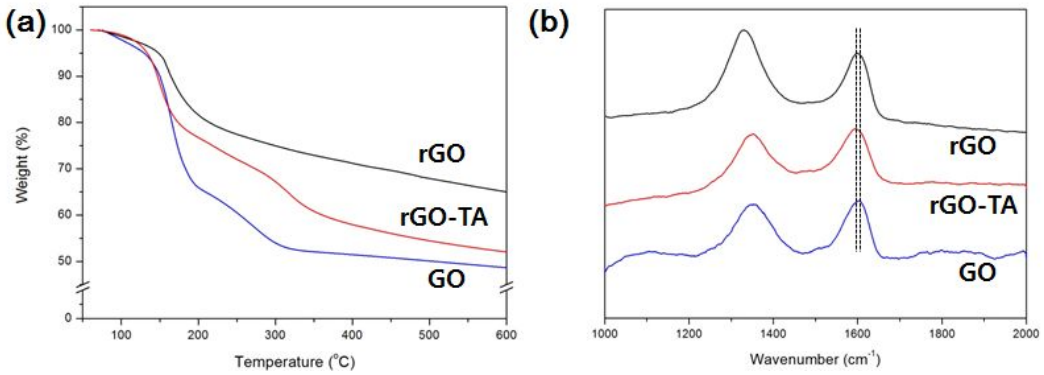

Fig. 4.2 (a) TGA curves of GO, rGO, and rGO-TA and (b) Raman spectra of GO and rGO-TA

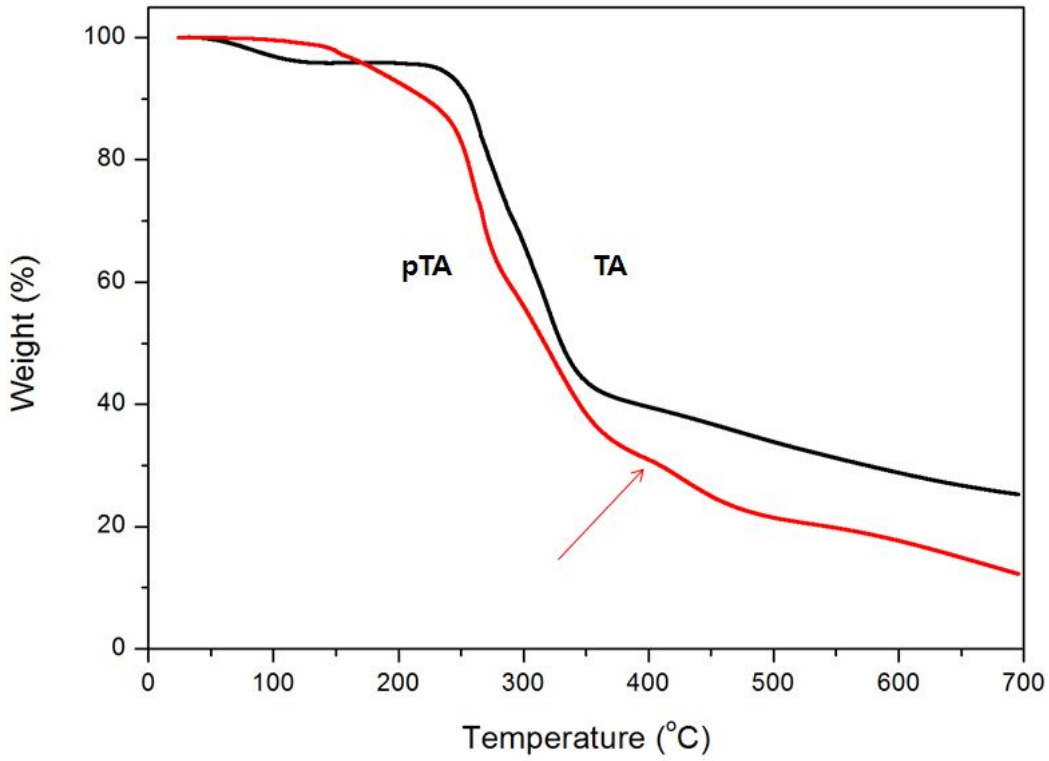

Fig. 4.3 TGA curves of TA and pTA

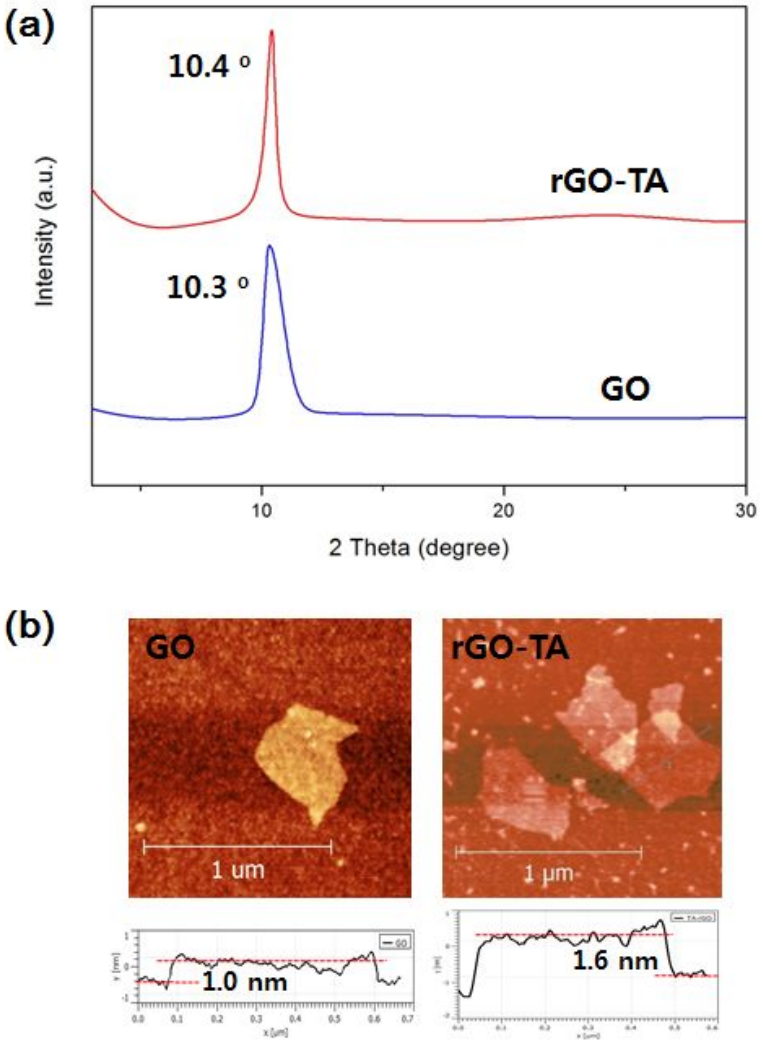

Fig. 4.4 (a) XRD patterns and (b) AFM images of GO and rGO-TA

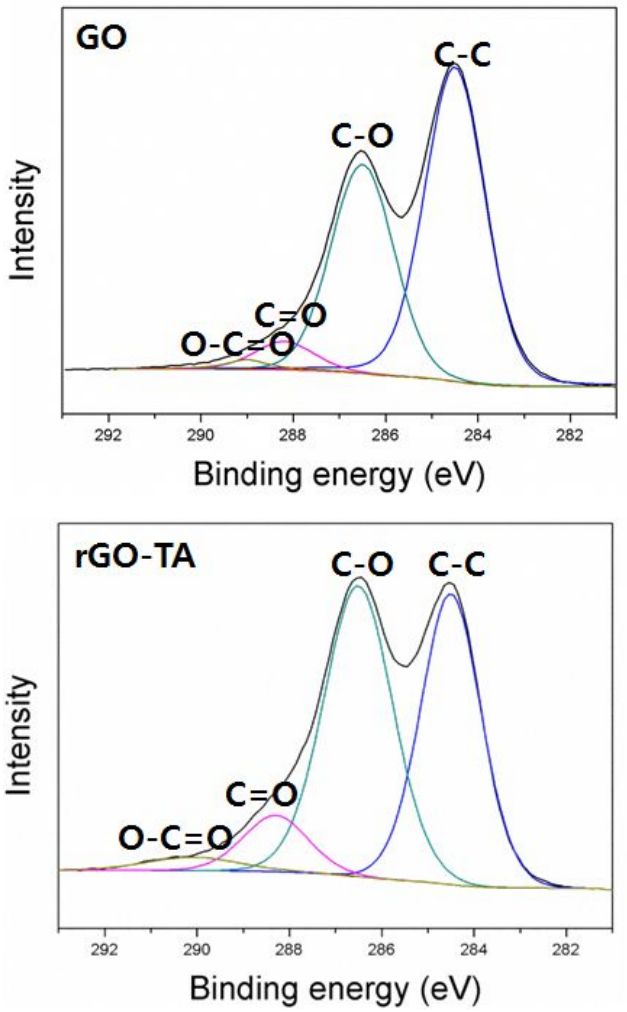

Fig. 4.5 C1s XPS spectra of GO and rGO-TA

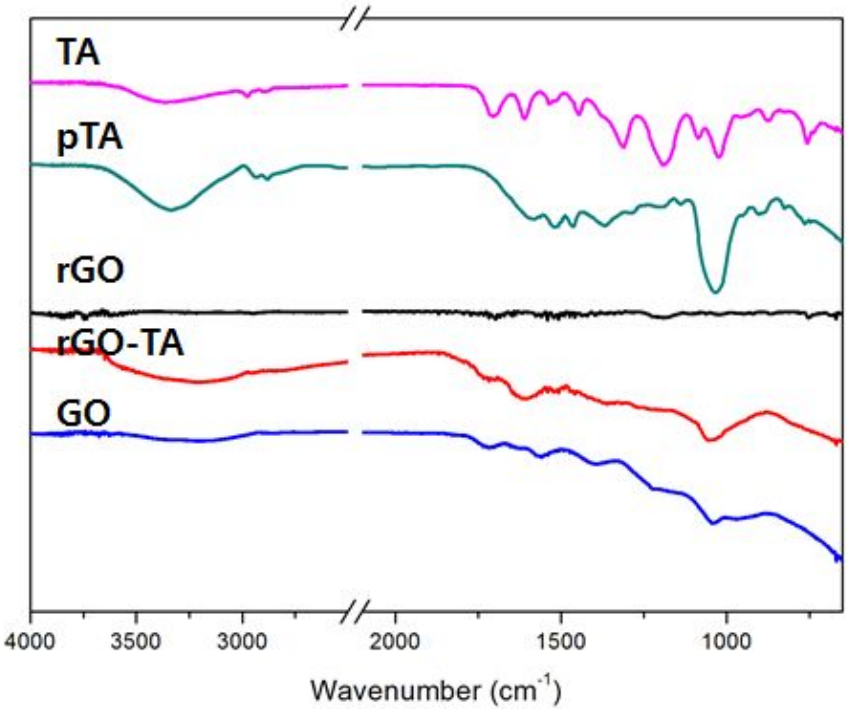

Fig. 4.6 FT-IR spectra of GO, rGO, rGO-TA, pTA, and TA

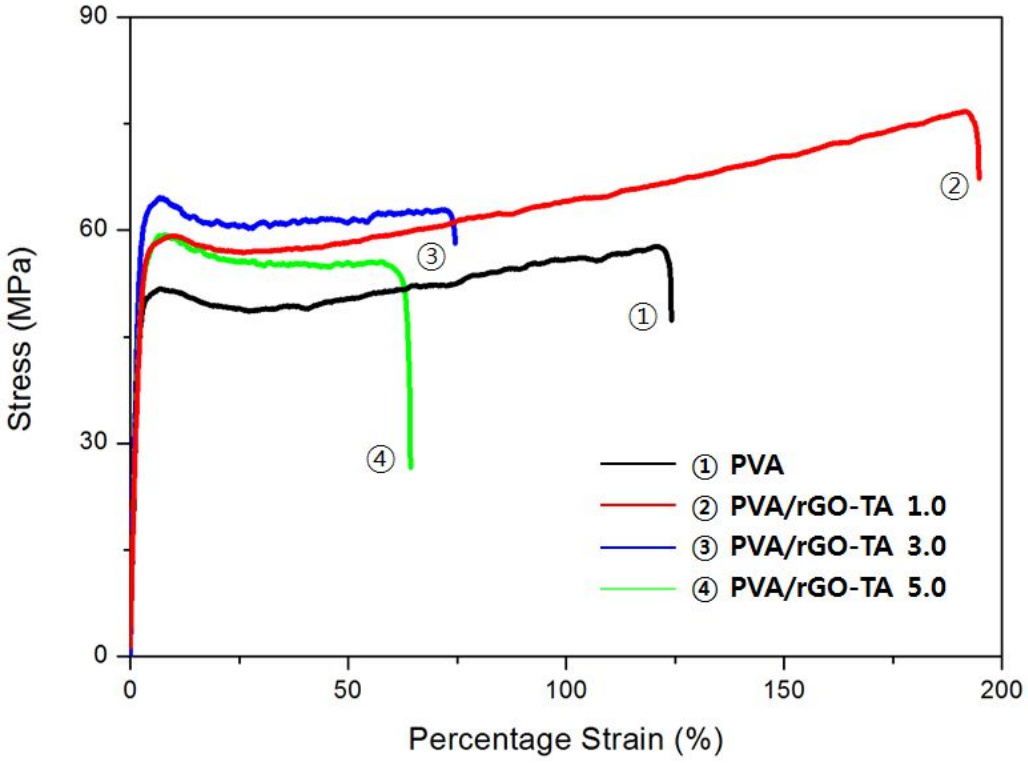

Fig. 4.7 Stress-strain curves of PVA and the PVA nanocomposites

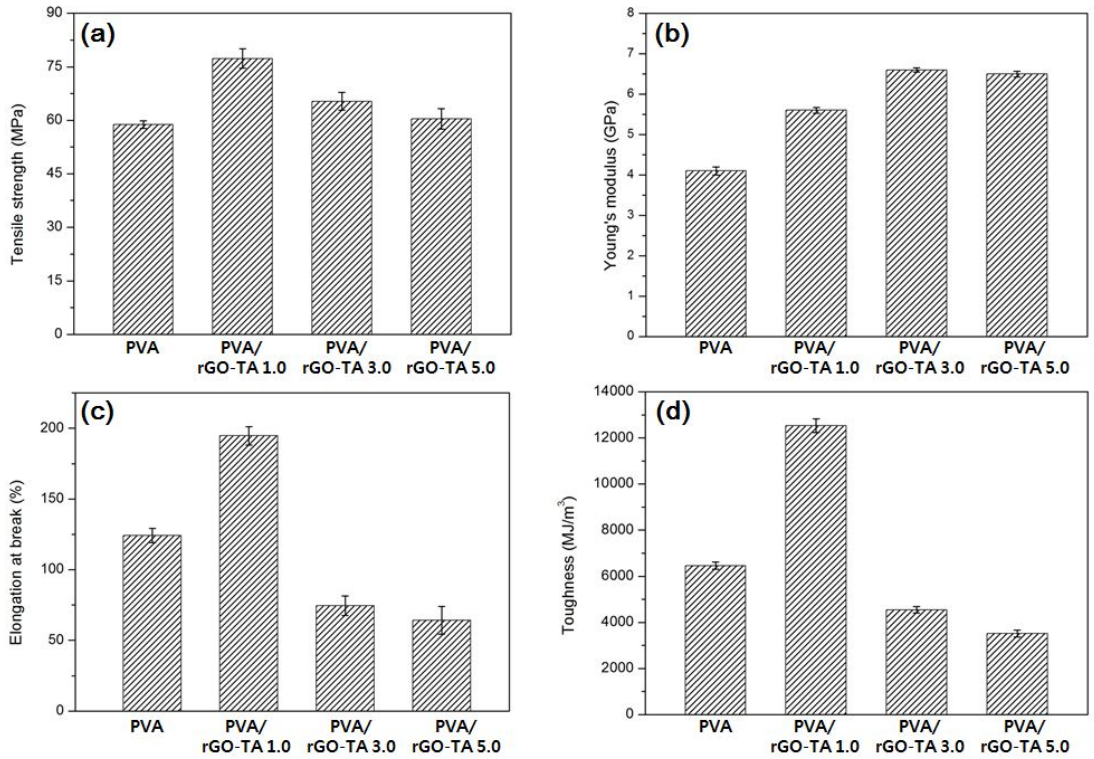

Fig. 4.8 Mechanical properties of PVA and the PVA nanocomposites

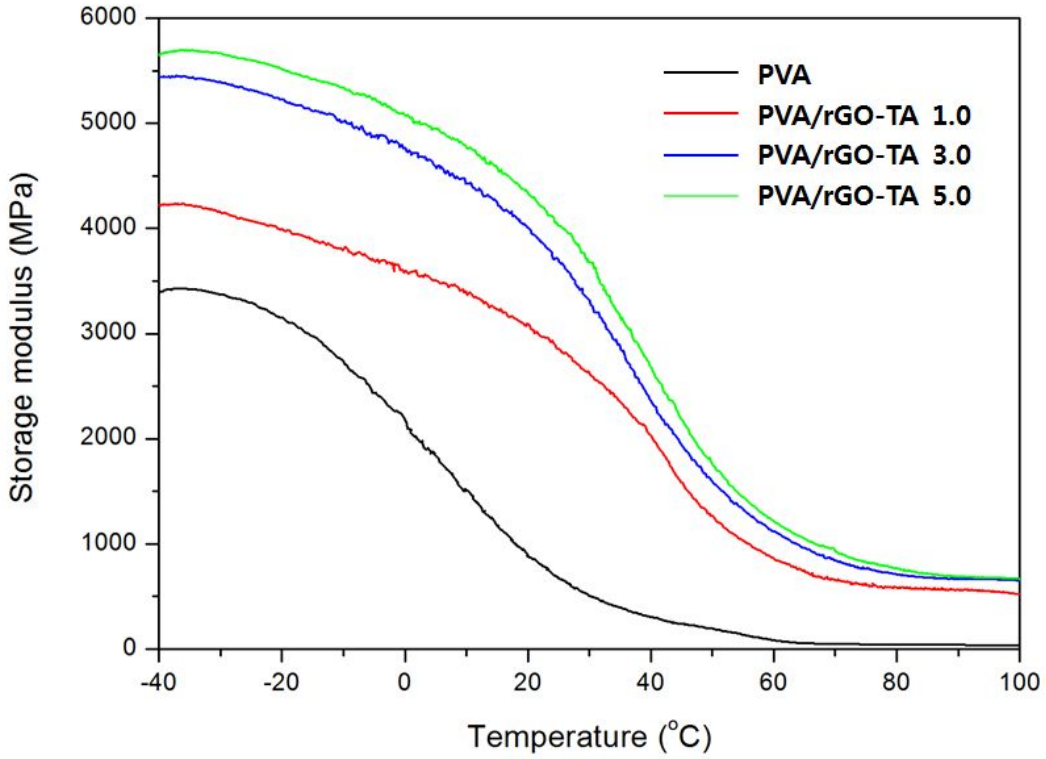

Fig. 4.9 Storage modulus versus temperature for PVA and the PVA nanocomposites as measured by DMA

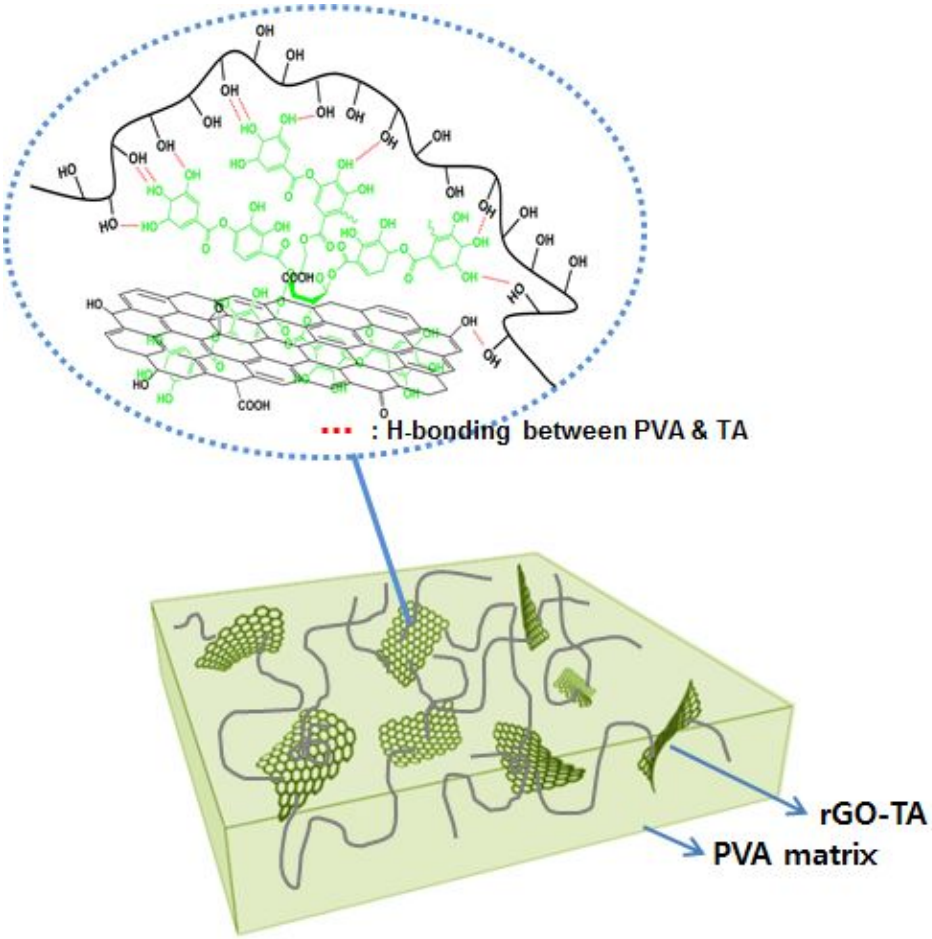

Fig. 4.10 Schematic of the toughening mechanism: formation of sacrificial bond and hidden length

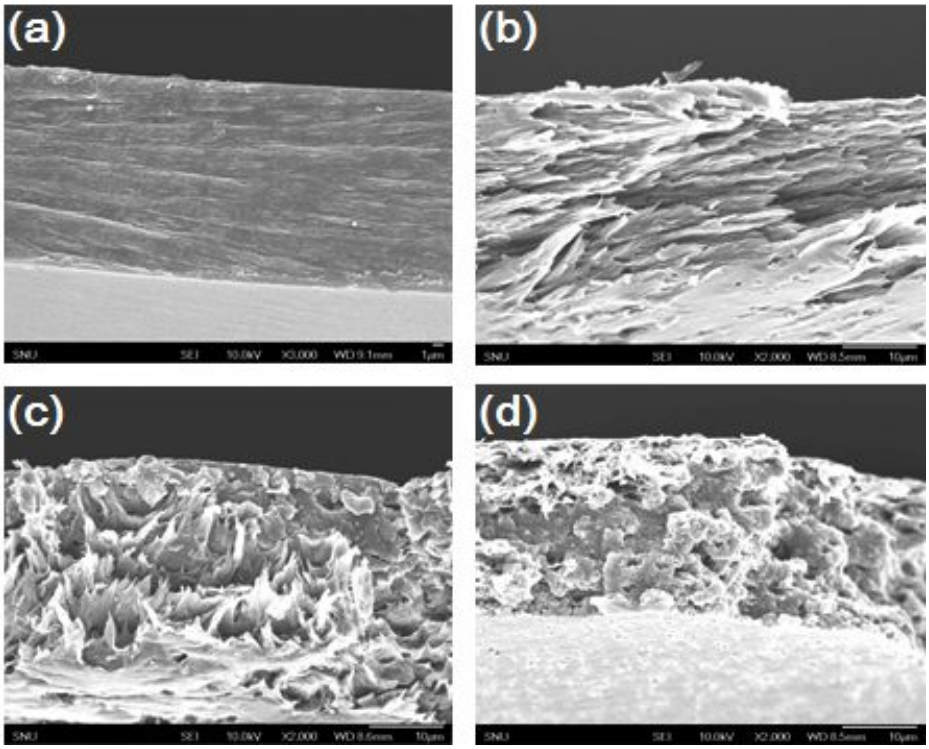

Fig. 4.11 SEM images of fractured surfaces of PVA and the PVA nanocomposites films. (a) PVA, (b) PVA/rGO-TA 1.0, (c) PVA/rGO-TA 3.0, and (d) PVA/rGO-TA 5.0

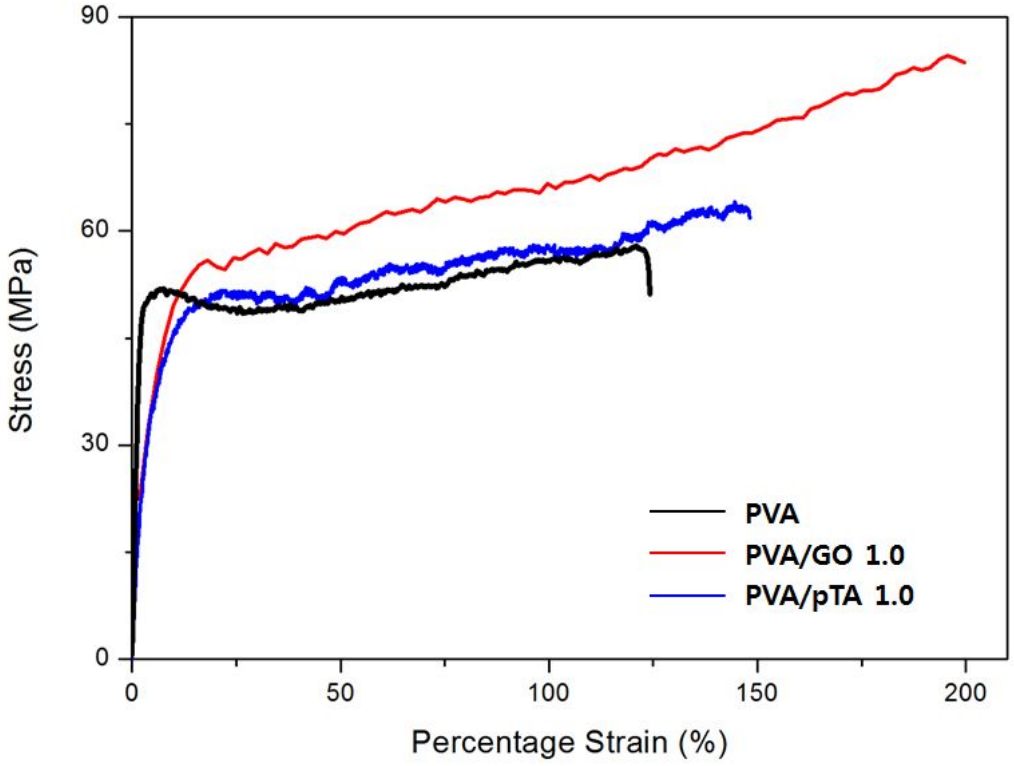

Fig. 4.12 Stress-strain curves of PVA nanocomposites containing 1.0 wt% of GO and pTA

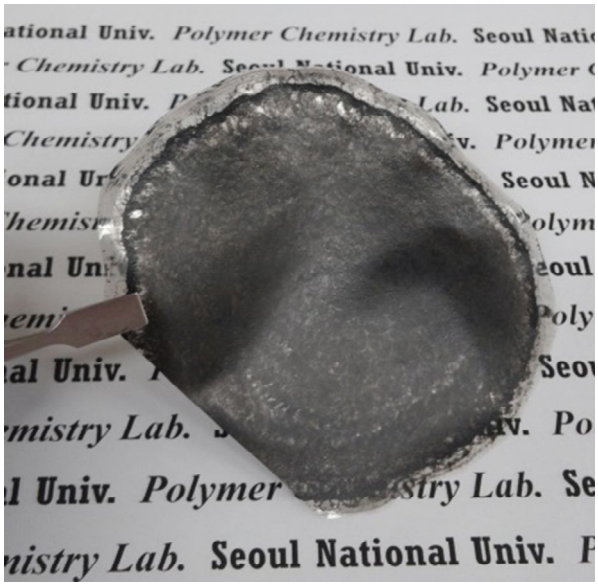

Fig. 4.13 Photograph of PVA nanocomposite film containing 1.0 wt% of rGO

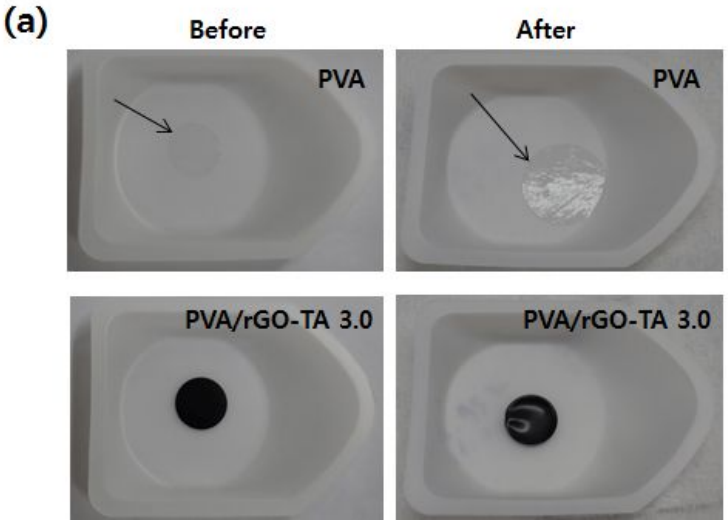
(a)
Before
After
PVA
PVA
PVA/rGO-TA 3.0
PVA/rGO-TA 3.0

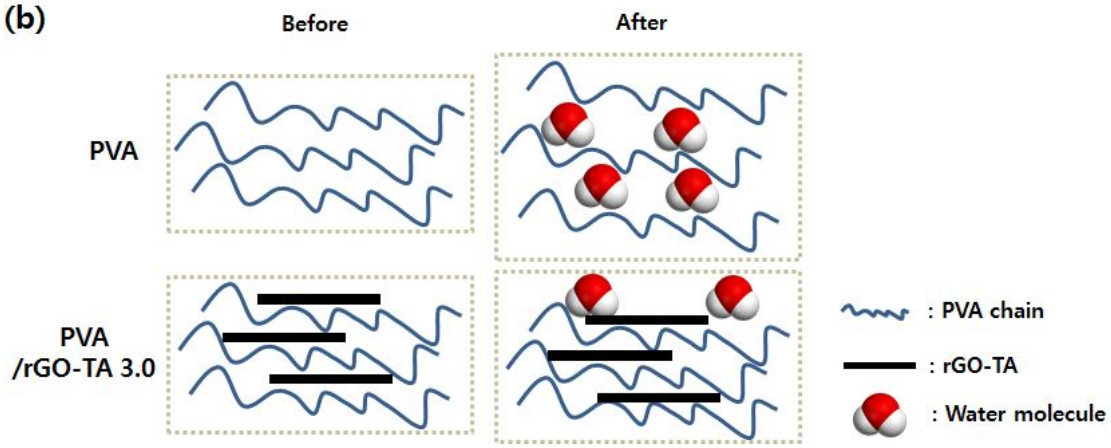
(b)
Before
After
PVA
PVA
/rGO-TA 3.0
: PVA chain
: rGO-TA
: Water molecule

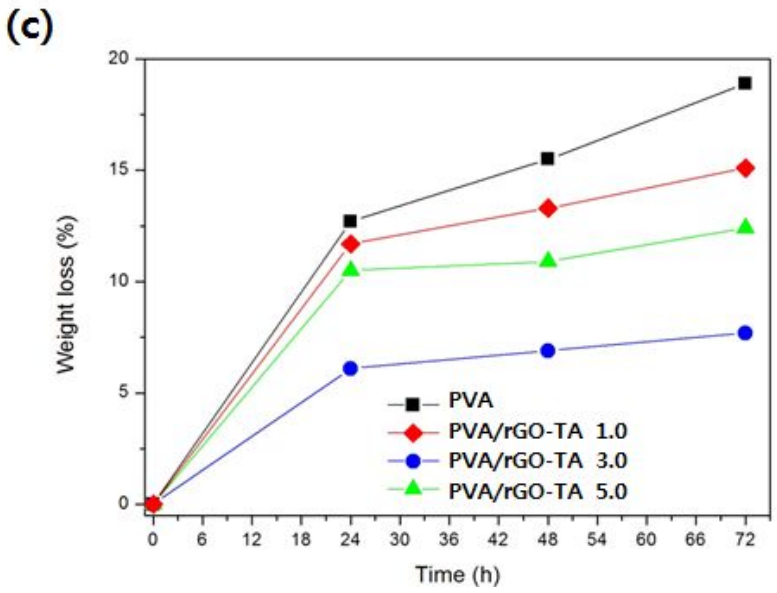

Fig. 4.14 (a) Optical photographs of PVA and PVA/rGO-TA 3.0 before and after 24 hours of water dipping test, (b) illustration of the physical stability of PVA and PVA/rGO-TA 3.0 after water dipping test, and (c) weight loss of PVA and the PVA nanocomposites after water dipping test

(a)

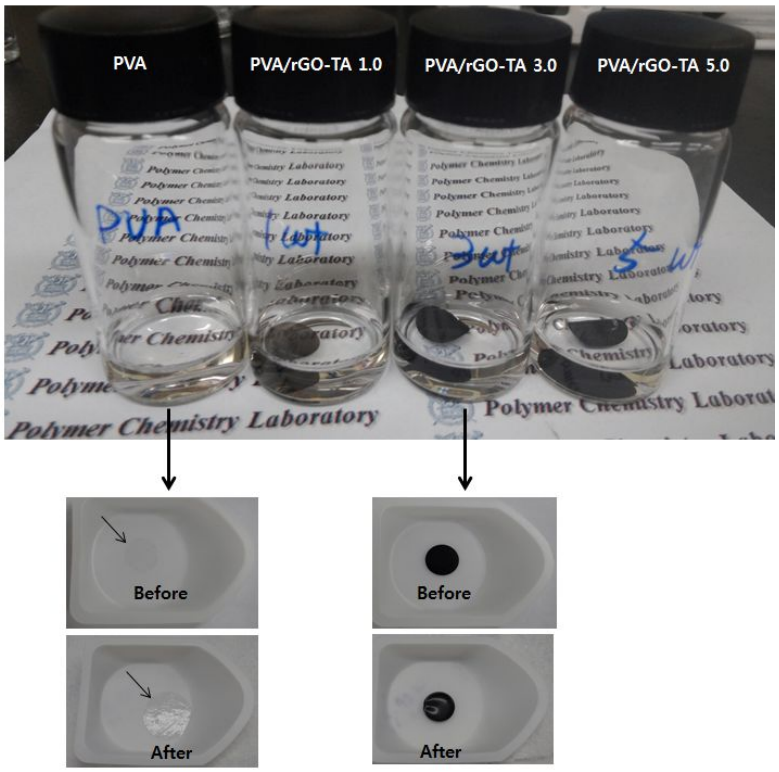
PVA
PVA/rGO-TA 1.0
PVA/rGO-TA 3.0
PVA/rGO-TA 5.0
Polymer Chemistry Laboratory
Before
After
Before
After

(b)

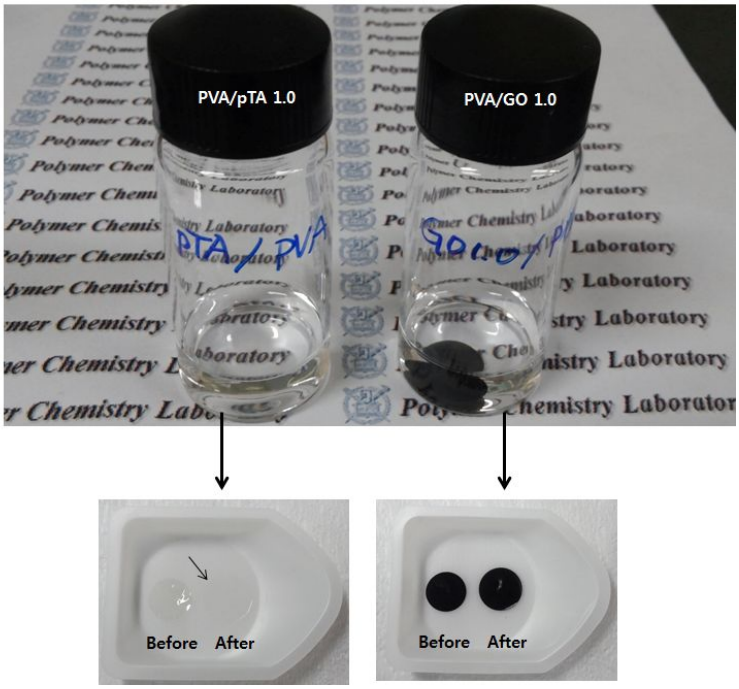

Fig. 4.15 Optical photographs of (a) PVA and PVA/rGO-TAs and (b) PVA/pTA and PVA/GO after 24 hours of water dipping test

No.	Sample	Water contact angle (°)	Weight swelling ratio (%)
①	PVA	 33.7	110.5
②	PVA /pTA 1.0	 34.0	114.1
③	PVA /GO 1.0	 38.9	109.2
④	PVA /rGO-TA 1.0	 51.2	104.4
⑤	PVA /rGO-TA 3.0	 62.8	64.7
⑥	PVA /rGO-TA 5.0	 60.5	75.6

Fig. 4.16 Water contact angles of PVA and the PVA nanocomposites

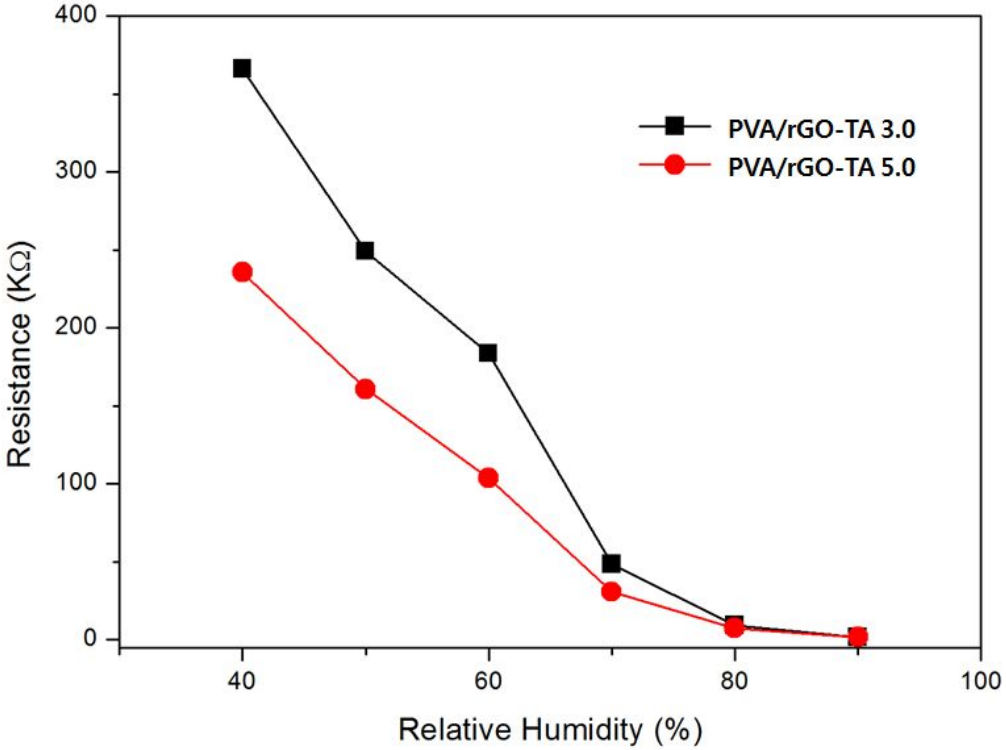

Fig. 4.17 Resistances of PVA/rGO-TA 3.0 and PVA/rGO-TA 5.0 films to RH

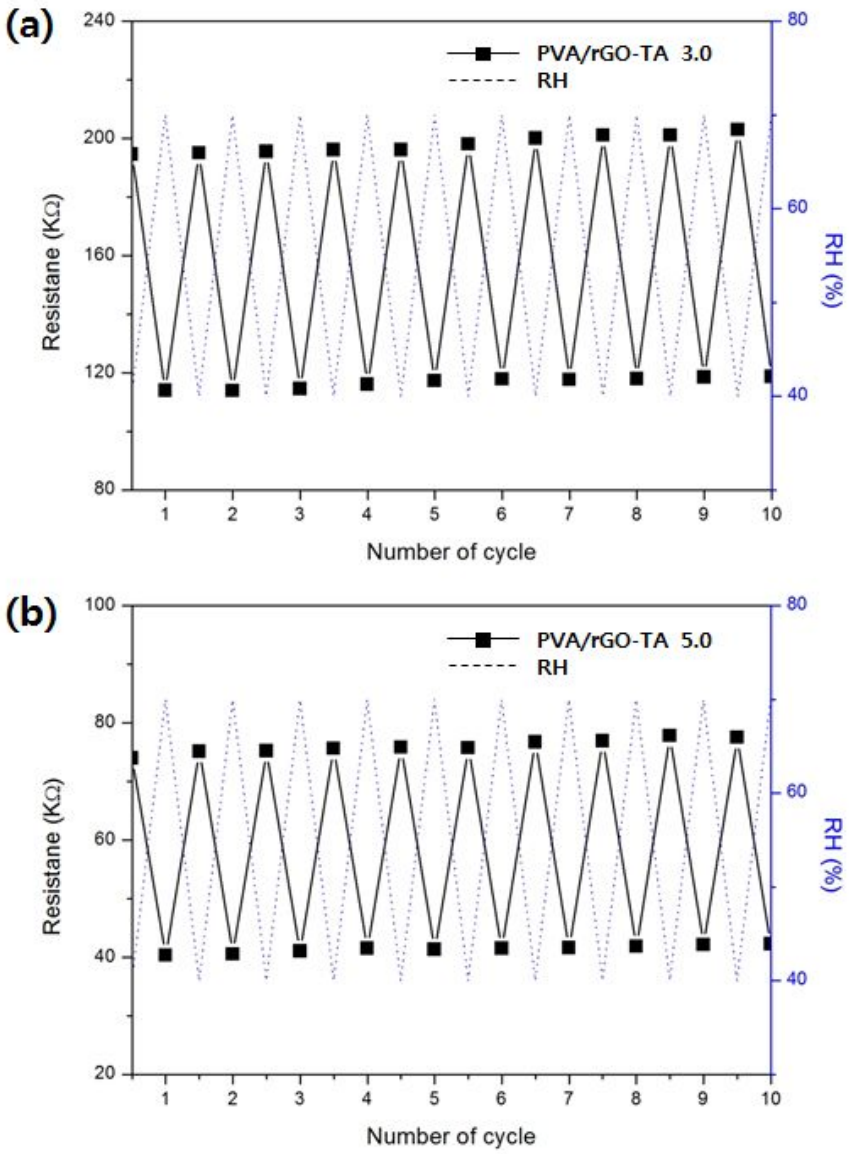

Fig. 4.18 Resistance reversibility of PVA/rGO-TA 3.0 and PVA/rGO-TA 5.0 films at 30 ºC

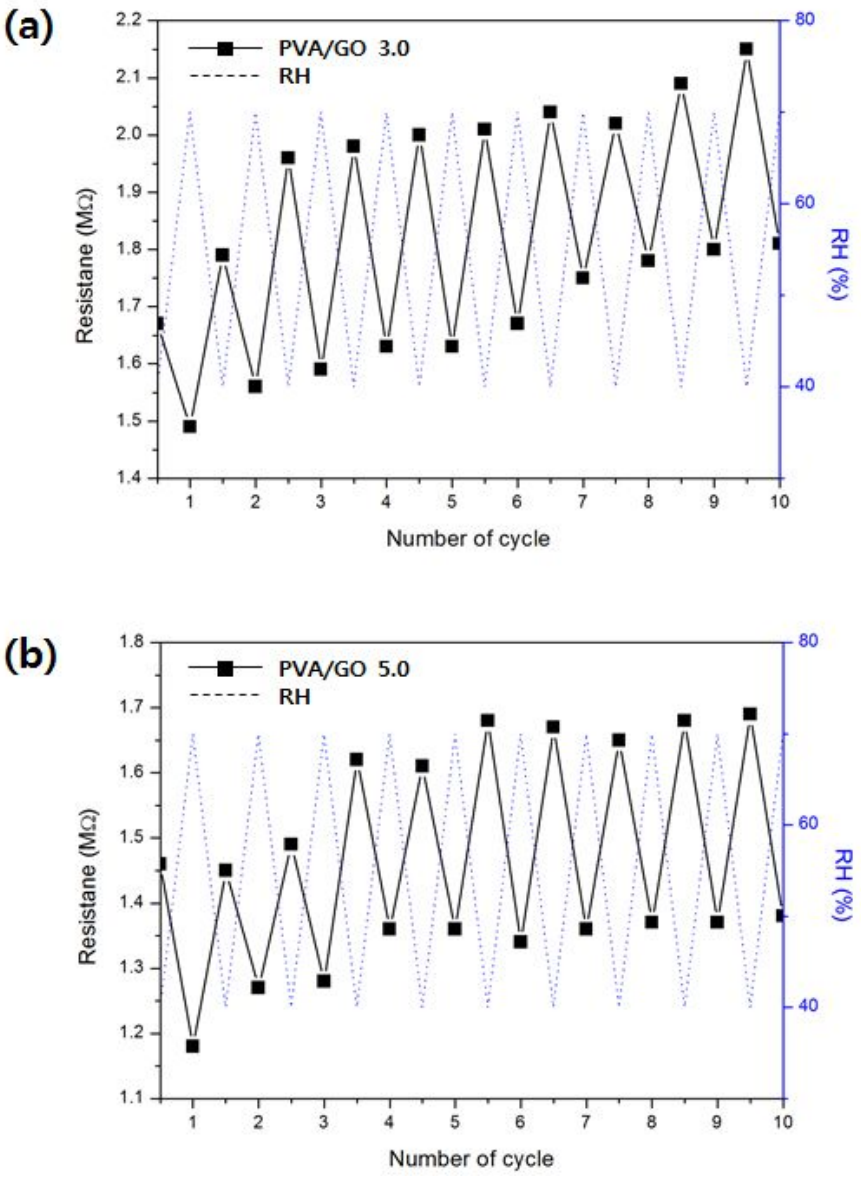

Fig. 4.19 Resistance reversibility of PVA/GO 3.0 and PVA/GO 5.0 films at 30 ºC

초 록

그래핀은 탄소 원자 하나의 두께를 가진 2차원 평면구조의 물질로서 기존의 탄소 소재를 뛰어넘는 우수한 물리화학적 성질을 가지고 있기 때문에 다양한 분야에서 차세대 기능성 소재 산업을 이끌어 갈 핵심소재로 떠오르고 있다. 특히 그래핀을 필러로 사용하는 경우, 아주 소량 첨가하는 것만으로도 고분자의 물성을 크게 증가시킬 수 있으므로 고분자 나노복합재료 분야에서 차세대 나노필러로 주목받고 있을 뿐만 아니라, 복합소재분야의 시장성장 가능성이 높아 그래핀의 조기 상용화도 가능할 것으로 예상되고 있다.

한편 폴리케톤은 전세계적으로 효성이 유일하게 개발하여 상업화한 미래 산업용 신소재로써 원료로 대기오염물질인 일산화탄소를 사용하여 제조한 친환경적인 새로운 고분자 소재이다. 또한 폴리케톤의 기계적 특성과 내열성, 내화학성, 연료투과성, 내마모성 등이 매우 우수하여 기존 엔지니어링 플라스틱 소재를 대체할 수 있는 환경 친화적인 소재로 주목을 받고 있다. 하지만, 이러한 폴리케톤은 높은 항복응력과 강성을 보이는데 반해 부서지기 쉬운 파단특성을 가지며, 장기내열노화에

따른 물성저하가 큰 약점으로 보고되고 있어 새로운 산업환경에 대응하는 신소재로 더욱 성장해 나아가기 위해서는 이의 보완이 시급하다고 할 수 있다.

본 연구에서는 그래핀 기반의 기능성 나노필러를 합성하고 이를 폴리케톤에 미량 도입하여 폴리케톤의 물성을 개선하고자 하였다. 고성능 고분자 나노복합재료를 제조하기 위해서는 그래핀이 고분자 내에서 균일한 분산상을 형성해야 하고 고분자와 강한 계면 결합을 형성하여야 한다. 하지만 그래핀은 극성 유기용매에 잘 분산되지 않고, 또한 대부분의 고분자와의 상용성(compatibility)이 부족하기 때문에 제조한 복합재료가 상 분리된 상태를 나타게 된다. 따라서 그래핀의 표면 개질은 그래핀을 충전제로 사용하기 위해 필수적으로 요구되는 사항이다. 따라서 본 연구에서는 그래핀을 다양한 합성 방법을 통하여 개질함으로써 그래핀 기반의 기능성 나노필러를 제조할 수 있었고 폴리케톤 나노복합재료의 목적 물성을 효과적으로 구현하였으며, 필러의 구조와 물성 사이의 상관관계를 규명함으로써 물성 구현 메커니즘 또한 밝히었다. 그 예로, 그래핀이 폴리케톤 고분자 내에서 균일한 분산상을 형성하면서 계면에서 고분자와의 강한 결합을 형성하도록 폴리아마이드 6를 도입하여 그래핀의 표면을 개질하였으며, 그 결과 폴리케톤의 기계적 물

성이 크게 향상하였다. 이는 그래핀 표면에 도입된 폴리아마이드 6와 폴리케톤 사슬간에 작용하는 수소결합뿐만 아니라 그래핀 표면에 존재하는 산소 작용기와 폴리케톤과의 추가적인 상호작용에 의한 것으로, 폴리아마이드 6 구조가 도입된 그래핀을 기반으로 하는 나노필러를 0.01 wt% 사용한 결과, 폴리케톤 복합재료의 인성이 크게 증가하는 놀라운 결과를 얻었다. 또한 그래핀의 높은 종횡비(aspect ratio)에 의한 배리어 특성과 화학 구조에서 기인한 라디컬 스케빈징 특성으로 인해서 그래핀/폴리케톤 복합재료의 열안정성 또한 크게 증가하였다. 따라서 분산성과 기능성을 고려하여 적절하게 개질한 그래핀 옥사이드를 필러로 사용하면 고분자 복합재료의 기계적 물성을 향상시킬 뿐만 아니라, 열안정제로써 열적 특성까지 향상시키는 것으로 확인되었다. 두 번째로 산화방지제 구조를 그래핀에 도입한 다기능성 필러를 합성하고 폴리케톤에 필러로 적용한 결과, 폴리케톤의 열안정성을 크게 향상되는 것을 확인할 수 있었다. 이러한 개질 방법은 폴리케톤 내의 그래핀의 분산성을 높여 고분자 복합재료의 기계적 물성을 강화시킬 뿐만 아니라, 열안정제라는 추가적인 기능도 부여할 수 있으므로 폴리케톤의 열안정성 또한 크게 증가시킬 수 있었다.

이 외에도 폴리비닐 알코올에 탄닌산으로 개질한 그래핀 옥사이드를

도입함으로써 폴리비닐 알코올의 다양한 물성을 동시에 향상시켰을 뿐만 아니라, 폴리비닐 알코올과 같은 수용성 고분자를 습도센서에 적용할 때 나타나는 장기 내구성 문제를 보완하고 습도 감도가 우수한 기능성 그래핀/고분자 복합소재를 제조할 수 있었다.

주요어: 그래핀, 고분자 복합재료, 폴리케톤, 폴리비닐알코올, 기계적 물성, 열안정성.

학번: 2012-30956 **성명 : 임민영**